

**PREDICTING THE EXTENT OF ROCK FAILURE/LOOSENING ABOVE
UNDERGROUND EXCAVATIONS IN MASSIVE AND JOINTED ROCK**

By

Hongdeng Deng

A thesis
Presented to the Faculty of Graduate Studies
in Partial Fulfillment of the Requirements
for the Degree of

Master of Science

Department of Civil & Geological Engineering
University of Manitoba
Winnipeg, Manitoba

© March, 2000



National Library
of Canada

Acquisitions and
Bibliographic Services

395 Wellington Street
Ottawa ON K1A 0N4
Canada

Bibliothèque nationale
du Canada

Acquisitions et
services bibliographiques

395, rue Wellington
Ottawa ON K1A 0N4
Canada

Your file *Votre référence*

Our file *Notre référence*

The author has granted a non-exclusive licence allowing the National Library of Canada to reproduce, loan, distribute or sell copies of this thesis in microform, paper or electronic formats.

The author retains ownership of the copyright in this thesis. Neither the thesis nor substantial extracts from it may be printed or otherwise reproduced without the author's permission.

L'auteur a accordé une licence non exclusive permettant à la Bibliothèque nationale du Canada de reproduire, prêter, distribuer ou vendre des copies de cette thèse sous la forme de microfiche/film, de reproduction sur papier ou sur format électronique.

L'auteur conserve la propriété du droit d'auteur qui protège cette thèse. Ni la thèse ni des extraits substantiels de celle-ci ne doivent être imprimés ou autrement reproduits sans son autorisation.

0-612-53148-1

Canada

**THE UNIVERSITY OF MANITOBA
FACULTY OF GRADUATE STUDIES

COPYRIGHT PERMISSION PAGE**

**Predicting the Extent of Rock Failure/Loosening Above Underground Excavations in
Massive and Jointed Rock**

BY

Hongdeng Deng

**A Thesis/Practicum submitted to the Faculty of Graduate Studies of The University
of Manitoba in partial fulfillment of the requirements of the degree**

of

M.SC

HONGDENG DENG © 2000

Permission has been granted to the Library of The University of Manitoba to lend or sell copies of this thesis/practicum, to the National Library of Canada to microfilm this thesis/practicum and to lend or sell copies of the film, and to Dissertations Abstracts International to publish an abstract of this thesis/practicum.

The author reserves other publication rights, and neither this thesis/practicum nor extensive extracts from it may be printed or otherwise reproduced without the author's written permission.

Abstract

This study is primarily a numerical investigation into the geomechanical response and deformation of two kinds of rock materials, massive and jointed rocks to excavation. Two finite element programs Phase² and InSight^{2D} were used to study the development of the failure/damage zones above an underground opening in massive rock. The results of simulations using a number of damage/failure criteria were compared to crack observations made by borescope in a potash mine near Esterhazy, Saskatchewan. The distinct element code UDEC was employed to identify modes of failure of roof in underground openings excavated in horizontally layered, vertically jointed rock.

Summary

In conventional rock engineering, the design and analyses of roofs for an underground opening in massive rock are generally based on the stress-strength method. This method was adopted in this thesis to predict the state of stress throughout a region near an underground excavation, assuming that the rock mass behaves elastically. The calculated stresses were then compared with the stresses required for damage/failure as defined by an appropriate damage/failure criterion.

Establishment of an appropriate damage/failure criterion for a specific rock mass at a certain site needs careful examination of the mechanical properties of the intact rock and the geologic setting of this site, and *in situ* observations of cracking near the underground openings. To evaluate the rock mass strength, it is also important to take account of the effect of stress rotation near the advancing tunnel face, and the potential for a significant reduction of the uniaxial compressive strength of the rock mass around the opening. Based on these principles, an empirical damage/failure criterion was proposed for the salt rock for potash mines near Esterhazy, Saskatchewan.

To apply the proposed Esterhazy damage/failure criterion, two-dimensional numerical modelling of the damage/failure process was carried out using the finite element tools Phase² and InSight^{2D}. With Phase² the predicted zones of damage/failure in the roof of an underground potash opening are comparable to the field observation data although the upper boundary of the damage zone is a little bit higher. This discrepancy arises mainly from the built-in assumption in the empirical damage/failure criterion that the entire rock mass strength around the underground opening has been degraded. Modelling of discrete fracturing around the opening was carried out using InSight^{2D}. The predicted shape and size of the failure zone above the opening matches the *in situ* observation data much more closely than the Phase² simulations.

Studies of failure mechanisms and roof stability of an underground opening in horizontally layered, vertically jointed rock were carried out using the distinct element code UDEC. This study reveals that buckling and shear failure along the abutments of the opening are the primary failure modes. Roof stability can be reached if a developed compressive arch is able to resist the tendency to downward movement.

The major conclusions and comments on the understanding of strength and failure propagation that have resulted from the investigations and analyses carried out during the course of this thesis are noted below:

Massive Rock

- 1) Salt rocks around underground openings, if undergoing tensile fracturing, could be assumed to behave elastically for a short time frame, and deformation and fracture could be analyzed by the stress-strength method using an appropriate damage/failure criterion.
- 2) The reduction of rock mass strength in the modelling studies of this thesis provides a reasonable approximation to the problem.
- 3) Numerical modelling studies should be based on detailed investigation of the mining environments (*in situ* rock conditions, shape, size and orientation of *in situ* cracks, mining procedures, etc.). Anomalous presence of faults, clay seams or other types of geologic weakness structures can direct cracking and failure to propagate in a “non-ideal” way, which is difficult for numerical modelling to cope with.

Jointed Rock

- 1) The failure modes of the roof of a rectangular opening in horizontally layered, vertically jointed rock are related to the geometry of the opening, joint spacing, bed thickness, joint friction angle, and the mining sequence.
- 2) UDEC is a promising numerical tool for gaining insights into failure mechanisms of jointed rock mass.

Acknowledgments

I would like to extend my sincere appreciation and gratitude to my supervisor, Dr. Brian Stimpson, for creating the opportunity for me to carry out this research, and for the much valued advice in keeping the topic in focus during the preparation of this thesis. He was still concerned about how and what I did on my thesis even though I had left the university. He spent a significant portion of his research-leave period to review the various drafts of this text word by word. Thank you, Dr. Stimpson, from the bottom of my heart.

I would like to thank Dr. Emery Lajtai, for fruitful discussions and access to his research results. His knowledge in fracture mechanics helped me a lot in numerical modelling using InSight^{2D}.

I would like to thank Dr. Jim Graham, who taught me soil mechanics with interesting practical case studies, widened my knowledge in soil engineering, and opened up my way to a career in Canada.

I also wish to express my appreciation to the following people. Dr. L. Castro of Golder Associates for constructive discussions on damage thresholds and Mr. J. D. Unrau of International Mineral & Chemical (Canada) Ltd. for providing me information on crack development above openings in the K2 mine, Esterhazy, Saskatchewan.

It is with particular admiration that I wish to express my sincere gratitude to my wife Yan for her patience, support, and love throughout this endeavour. To my daughter Susan, I give thanks for her smiling face and loving eyes.

CONTENTS

ABSTRACT	i
SUMMARY	ii
ACKNOWLEDGMENTS	iv
TABLE OF CONTENTS	v
LIST OF FIGURES	vii
LIST OF TABLES	xii
PART I INTRODUCTION	1
1.1 Failure in Roofs/Backs of Underground Openings	2
1.2 Numerical Modelling of Roof/Back Failure	4
1.3 Scope of Work and Thesis Layout	6
PART II MASSIVE ROCK	8
Chapter 1 Literature Survey on Stress-Strength Design Approach	
1.1 Stresses Around Underground Openings	9
1.1.1 Initial State of Stress	9
1.1.2 Induced Stresses Around Underground Openings	10
1.2 Deformation and Failure Processes of Rock in a Stress Field	13
1.3 Strength and Failure Criteria for Massive Rock	15
Chapter 2 Predicting Zone of Damage in Roofs of Esterhazy Potash Mines	
2.1 General Descriptions of Potash Mines in Esterhazy, Saskatchewan	24
2.2 Deformation and Fracture Around An Opening in Salt Strata	26
2.3 Importance of Knowing Zone of Failure	34
2.4 Roof Control Strategies in Saskatchewan Potash Mines	38
2.5 The Properties of Salt Rock	40
2.6 Selection of Damage Criteria for Numerical Modelling	47
Chapter 3 Numerical Simulation of the Damage Zones Using Phase² and InSight^{2D}	
3.1 Numerical Modelling Using Phase ²	54
3.2 Discussion	81
3.3 Discrete Fracture Modelling Using InSight ^{2D}	82
3.4 Discussion	94
3.5 Conclusions	101

PART III JOINTED ROCK	105
Chapter 4 Stability of a Layered Roof	
4.1 Introduction	105
4.2 The UDEC Model	109
4.3 Simulation Using Rigid Block Models	110
4.4 Deformable Block Models	118
4.5 Physical Modelling	130
4.6 Conclusions	130
4.7 Rock Bolting	136
PART IV SUMMARY	138
REFERENCES	142
APPENDIX Definition of Stiffness	151

LIST OF FIGURES

1.0	Classification of failure modes in underground openings (modified after Aydan et al. 1993).	3
1.1	Stresses in the material surrounding a circular hole in a stressed elastic body.	12
1.2	Stress-strain diagram showing the elements of crack development including the crack initiation and crack damage thresholds (after Eberhardt 1998).	14
1.3	Core discing. The core is 45 mm in diameter (after Martin 1993).	20
1.4	Location of microseismic events at the end of Round 13. Note the strong clustering of events in the roof where the notch will eventually develop. Also note the cracking occurring ahead of the face (after Martin 1993).	21
1.5	Idealize strain-time and strain rate-time curves.	23
2.1	Isopach and depth of burial map of the Prairie Evaporite Formation in Elk Point Basin (after Jones and Prugger 1982).	25
2.2	Immediate overhead stratigraphy of Esterhazy mining zones (after Jones and Prugger 1982).	27
2.3	Vertical stress distribution around openings in potash mines (after Mackintosh 1975)	28
2.4	Failure examples (after Jones and Prugger 1982).	30
2.5	Physical modelling of crack propagation around an opening (after Carter 1992)	31
2.6	Typical layout of observation boreholes in the back of an opening at Esterhazy	33
2.7	Mapping of cracking in the roof of Room 1 (The lines in the hatched zone of damage are not actual cracks)	33
2.8	Mapping of cracking in the roof of Room 2 (The lines in the hatched zone of damage are not actual cracks)	35
2.9	Mapping of cracking in the roof of Room 3 (The lines in the hatched zone of damage are not actual cracks)	35

2.10	Layout of observation boreholes in the back of a travelway	36
2.11	Mapping of cracking in the roof of a travelway (The lines in the hatched zone of damage are not actual cracks)	37
2.12	Formation of stress-relieved ground for stabilizing mine openings (after Serata 1983)	39
2.13	Stress-strain response of potash measured from axial and lateral clip-on gauges (after Duncan 1990)	41
2.14	Summary illustration of the principal stress relationship at the ductile yield point, point of volume reversal and ultimate strength for Patience Lake potash tested at a strain rate of $1.75 \mu\epsilon/s$ (after Duncan 1990)	43
2.15	Stress-strain response under unloading triaxial tests (after Chen 1993)	45
2.16	Plot of the AE event count and the AE event elastic impulse “energy” rate vs axial stress for a Saskatchewan sample (after Eberhardt 1998)	48
2.17	Plots of volumetric strain and stiffness vs axial stress for a Saskatchewan sample (after Eberhardt 1998)	49
2.18	Stress-volume strain response of a Saskatchewan sample (after Duncan 1991)	51
3.1	Finite element mesh for Case Model 1	57
3.2a	Contours of strength factor (Hoek-Brown failure criterion, $m=4.7$, $s=1$)	58
3.2b	Contours of deviatoric stress (MPa) and zone of failure by the Esterhazy failure criterion (Equation 3)	58
3.3	Contours of minimum principal stress σ_3 (MPa)	59
3.4	Finite element mesh for Case Model 2	61
3.5	Contours of the major principal stress σ_1 (MPa)	62
3.6	Contours of the minor principal stress σ_3 (units in MPa)	63
3.7	Principal stress distributions at different heights in the roof	64
3.8	Contours of strength factor using the Hoek-Brown criterion ($m=4.7$, $s=1.0$)	65

3.9a	Contours of strength factor and predicted zone of failure for Hoek-Brown criterion ($m=4.7$, $s=1$, s_c reduced to 65%)	67
3.9b	Contours of strength factor and zone of failure for Hoek-Brown failure criterion (σ_c reduced to 80%)	68
3.10	Contours of strength factor and zone of failure for Duncan failure criterion	69
3.11a	Contours of strength factor for modified Duncan failure criterion (σ_c reduced to 65%)	70
3.11b	Contours of strength factor for modified Duncan failure criterion (σ_c reduced to 80%)	71
3.12	Contours of deviatoric stress and zone of failure (units in MPa)	72
3.13	Contours of strength factor and zone of damage growth for the proposed Esterhazy damage criteria	73
3.14	Finite element mesh for Case Model 3 for incorporating a clay seam	74
3.15	Contours of minor principal stress σ_3 (MPa)	76
3.16a	Contours of strength factor and zone of failure for the Hoek-Brown criterion ($m=4.7$, $s=1$)	77
3.16b	Contours of strength factor and zone of failure for the Duncan failure criterion	78
3.17	Contours of deviatoric stress and zone of failure for the Esterhazy failure criterion (Equation 3)	79
3.18	Contours of horizontal displacement (mm)	80
3.19	Finite element mesh of block under uniaxial compression	85
3.20	Factor of safety around the crack tip	87
3.21	Contours of minimum principal stress (MPa)	88
3.22	Finite element mesh of block under biaxial compression	89
3.23	Contours of minimum principal stress	90
3.24	Finite element mesh for a tabular opening	91

3.25	Contours of safety factor (USR yield criterion, $R=0.34$; the dash lines represent s_1 directions)	92
3.26	Introducing cracks in the failure region along s_1 direction	93
3.27	Contours of minimum principal stress (units in MPa)	95
3.28	Introduction of the second cracks along the s_1 direction	96
3.29a	Contours of safety factor	97
3.29b	Contours of minimum principal stress (units in 10 MPa)	98
3.29c	Trajectories of the maximum principal stress after the second crack is inserted	99
3.30	Deduced ultimate zone of failure	100
3.31	Conceptual sketch of the loosened zone in the roof	102
4.1	Four failure modes of voussoir beams (after Sterling 1980)	107
4.2	Two-hinge failure model (after Stimpson 1989)	108
4.3	Effect of joint spacing on failure modes	112
4.4a	Effect of span on the failure modes (span 1.6m, arrows are velocity vectors)	113
4.4b	Effect of span on the failure modes (span 3.6m)	114
4.4c	Effect of span on the failure modes (span 4.8m)	115
4.5	Effect of friction angle of joints on the failure modes	116
4.6	Effect of dimensions on the failure modes	117
4.7a	Effect of dimensions on the failure modes (Block size: width 1.0m, height 0.5m)	119
4.7b	Effect of dimensions on the failure modes (Block size: width 1.0m, height 1.0m)	120

4.7c	Effect of dimensions on the failure modes. The anomalous velocity vectors indicate the whole system is at equilibrium (Block size: width 1.0m, height 1.5m)	121
4.8	Effect of block dimensions on the failure modes	122
4.9	Principal stress distributions	124
4.10	Principal stress trajectories show development of a compressive arch	125
4.11	Roof failure by the two-hinge mode resulting from the collapse of a full arch	125
4.12	Stress trajectories in deformable blocks showing a compressive arch developing in the roof (size of block: width 0.4m, height 0.8m)	126
4.13	Major principal stress contours	127
4.14	Minor principal stress contours	128
4.15	Stress trajectories showing the compressive arches developing in each layer	129
4.16	Physical modelling of sequential excavation (after Stimpson 1989)	131
4.17a	Roof failure is characterized by sagging and layer separation (step 6000)	132
4.17b	Roof failure by the two-hinge mode with increase of span (step 11000)	132
4.18	Simulation of sequential excavation	133
4.19	Relationship of failure modes to dimensions of block and roof span	135

LIST OF TABLES

3.1	Material properties for salt and potash rock	55
3.2	Saskatchewan potash strength (after Lajtai et al 1991)	60

PART I INTRODUCTION

The response of a rock mass to an external perturbation such as the excavation of an underground opening depends on many factors such as the mechanical properties and the geometrical and spatial characteristics of the discontinuities, the properties of the intact rock, the shape, size, and orientation of the opening, the magnitude and orientation of the pre-mining stresses, and the existence and magnitude of any groundwater pressures. The prediction of the response of such a system is therefore highly complex and has been approached by researchers in three ways: closed-form analytical solutions (Kirsch 1898, Jaeger and Cook 1969, Poulos and Davis 1974, Brady 1977), physical models (Patton 1966, Ladanyi and Archambault 1970, Indraratna and Hague 1977, Stimpson 1989) and numerical modelling (Southwell 1940, Otter et al. 1966, Cundall 1971, Zienkiewicz 1977, Brady 1979). In this study, numerical and physical modelling are used.

Two approaches to numerical modelling of rock masses can be identified. A continuum approach treats the rock mass as a continuum intersected by a number of discontinuities, while the discontinuum approach views the rock mass as an assemblage of independent blocks or particles (Goodman and St. John 1977).

The differential models of the continuum approach, such as the finite element and finite difference methods, characterize the entire region of interest, and are capable of handling complex geometries and heterogeneous rock masses. Discontinuum models feature numerical procedures involving the equations of motion of particles or blocks and their interactions and should be used whenever independent rock block movements must be specifically recognized and modelled. This is the case of excavation within a low stress field in jointed rock which may induce large movements and rotations of the rock blocks defined by existing geological discontinuities or by stress or blasting-induced rock fractures around the opening.

Practical applications of the numerical methods are particularly useful for modelling the effects of different geological features and for determining the potential fracture zones around excavations at depth (Hoek and Brown, 1980). By using a suitable rock

fracture criterion, it is possible to identify failed or highly stressed zones around excavations and thereby to assist in the proper selection of rock support or alternative mine geometries and sequencing.

The research described in this thesis had two primary goals. First, data on roof cracking was obtained from a potash mine near Esterehazy, Saskatchewan, and various approaches were employed in an attempt to simulate the field observations using two finite element programs – Phase² and InSight^{2D}. Phase² was used to assess the application of damage and failure criteria in predicting cracked zones in the roof. InSight^{2D} was applied for the first time to simulating discrete crack development around a mine opening. Second, the UDEC code was employed to investigate the behaviour of a particular class of roof, namely, horizontally bedded and vertically jointed. Patterns of behaviour were related to joint spacing, friction angle, block size, and span, and compared to results from a physical model. An original finding was that with increasing span a roof can initially be unstable, then pass through a self-supporting phase, before passing into another unstable mode.

1.1 Failure in Roofs/Backs of Underground Openings

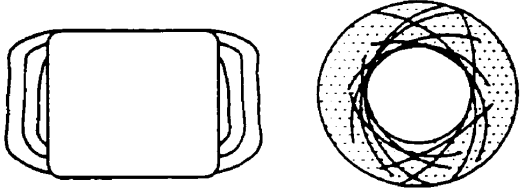
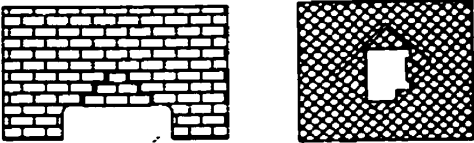
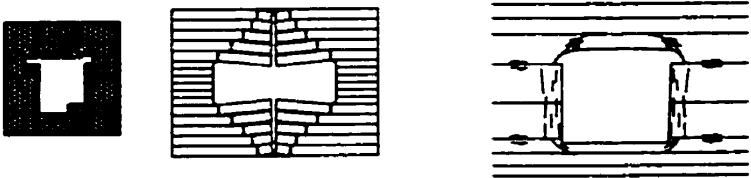
Underground excavations are created in a compressive-stress field where the components of stress and their magnitudes reflect the depth and geological history of the rock mass. The presence of an opening alters the stress field, producing compressive and perhaps tensile stress concentrations around the opening. Damage, fracture or failure may occur within these zones of stress concentration.

The modes of instabilities likely to take place in the vicinity of underground openings may be classified (Aydan et al 1993), on the basis of the structure and strength of the rock mass as (Figure 1.0):

1) Failure modes involving only intact rock

- Rockbursting

- Squeezing

<p>Failure Involving Only Intact Rock</p> <p>Rockbursting Squeezing failure</p>	
<p>Failures Involving only Discontinuities</p> <p>Falls Sliding Toppling</p>	
<p>Failure Involving Intact Rock and Discontinuities</p> <p>Bending failure Buckling failure Tensile splitting Shearing and sliding Flexural toppling</p>	

**Figure 1.0 Classification of failure modes in underground openings
(modified after Aydan et al. 1993)**

2) Failure modes involving only discontinuities

Block falls

Sliding

Toppling

3) Failure modes involving discontinuities and intact rock

Bending

Buckling

Punching and sliding

Shearing and sliding

The failure modes of Type 1 are usually observed in massive rock, while Type 2 are commonly encountered in jointed rock at a shallow depth. The failure modes of Type 3 occur in both massive and jointed rocks. The rock mechanics engineer must be familiar with conditions required for the development of these instabilities and the means to prevent them.

1.2 Numerical Modelling of Roof/Back Failure

In this thesis two specific types of underground opening and rock mass were studied for modes of failure using numerical modelling, namely

- (1) openings with large span/height ratio in massive, soft rock, and
- (2) rectangular openings in thin layered, vertically jointed, hard rock.

To study the failure/damage processes for these two kinds of rock mass, two different numerical approaches are adopted in this thesis: finite element methods for the massive rock with calibration against data from a potash mine in Saskatchewan, and the distinct element technique for the thin layered, vertically jointed rock with a comparison to results from physical modelling.

Massive Rock

Salt rock in Saskatchewan is associated with potash deposits of great lateral extent that are mined by the room-pillar method at a depth of approximately 1,000m. Roof cracks are found in a dome-shaped zone with an apex of about 3.5 m above some of the mining rooms. In addition, cracks are open and rough, which implies the presence of tensile stresses. Preliminary 2D elastic stress analyses of these rooms predicted a damage zone only in the side walls using the Hoek-Brown failure criterion. The difference in the extent and location of failure/damage zones between the predicted and the observed provided the first issue to be addressed in this research. In order to solve this problem the writer started with a review of the basic salt rock properties obtained in laboratory testing, i.e., uniaxial compression tests, triaxial compression tests and acoustic emission response. Detailed field data on the development of cracks and deformation of salt rock backs in a potash mine were also acquired from the K2 Mine near Esterhazy, Saskatchewan. Based on this information a new empirical damage criterion for salt rock was established. The new damage criterion was then applied in numerical modelling and the results compared to the field data.

Jointed Rock

With respect to the jointed, strong rock at a shallow depth, failure of the rock mass is governed by the discrete joints rather than by the intact rock itself, as the strength of the intact rock is much higher than any mining-induced stresses. As the rock mass is not a continuum, continuum elastic stress analysis is not appropriate. The distinct element method, which treats the rock mass as a discontinuum, has become one of the most powerful numerical tools for the study of jointed rock developed so far in either mining or civil engineering.

Two specific issues of thinly layered, vertically jointed rock are dealt with in this thesis:

1) Failure of the jointed rock mass is affected by many factors, including the orientations, spacings and roughness of the joints, the size of rock blocks, the dimension and shape of the openings, and even the sequence of excavation. Sensitivity studies of these factors were carried out using distinct element modelling to increase understanding of how these factors influence the failure mechanisms.

2) A 2-hinged failure mechanism was proposed by Stimpson (1989), and analytically and physically modelled. In this study, the distinct element method was used in an attempt to model the 2-hinge failure mechanism.

1.3 Scope of Work and Thesis Layout

This thesis involves numerical modelling of damage and failure in jointed rock and massive rock around shallow and deep underground excavations. The finite element programs Phase² and InSight^{2D} are used for studies of massive rock, and the Universal Distinct Element Code, UDEC, for analysis of thinly layered, vertically jointed rock. The whole thesis consists of four parts, Part I acts as preface, Part II and Part III form the core part of the research, and Part IV summarizes the research.

Part I summarized rock mass instability and failure modes around openings in massive and jointed rock mass. A general description of methodologies for studies of the massive and jointed rocks was then provided, and followed by this description of the work scope and the thesis outline.

Part II describes numerical modelling of damage zones in a massive rock. This part begins with Chapter 1 - a literature review on the stress-strength design approach, which contains a discussion of stress distributions around underground openings, deformation and failure processes of rock in a stress field, and strength/failure criteria for massive rock currently in use. Chapter 2 briefly describes potash mines in Esterhazy, Saskatchewan, field observations of roof damage, the properties of salt rock, and an empirical damage/failure criterion is provided. Chapter 3 provides numerical simulation of damage zones around openings in the Esterhazy potash mines using numerical tools Phase² and InSight^{2D}. Results from these case models are used to demonstrate the differences between predicted damage zones produced by employing various failure

criteria. This chapter ends with conclusions and a discussion of numerical modelling and its capability in prediction of damage zones around openings at Esterhazy.

Part III describes application of a distinct element code UDEC for study of failure mechanisms around an opening in a thin layered, vertically jointed rock mass. Chapter 4 contains a literature review of failure modes of fractured rock, various numerical models and physical model studies. It illustrates basic features of UDEC models and the application of UDEC, where sensitivity studies of rigid blocks are conducted to evaluate the effects on failure modes of spacing of joints, the span of the underground openings, the friction angle of the block surface, and the dimensions of blocks. The development of arching in the horizontally-layered, vertically-jointed rock mass system is then examined using a deformable block model. Finally, a UDEC modelling of sequential excavation is demonstrated to verify the failure mode observed in a physical model study.

The primary steps and conclusions of the research are reviewed in Part IV.

PART II MASSIVE ROCK

Massive rock is not necessarily geologically structureless, but where there are faults, joints or other weak interfaces, their spacing is wide compared with the thickness of the rock unit and/or the dimensions of openings excavated in it.

Although there are few structural flaws in massive rock, rock engineering problems around underground openings in these materials still challenge rock engineers in various ways, including rock bursting in high strength, brittle rock and squeezing in a weak, creep-prone rock.

Studies of failure or damage in rock masses are of fundamental and practical interest in rock/mining engineering. For rock/mining engineers, the ultimate goal is to precisely predict those regions around underground openings where failure will occur and to estimate the degree to which the rock in such regions will be fractured. One approach to this challenge makes use of the theory of elasticity to predict the state of stress throughout the region of interest (i.e. near the excavations), and, therefore, assumes that the rock mass behaves elastically. The stresses calculated in this way are then compared with the stresses required for failure as defined by an appropriate failure criterion. Zones of predicted rock failure can then be mapped. This procedure has been applied with some success to rock/mining engineering problems. The primary limitation of the method is that once failure is initiated at some point, stresses are redistributed. This redistribution may bring the rock mass into a state of equilibrium or failure may propagate if the new stresses still exceed the failure criterion at some points. The applicability of this approach is evaluated in this thesis using the observed extent of salt rock loosening above an underground potash room in an Esterhazy potash mine (Saskatchewan) as the measure of success.

Chapter 1 Literature Survey on Stress-Strength Design Approach

1.1 Stresses Around Underground Openings

The final state of stress around an underground opening is the resultant of the initial, undisturbed state of stress and stresses induced by the excavation. Since the induced stresses are related to the initial, undisturbed stress state, it is clear that the accuracy of determination of the pre-excavation state of stress is of primary importance to any design.

1.1.1 *Initial State of Stress*

The initial state of stress (i.e. virgin ground stress) originates from overburden load and tectonic history of the rock mass. The vertical normal stress underground is normally proportional to the depth of overburden and the density of the overlying strata. The gravitational component of the horizontal normal stress is a function of Poisson's ratio of the material and the vertical stress. These relationships can be theoretically expressed by the following formulae, assuming plane strain, linear elasticity, and a uniform overburden:

The vertical stress:

$$\sigma_v = \gamma z$$

The horizontal stress:

$$\sigma_h = \sigma_v \left(\frac{\nu}{1 - \nu} \right)$$

where γ is the unit weight of the overburden, z is the depth, and ν is Poisson's ratio of the rock.

Measured *in situ* horizontal stresses are often higher than those predicted by the above equation because they are modified by topography, tectonic stresses, folding uplift, faulting, stiffness variations between strata, etc. Therefore, the prediction of field stresses at a particular point is almost impossible. Consequently, it is essential to carry out *in situ* stress measurements as part of a site investigation program.

It is well known, however, that the precise measurement of *in situ* stresses is also difficult. Also, a large number of measurements must be made in order to acquire an accurate estimate of the *in situ* stress field for a particular site, and this is very time-consuming and costly work.

For an estimate of the *in situ* state of stress, Heim (1912) provided a well-known rule of thumb. He suggested that most material cannot support stress differentials for extended periods of time (i.e. geological time scales) due to time-dependent deformation properties (creep, viscous behaviour, etc.). The lateral and vertical stresses should thus equalize at least at sufficiently high stress levels. Heim's rule is widely used by workers in weak rocks such as coal measures and evaporites, and it has been found to give a good approximation of the *in situ* stress field in these materials. It has also been shown that Heim's rule gives a reasonable estimate of the horizontal stresses at depths in excess of one kilometre (Hoek and Brown 1980).

1.1.2 Induced Stresses Around Underground Openings

Several analytical solutions for the stress distribution around an underground excavation are described in many standard rock mechanics texts. A solution requires the following (Brady and Brown 1985):

- (a) The boundary conditions for the problem
- (b) The differential equations of equilibrium
- (c) The constitutive equations for the material
- (d) The strain compatibility equations

One of the earliest solutions for the distribution of stresses around an opening in an elastic body was published by Kirsch (1898) for a 2-D circular hole. The stresses at a point near the opening (Figure 1.1) are defined by the Kirsch equations for plane strain and linear elasticity:

Radial stress:

$$\sigma_r = \frac{1}{2} p_z \left\{ (1+k) \left(1 - \frac{a^2}{r^2}\right) + (1-k) \left(1 - 4\frac{a^2}{r^2} + 3\frac{a^4}{r^4}\right) \cos 2\theta \right\}$$

Tangential stress

$$\sigma_\theta = \frac{1}{2} p_z \left\{ (1+k) \left(1 + \frac{a^2}{r^2}\right) - (1-k) \left(1 + 3\frac{a^4}{r^4}\right) \cos 2\theta \right\}$$

Shear stress

$$\sigma_{r\theta} = \frac{1}{2} p_z \left\{ -(1-k) \left(1 + 2\frac{a^2}{r^2} - 3\frac{a^4}{r^4}\right) \sin 2\theta \right\}$$

where p = vertical field stress, k = ratio of the horizontal to vertical stress, a = radius of the circular hole, r = radius of the stress element, θ = polar angle of the stress element.

Theoretical solutions for stresses around other excavation shapes are available from numerous publications (Muskhelishvili 1953, Savin 1961, Greenspan 1944, Heller et al 1958, Jaeger and Cook 1969, Obert and Duvall 1967). These solutions played a very important role in the early development of rock mechanics before the advent of the digital computer and numerical techniques.

Numerical techniques are widely used in modern rock engineering as they are capable of handling more complex excavation shapes, non-homogeneity of the rock mass, and non-linear constitutive behaviour of the medium. These conditions generally present difficulties which are not amenable to closed-form solutions.

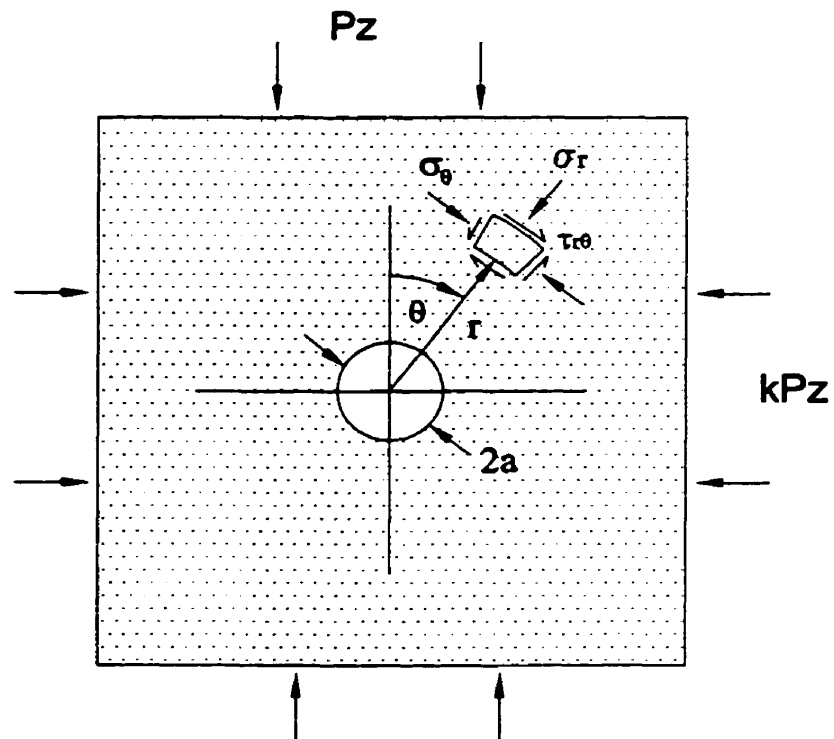


Figure 1.1 Stresses in the material surrounding a circular hole in a stressed elastic body

Numerical techniques have led to many important insights into rock behaviour around underground openings. For example, in studies of the strength of massive Lac du Bonnet granite around underground openings at the Underground Research Laboratory (URL), Martin (1993) noted that, state of stress induced ahead of the tunnel face was critical to the understanding of how failure around the tunnels developed. These findings were accomplished using the 3-D boundary element program Examine^{3D}.

There are two primary numerical methods used in solving problems in rock mechanics in massive rock. They are (1) The Finite Element Method (FEM) and (2) The Boundary Element Method (BEM). Of these, the finite element method is the most popular. It involves dividing the problem body in smaller “elements” of various shapes connected by “nodes”. Each finite element can have different material properties. Displacements at the nodes are treated as unknowns and solved for. Stresses are then calculated at one or more points inside each element using the stress-strain relationship and the nodal displacements. The major limitation of the finite element method for application to engineering rock mechanics lies in the need to arbitrarily define the outer boundaries of the problem domain. This can introduce inaccuracies into the solution because the far-field stress conditions may not be satisfied completely.

As mentioned earlier in this section, a solution for deformations, strains and stresses throughout the rock mass must satisfy four conditions. All numerical methods satisfy the conditions (a), (b) and (d) in almost a routine manner. The most crucial on which the usefulness of the solution depends is condition (c) - the constitutive equations for the rock masses.

A detailed description of the advantages and disadvantages of numerical tools is not the purpose of this thesis. The interested reader can refer to related literature.

1.2 Deformation and Failure Processes of Rock in a Stress Field

When the *in situ* stress field is disturbed by underground excavation, deformation and, possibly, fracture of the rock mass takes place. The behaviour of rock under increasing load is shown by the stress-strain curve obtained from laboratory testing of rock samples in Figure 1.2. The deformation and fracture processes can be divided into several stages:

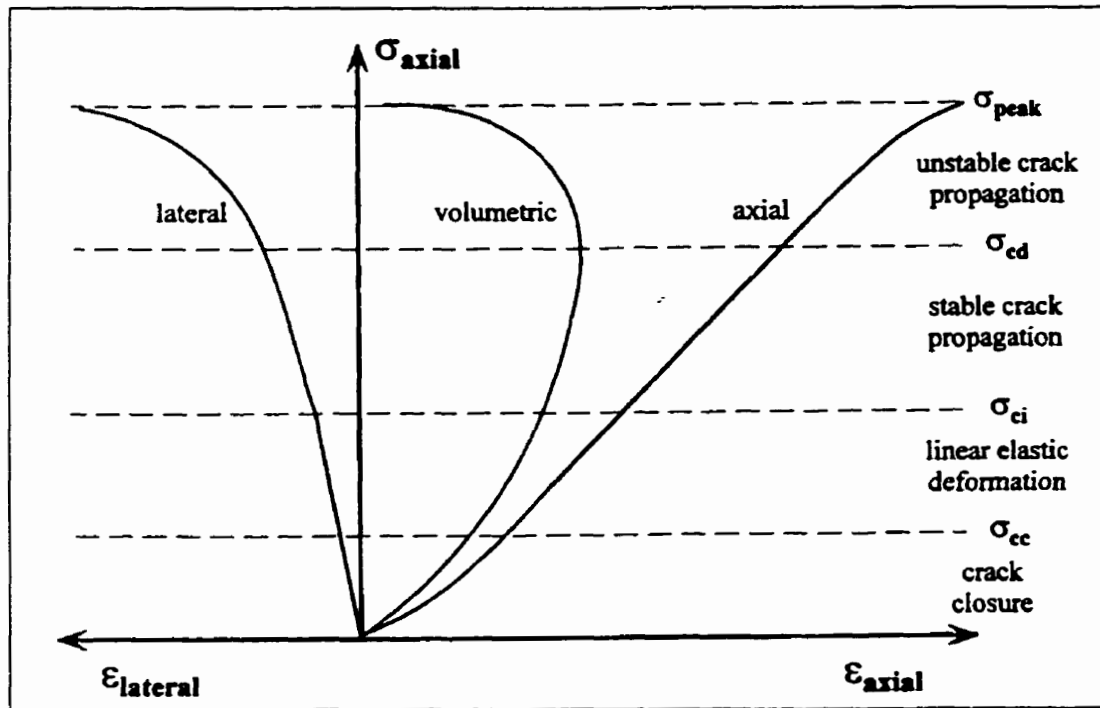


Figure 1.2 Stress-strain diagram showing the elements of crack development including the crack initiation and crack damage thresholds (after Eberhardt 1998)

- Crack closure
- Linear elastic deformation
- Crack initiation and stable crack growth
- Critical energy release and unstable crack growth
- Failure and post peak behaviour

Crack closure occurs during the initial stages of loading when existing cracks orientated at an angle to the applied load close. During crack closure, the stress-strain response is non-linear, exhibiting an increase in axial stiffness (i.e. Young's modulus). The extent of this non-linear region is dependent on the initial crack density and geometrical characteristics of the crack population. Once the majority of existing cracks have closed, linear elastic deformation takes place. The elastic constants of the rock are calculated from this linear portion of the stress-strain curve.

Crack initiation represents the stress level where microfracturing begins and is marked as the point where lateral and volumetric strain curves depart from linearity. Crack propagation at this point is considered as being stable, and controlling the applied load can stop crack growth. Bieniawski (1967) defines unstable crack propagation as the condition that occurs when the relationship between the applied stress and the crack length ceases to exist and other parameters, such as the crack growth velocity, take control of the propagation process. Under such conditions, crack propagation would be expected to continue even if loading was stopped and held constant. Bieniawski (1967) correlated the threshold for unstable crack growth, also referred to as the point of critical energy release and the crack damage threshold, with the point of reversal in the volumetric stress-strain curve.

Unstable crack propagation continues to the point where the numerous microcracks coalesce into large cracks and the rock can no longer support an increase in load. This point (the maximum load bearing capacity) is defined as the peak strength of the rock sample.

The mechanisms by which fractures initiate, grow and coalesce and form large-scale fractures and faults have been studied and well documented (Wawersik and Brace, 1971;

Wong, 1982; Fredrich et al, 1989). These mechanisms include sliding along pre-existing cracks and grain boundaries, pore crushing, elastic mismatch between mineral grains, grain-grain contact, and dislocation movement. The result of these processes is gradual degradation of the rock, starting well before the peak strength of the rock is reached, and continuing past the peak stress into the post-peak region.

It is found from numerous studies that the majority of fracturing occurs between grain boundaries with secondary fracturing occurring within weaker grains along cleavage planes and at points where harder minerals induce a point load in neighbouring softer minerals (Waversik and Brace, 1971; Bombolakis 1973; Sprunt and Brace 1974; Mosher et al. 1975; Kranz 1979).

1.3 Strength and Failure Criteria for Massive Rock

Each type of rock has its own strength surface in 3-D stress space which, if a suitable form of equation were found, could be represented algebraically as a strength criterion. The early attempts to develop strength criteria for rock were mainly theoretical and evolved from yield criteria for metals and Griffith crack theory for glass. They led to an improved understanding of micromechanics, but none of them fit the experimental data particularly well (Jaeger and Cook 1969). For this reason, the strength criteria most used in practice are empirical. The approach is to fit a curve (or a surface in three-dimensional stress space) to a real set of experimental data. The formula may have a theoretical justification, but is chosen mainly to give a good fit and for its simplicity. The method gives a sufficiently accurate prediction of strength for most practical purposes.

To be useful to the underground excavation designer, a rock failure criterion should satisfy the following requirements (Hoek and Brown, 1980):

- a) It should adequately describe the response of an intact rock sample to the full range of stress conditions likely to be encountered underground.
- b) It should be capable of predicting the influence of one or more sets of discontinuities upon the behaviour of a rock mass

- c) It should provide some form of projection, even if approximate, for the behaviour of a full scale rock mass containing several sets of discontinuities.

Several commonly used failure criteria are briefly described in the following section:

(1) Bieniawski Criterion

Bieniawski (1967) proposed the following empirical power law strength criterion:

$$\frac{\sigma_1 - \sigma_3}{2\sigma_c} = 0.1 + B \left(\frac{\sigma_1 + \sigma_3}{2\sigma_c} \right)^a$$

where σ_1 is the major principal stress at failure, σ_3 is the minor principal stress applied to the specimen, σ_c is the uniaxial compressive strength of the intact rock material, and the exponent a represents the curvature of the strength surface and assumes values in the range of 0.85 - 0.93. The constant B controls the position of the envelope, and varies from 0.7 to 0.8 for most rock types.

(2) Hoek and Brown Criterion

Hoek and Brown (1980) developed the following criterion for the prediction of rock mass strength:

$$\frac{\sigma_1}{\sigma_c} = \frac{\sigma_3}{\sigma_c} + \sqrt{m \frac{\sigma_3}{\sigma_c} + s}$$

where m and s are constants which depend upon the properties of the rock and upon the extent and characteristics of discontinuities. Both m and s have been correlated with, and can be predicted from, the rock mass quality index, Q , and the rock mass rating (RMR).

(3) Martin's Cohesion-Reduction Concept and the Castro Criterion

While investigating the significant reduction (from about 200 MPa to about 100 MPa) of the uniaxial compressive strength of massive granite around the tunnel at the 420 m Level of the Underground Research Laboratory, Pinawa, Manitoba, Martin (1993) noted that this reduction could not be simply attributed to scale effects because a 100-mm diameter borehole displayed the same failure as a 3.5-m diameter tunnel. It was observed that excavating tunnels at the 420 Level caused crack damage to the rock around the advancing tunnel face and that this sort of damage reduced the rock strength.

Further studies of unconfined compression tests revealed that cracking in compression initiates at about $0.4\sigma_c$. Martin (1993) then concluded that this crack damage stress ($0.4\sigma_c$) is the true strength or cohesion of the rock.

Similarly, Castro (1996) investigated the zones of stress-induced damage and failure around a deep underground opening in a moderately jointed, brittle rock mass. His studies suggested that movements of blocks along existing, non-continuous discontinuities have only a minor effect on rock mass damage initiation, because the blocks do not have the kinematic freedom for significant levels of translation and rotation. It was further proposed that valid information regarding the onset of damage can be extracted from small-scale laboratory tests. It was therefore proposed that the damage initiation zones (DI) started within the rock mass where the induced deviatoric stresses (i.e. difference of the major and minor principal stresses) exceeded the stress level for the onset of stable crack growth, σ_{sc} , as measured in uniaxial compression tests of the intact rock. The criterion for damage initiation through the intact rock material is expressed as follows (Castro 1996):

$$\sigma_1 - \sigma_3 \approx \sigma_{sc}$$

The σ_{sc} value is estimated from measurements of the crack volume or inelastic volumetric strain (Martin and Chandler, 1994), and is defined by the stress at which dilation just begins on a plot of crack volume versus axial strain.

As these strength criteria are established on the basis of data obtained from laboratory testing of intact rock specimens they may only be an approximation to the *in situ* rock strength. One must, therefore, be careful not to extrapolate far beyond the conditions for which data are available, since the criteria are then likely to give poor predictions. Several factors affect the measured strength of intact rock, including:

(1) Sample Disturbance

Samples are generally collected from the location where the underground excavation will be constructed or from a borehole. It is generally recognized that softer rocks, such as shales and porous sandstones, are susceptible to sample disturbance and in a high stress field, core from hard rock can suffer crack damage during drilling. The process of drilling a core sample from a stressed medium induces a stress concentration where the bit is penetrating the rock. Core discing is an extreme form of such sample disturbance (Figure 1.3). *In situ* stress magnitudes generally increase with depth, consequently, one should find that samples of the same rock obtained at increasing depths should contain a higher density of microcracks (Martin 1993).

(2) Face Effects during Tunnel Advance

“Overloading” of the rock ahead of the face and consequent damage of rock before it enters the tunnel has been reported. The occurrence of this damage is attributed to the stress concentrations caused by the tunnel face and was investigated by microseismic monitoring in the Mine-By tunnel at the 420 m Level of the Underground Research Laboratory, Pinawa, Manitoba (Carlson and Young 1992, Martin 1993). A typical record of the clustering of microseismic events in the roof and ahead of the face is shown in Figure 1.4. As noted by Martin (1993), the damage is indicated by microseismic events that have a wide range of moment magnitudes. These microseismic events represent the initiation of cracking and not ultimate failure. This type of damage results in a reduction of cohesion to 50% or more for the rock immediately adjacent to the tunnel. The rock



Figure 1.3 Core discing. The core is 45 mm in diameter (after Martin 1993)

strength was likely not degraded from its *in situ* value at distances beyond 0.5m (about 0.3 times the tunnel radius) from the tunnel boundary.

Stress rotation ahead of the tunnel face also occurs as the tunnel advances, a feature revealed by Martin (1993) using the boundary element program Examine^{3D}. This stress rotation influences the direction and origin of crack growth, causes additional crack growth without increasing the load (Wu and Pollard 1992), and contributes to the loss in cohesion.

(3) The Effect of Scale on Strength

The difference between the laboratory strength of rock samples and the *in situ* strength of rock mass may arise from the effect of specimen scale. An empirical strength/scale relationship for various rock types was proposed by Hoek and Brown (1980). The relationship is given by:

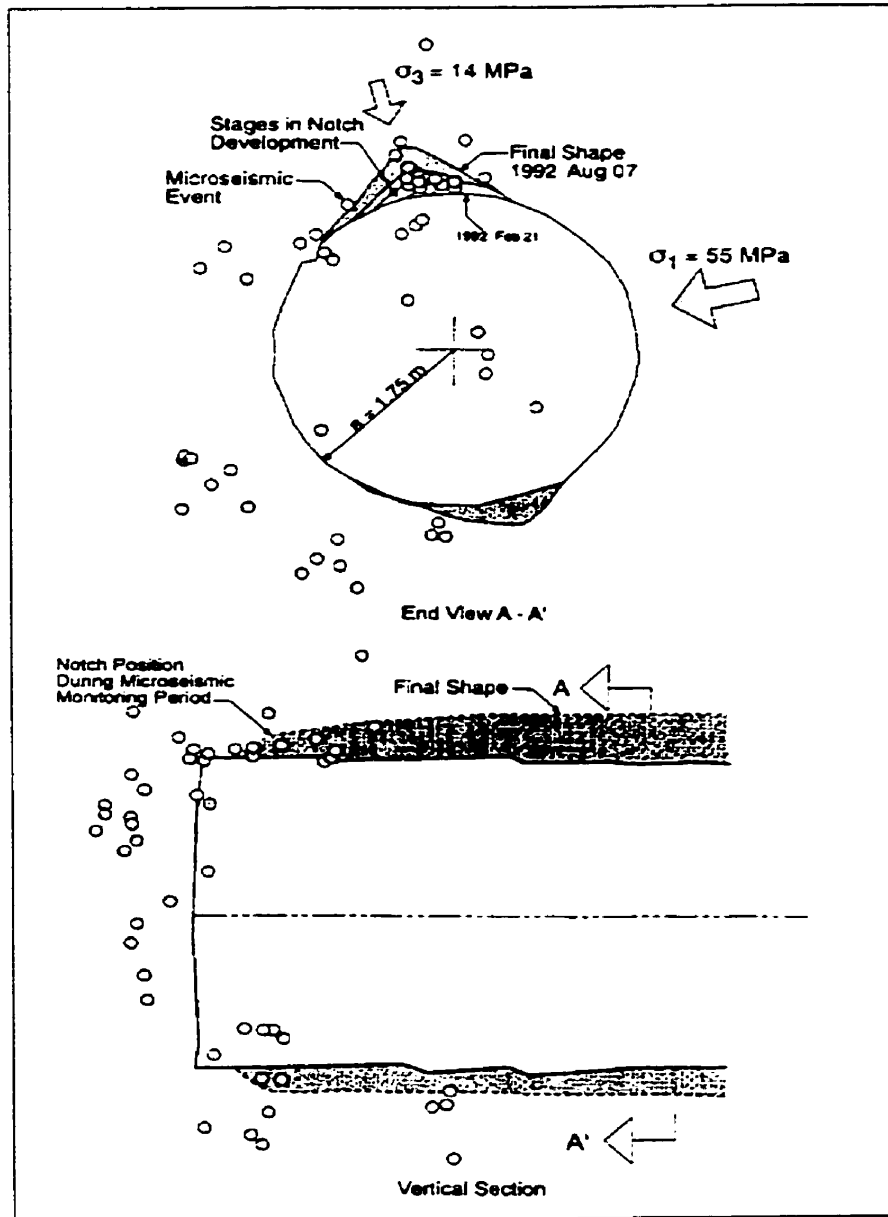


Figure 1.4 Location of microseismic events at the end of Round 13. Note the strong clustering of events in the roof where the notch will eventually develop. Also note the cracking occurring ahead of the face (after Martin 1993)

$$\frac{\sigma_c}{\sigma_{c50}} = \left(\frac{50}{d} \right)^{0.18}$$

where σ_{c50} is the uniaxial compressive strength of a specimen of 50 mm diameter, and d is the diameter of the specimen in mm.

(4) The Effect of Loading Rate on Strength

The effect of loading rate on the compressive strength of rock has been well studied. In general, the faster the rate of load application, the stronger the rock. For example, Sangha and Dhir (1972) tested a sandstone over loading rates ranging from 29 to 2.9×10^{-5} MPa/s. The results indicated that slow loading rates (<1 MPa/s) tend to reduce the strength to a level approaching about 0.8 of the maximum strength achieved. Similar results were reported by Jackson and Lau (1990) based on load-rate testing of Lac du Bonnet granite from the Underground Research Laboratory, Pinawa, Manitoba. The strength at low loading rates (0.075 to 0.00075 MPa/s) declined to about 0.8 of the strength obtained at the standard loading rate (0.75 MPa/s).

(5) Long-term Strength

In general, time-dependent properties are associated with rheological behaviour. From a practical point of view it is also useful to include the effects of weathering on long-term strength. In mining, time-dependent behaviour is typically associated with the softer rock types such as halite and potash, though it can occur in all types of rock mass. Time dependency can take various forms. One important form is a change in deformation with time at a constant stress or creep. A typical creep curve from laboratory testing is shown in Figure 1.5. It displays, in general, three characteristic sections known as the primary, secondary, and tertiary phases. Primary creep occurs for a short time after initial loading and is marked by a decelerating rate of strain. Secondary creep follows and, ideally, is

characterized by a steady rate of strain. After this stage comes tertiary creep, characterized by accelerating strain rates leading to failure.

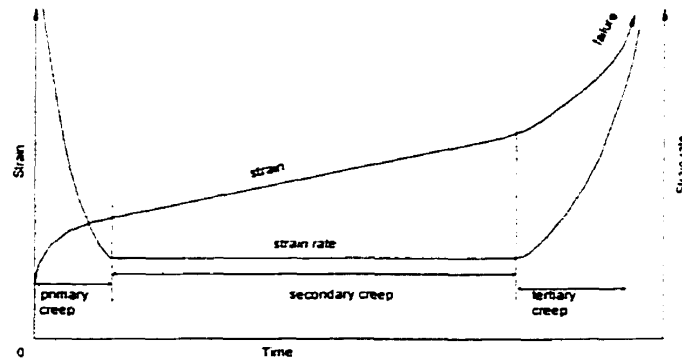


Figure 1.5 Ideal strain-time and strain rate-time curves

The long term strength of rock in creep can be compared to its short term strength (conventional uniaxial compressive strength). Wiid (1966) conducted creep tests on both wet and dry samples of dolerite. Two distinct behaviours were indicated. When the sample was dry and the applied axial stress was less than $0.8\sigma_c$, failure did not occur even after 360 hours of constant loading. When the sample was wet, failure was seen to occur at stress levels below $0.8\sigma_c$, suggesting that the presence of water aided the failure process. Uniaxial creep tests of potash were carried out by Duncan (1991) and a long term strength of approximately 95% of the conventional uniaxial compressive strength was reported.

It is important to note that creep behaviour is exceptionally sensitive to the test technique and procedure as well as test conditions such as humidity, temperature, and type of instrumentation. Thus, data from different investigators who use different techniques and test times yield results which in themselves are useful but not always comparable.

Chapter 2 Predicting Zone of Damage in Roofs of Esterhazy Potash Mines

The preceding section described a general method for predicting failure around underground excavations in massive rock. It shows that the accuracy of predicting damage zones is dependent on proper estimation of the virgin field stresses and the strength criterion of the rock mass. Therefore, an appropriate approach to prediction of the zone of damage around an underground opening must be based on a detailed study of the geological setting, geomechanical properties of the rock mass obtained from both *in situ* measurements and laboratory testing, and the specific procedures of excavation. The prediction of the zone of damage in roofs of an Esterhazy potash mine in this thesis, therefore, starts with a general description of potash mining in Esterhazy, followed by a summary of the mechanical properties of the salt rock and field observations of roof damage. An empirical failure criterion is then established and numerical modelling of the zone of damage is conducted and described in Chapter 3.

2.1 General Description of Potash Mines in Esterhazy, Saskatchewan

Potash was discovered in the southeastern part of Saskatchewan in 1943 during oil exploration drilling in two wells at a depth of about 2.29 km. With the development and introduction of gamma ray logging as a tool in oil exploration, potassium-bearing beds were indicated over a large area of southern Saskatchewan (Fuzesy 1982).

The first attempt to mine potash was made by the Western Potash Corp. in 1951 near Unity, 160 km west of Saskatoon. A shaft was sunk to approximately 550 m (1,804 ft) where water and sand of the Blairmore Formation were encountered and led to the project being abandoned in 1960 (Fuzesy 1982).

A New Mexico potash producer, Potash Co. of America, selected an area 8 km east of Saskatoon and began shaft sinking in 1956. In 1958 they began production from beds at 1,016 m (3333 ft) below surface. The first muriate of potash was shipped in March 1959.

The potash-bearing units in Saskatchewan occur in the Prairie Evaporite Formation that extends over 1000 miles from northernmost Alberta to North Dakota (Figure 2.1). The Formation rests conformably on the Winnipegosis Formation, is overlain

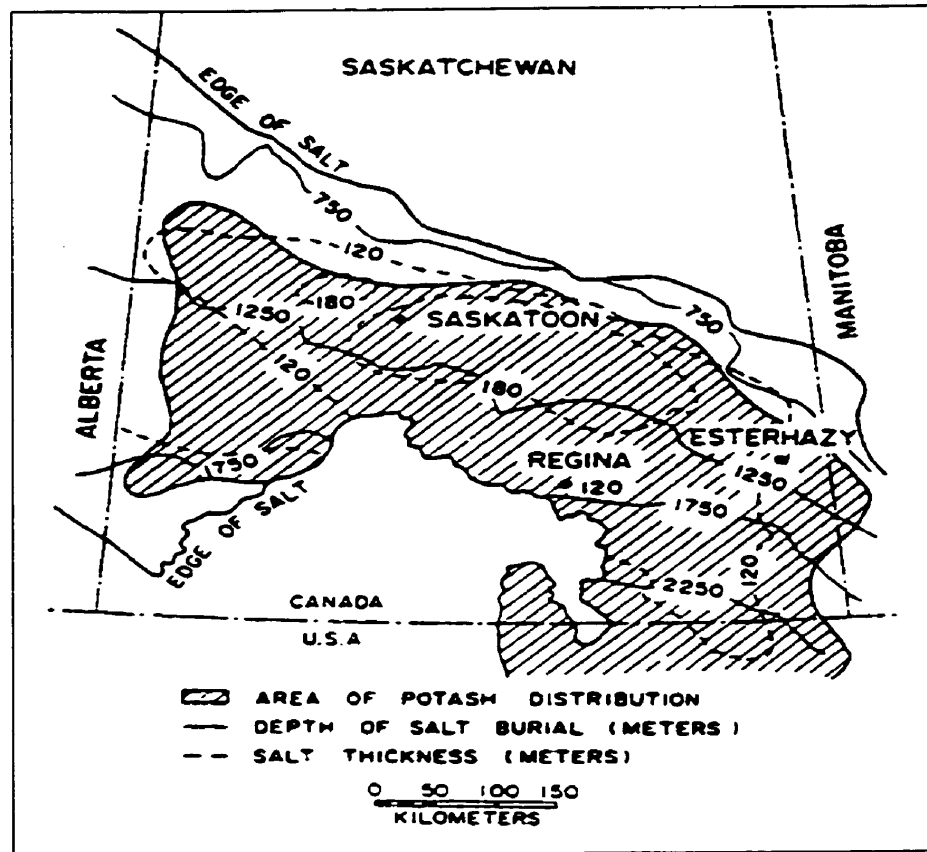


Figure 2.1 Isopach and depth of burial map of the Prairie Evaporite Formation in Elk Point Basin (after Jones and Prugger 1982)

disconformably by the Dawson Bay Formation, and is of Middle Devonian age. The Esterhazy mines, PCS (Potash Corp. of Saskatchewan) Rocanville and IMCC (the International Minerals and Chemical Corp.) K-1 and K-2 extend to approximately 960 m below the ground surface (Jones and Prugger, 1982). Several clay seams are encountered above the ore body. Detailed geological background can be found in Worsley and Fuzesy (1979) and Dunn (1982). Figure 2.2 is a stratigraphic column for the Esterhazy mining zones in PCS Rocanville (Jones and Prugger, 1982). The homogeneous, competent salt strata above and below the 2.5 m thick ore allows excavation of very wide rooms. These wide rooms, with closure of about 100 mm a year (decreasing exponentially with time), allow excellent local extraction ratios and the soft ore permits high rates of production by mining machines.

The potash ore is composed mainly of medium to coarse grained sylvite (KCl) and halite (NaCl) crystals with some carnallite ($\text{KMgCl}_3 \cdot 6\text{H}_2\text{O}$) and interstitial clay. The halite-dominated rock is the major component of the roof of the workings, and consists of halite (70%) and sylvite (25%) with clay making up the remaining 5% (Lajtai et al 1987). The halite rock is relatively coarse-grained with most crystals measuring in the 5 - 25 mm range. A few halite grains are larger than this and may reach 45 mm in size. The sylvite crystals are smaller, between 5 and 25 mm, and the clay pods are the smallest, less than 5 mm. The clay component occurs most commonly as interstitial pods and stringers. In addition, trace amounts of clay have been detected by X-ray diffraction of selected halite and sylvite crystals. This fraction is probably concentrated along grain boundaries.

2.2 Deformation and Fracture Around An Opening in Salt Strata

Deformation and fracture of salt rock under mining conditions has been investigated by many researchers (Baar 1971, Mackintosh 1975, Jones and Prugger 1982, Chen 1993). At approximately 1,100 m depth mine stresses are more or less hydrostatic, and estimated to be about 25 MPa according to the overburden depth. Cutting of a room under these high stress conditions results in immediate stress relief movement of the adjacent potash and salt into the room (Jones and Prugger, 1982). Vertical stresses are transferred into the

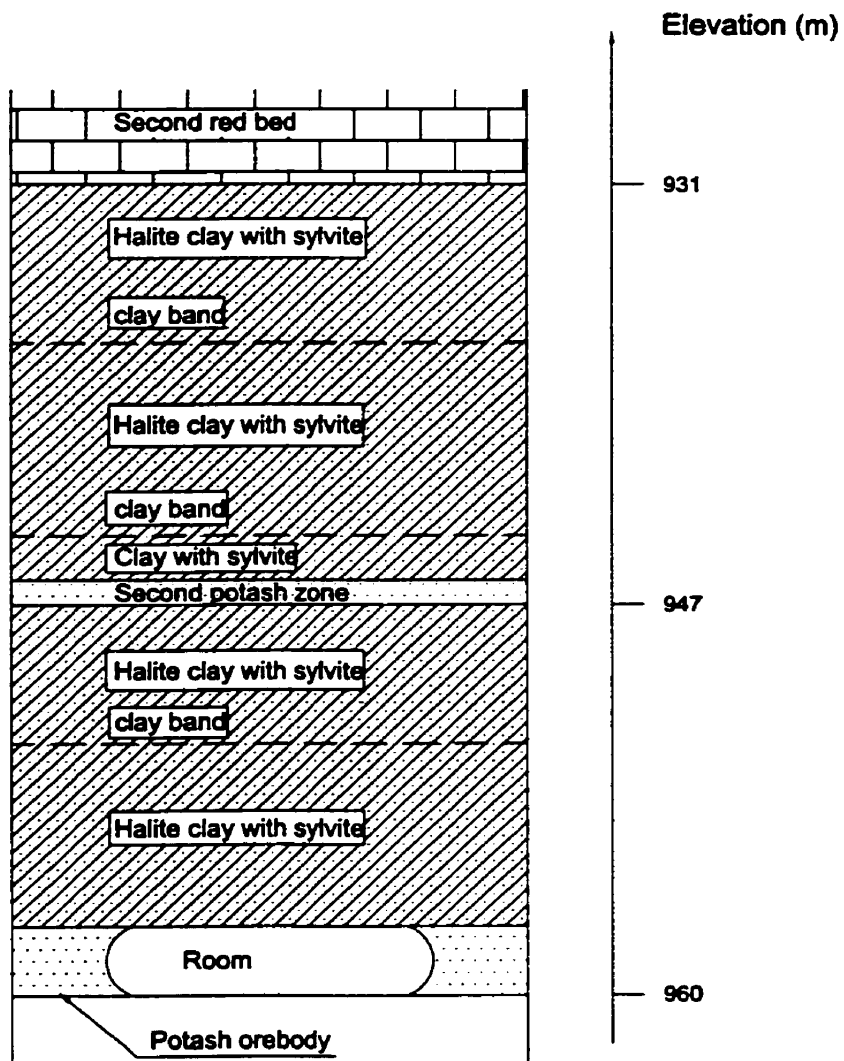


Figure 2.2 Immediate overhead stratigraphy of Esterhazy mining zones (after Jones and Prugger 1982)

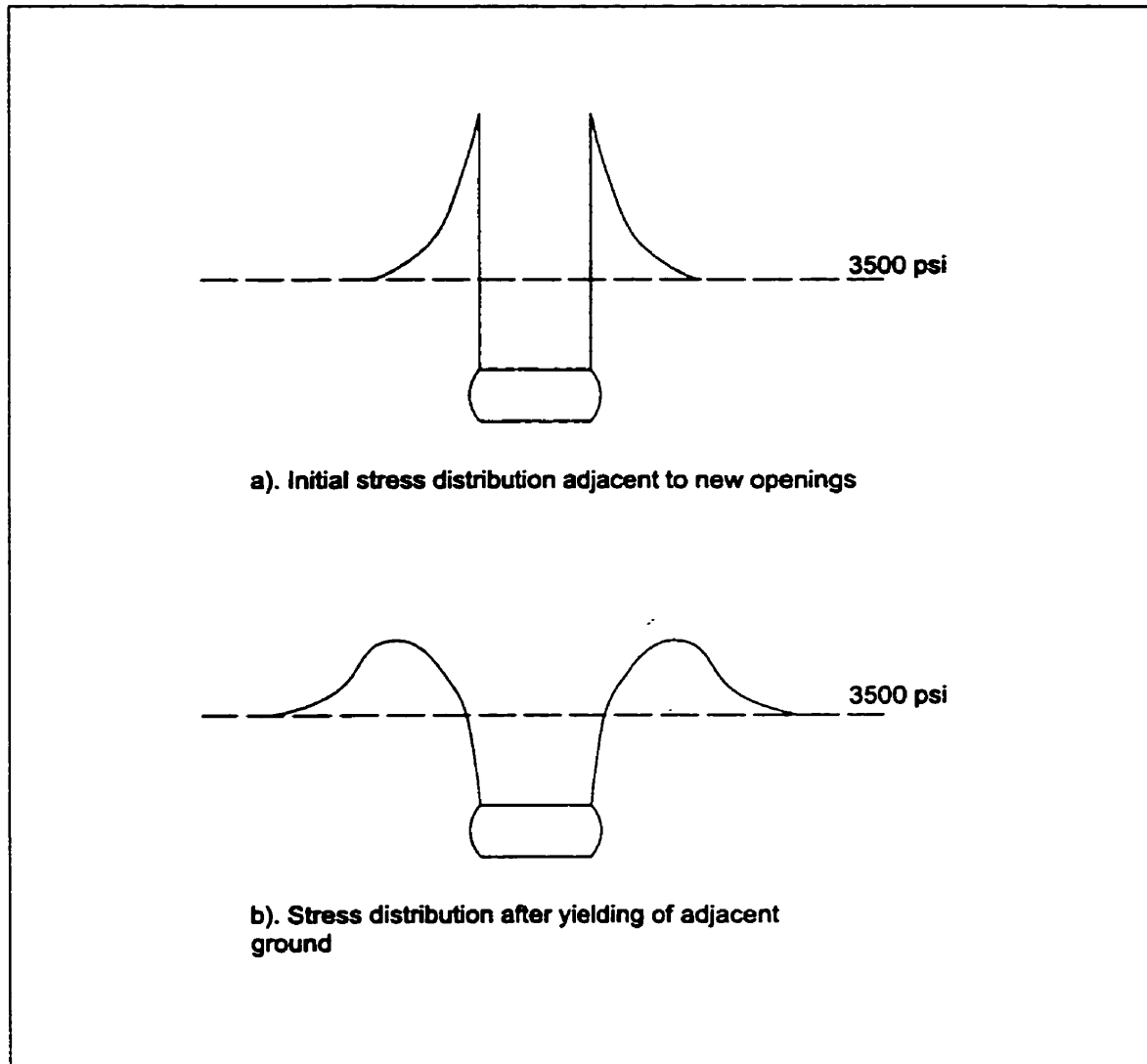


Figure 2.3 Vertical stress distribution around openings in a Cominco potash mine (after Mackintosh 1975)

abutments close to the opening, resulting in the vertical stress distribution as shown on Figure 2.3a. As the walls of the opening yield, the peak stresses transfer deeper into the wall and the near-wall stress gradient is reduced (Figure 2.3b). Horizontal stresses are transferred to the strata above and below the opening. The clay seams act as planes of weakness and if the roof layers are unable to withstand the increased loading, buckling or shear failure develops and transfers the stresses deeper into the “roof” and floor as shown in Figures 2.4a and 2.4b. In principle, failure of successive beds will continue until a competent salt bed thick enough to withstand the loading is encountered.

Failure by shear fracture or faulting is not the major deformation mechanism in potash under unconfined compressive loading i.e. near the opening. The major mechanism is similar to that for any other brittle rock - the buckling instability of slabs of rocks bounded by tensile fractures growing parallel to the compression axis (Peng and Johnson 1972).

In an attempt to study the deformation and fracture of salt rock around an underground opening under uniaxial compression, a layered physical model of a potash excavation was constructed by Carter (1992) and loaded in uniaxial compression. The fracture pattern evolved in the following manner. First, primary fractures formed in the salt rock back and in the potash floor at an applied stress range of 3.1 - 4.6 MPa (Figure 2.5a). The crack offset from the cavity centre may be due to nearness of the model boundary, the wide tensile stress distribution above the square opening, and variations in the strength of the crystals. Following the formation of the primary cracks, “remote” cracks formed at 5.5 MPa, starting in the salt back above the edge of the pillars (Figure 2.5b). The remote cracks above the pillars and the primary cracks in the floor extended slightly. At 8.7 MPa, remote cracks formed in the upper salt and limestone layers on both sides of the opening (Figure 2.5c). At the ultimate load of 13 MPa, further crack propagation occurred in the remote and sidewall regions, but the primary cracks remained stable. Eventually, the opening was severely damaged (Figure 2.5d).

This physical model verifies the predicted sequence of cracking to some degree. However, the stress conditions in the mine environment are more complex than the state of uniaxial compression in the physical model. The vertical primary cracks along the centreline of the opening in Carter’s model have never been observed in potash mines. In

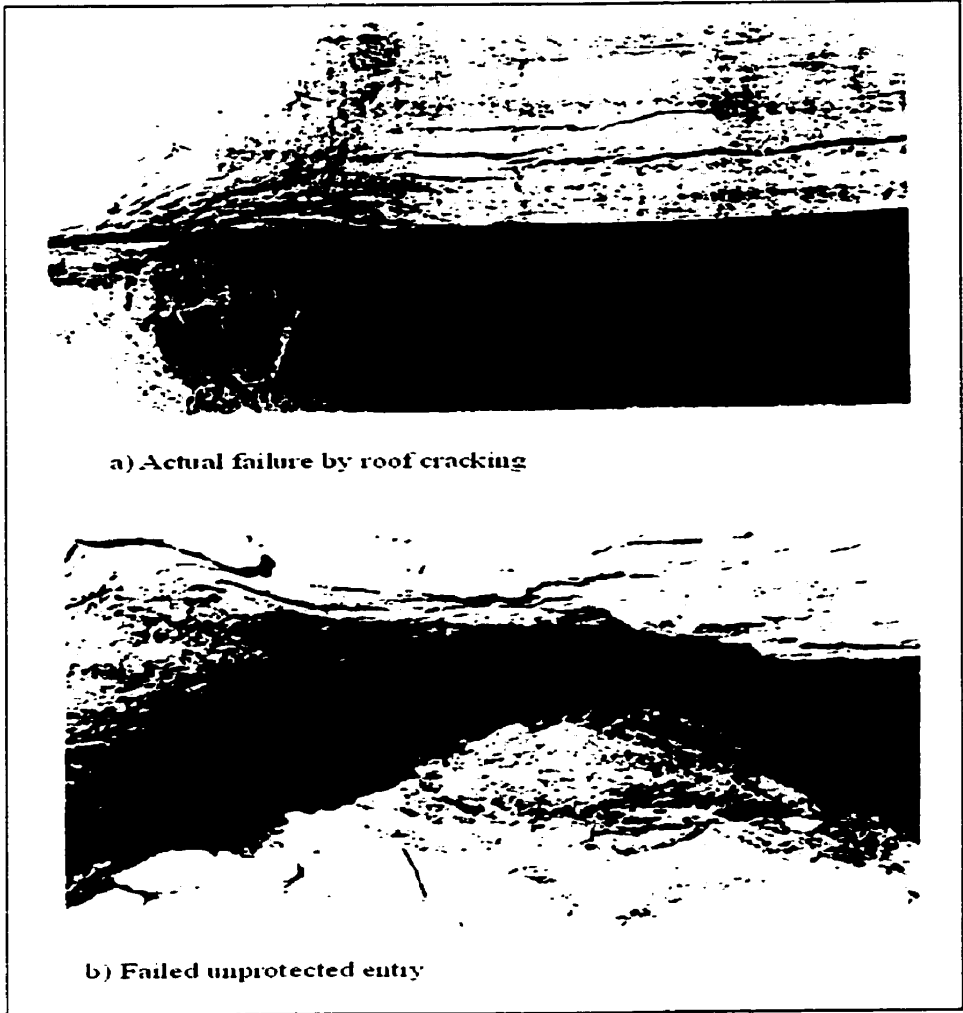


Figure 2.4 Failure examples (after Jones and Prugger 1982)

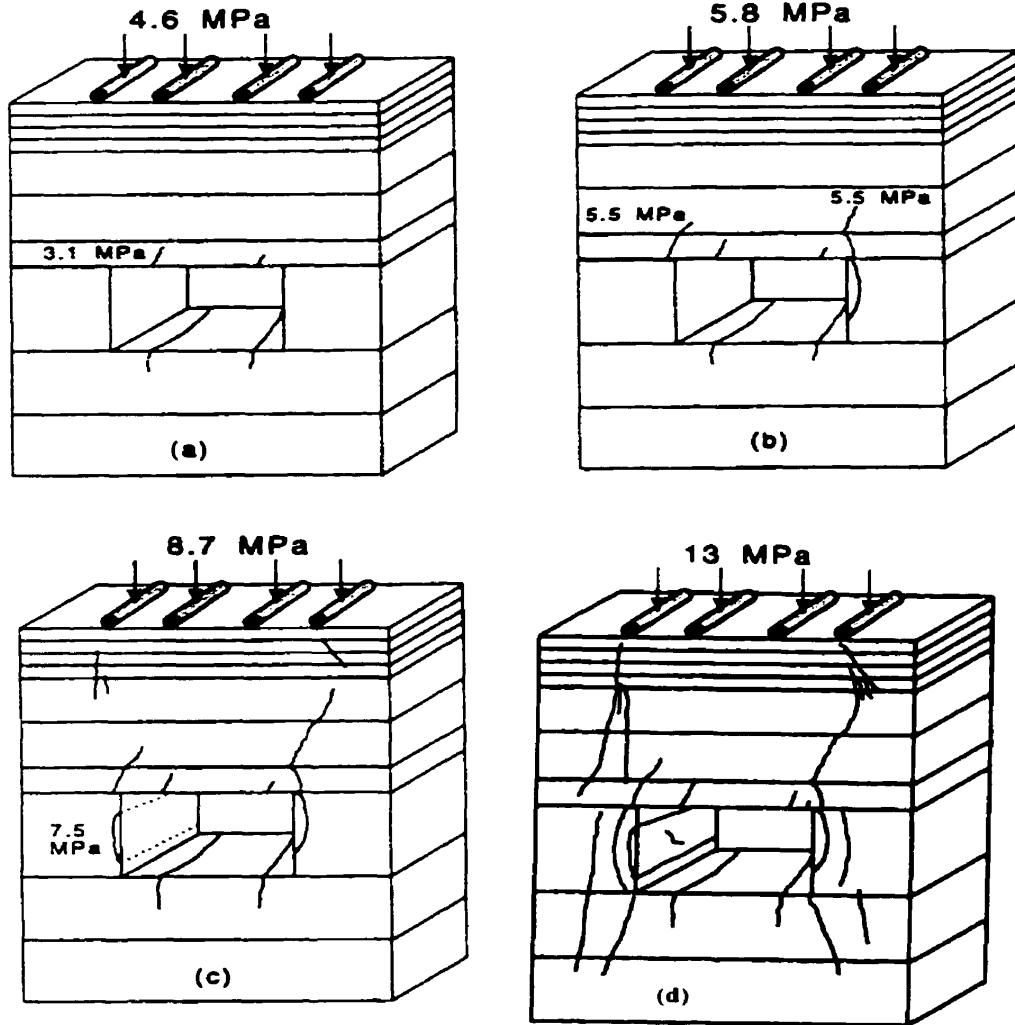


Figure 2.5 Physical modelling of crack propagation around an opening
(after Carter 1992)

a physical model of a single tabular opening under uniaxial compression with rigid lateral confinement (Napier and Ozbay, 1993), the initial cracking along the centreline of the opening seen in Carter's model was inhibited, while the extension cracks above the sidewalls initiated and propagated towards the centreline of the opening, eventually defining a dome-shaped failure zone above the rectangular opening.

In situ, the confining pressure increases with distance into the rock mass from the underground opening. It is expected that the application of a confining pressure would affect the mechanism of failure. It depresses the microcracking process, so there is the possibility that the failure mechanism changes from one characterized by "slabbing and buckling" at the surface to another in the interior of rock mass where a "shear mechanism" may operate and the failure mode is through faulting. Chen's (1993) studies of potash pillar mechanics in a mine near Saskatoon illustrate such a change in deformation and failure characteristics with distance into the pillars.

Fractures exist around the underground excavations of the IMC K1 and K2 potash mine at Esterhazy, Saskatchewan. Many of them are located in the yield pillars and in the walls as shallow spalling fractures, but there are also fractures in the roof and floor at some locations. Visual inspections of fractures in the roof are made with a borehole video borescope and provide a means of determining where cracking is occurring. The borescope also provides an opportunity to determine the geometry of the cracked region. A typical layout of monitoring boreholes is shown in Figure 2.6. Boreholes A and C were drilled 3.0 m from the edge of the pillar while borehole B was drilled at the centre of the opening.

Internal mapping of cracks in the roof of Room 1 is shown in Figure 2.7. The first open hairline crack to develop was at a depth of 0.32 m in borehole A. Hairline cracks formed at depths of 3.0 m to 3.5 m in the central borehole B two weeks later. Open cracks were observed in borehole B. No cracks were found in borehole C during the short period of inspection.

Figure 2.8 shows the crack development in Room 2. The first crack was found at a depth of 3.0 m in the central monitoring borehole B. Hairline cracks were observed at depths of 1.0 - 2.0m in borehole A and at 2.8 - 3.6 m in borehole B two weeks later. Cracks developed and propagated steadily thereafter. Open cracks were observed in

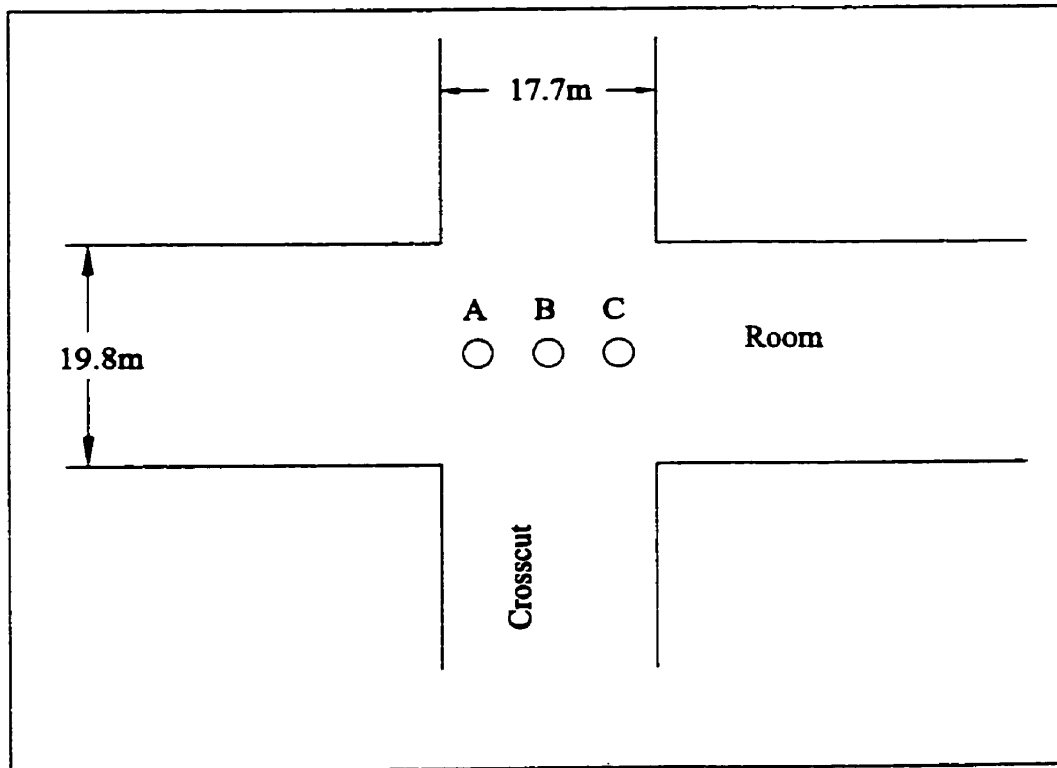


Figure 2.6 Typical layout of observation boreholes in the back of an opening at Esterhazy

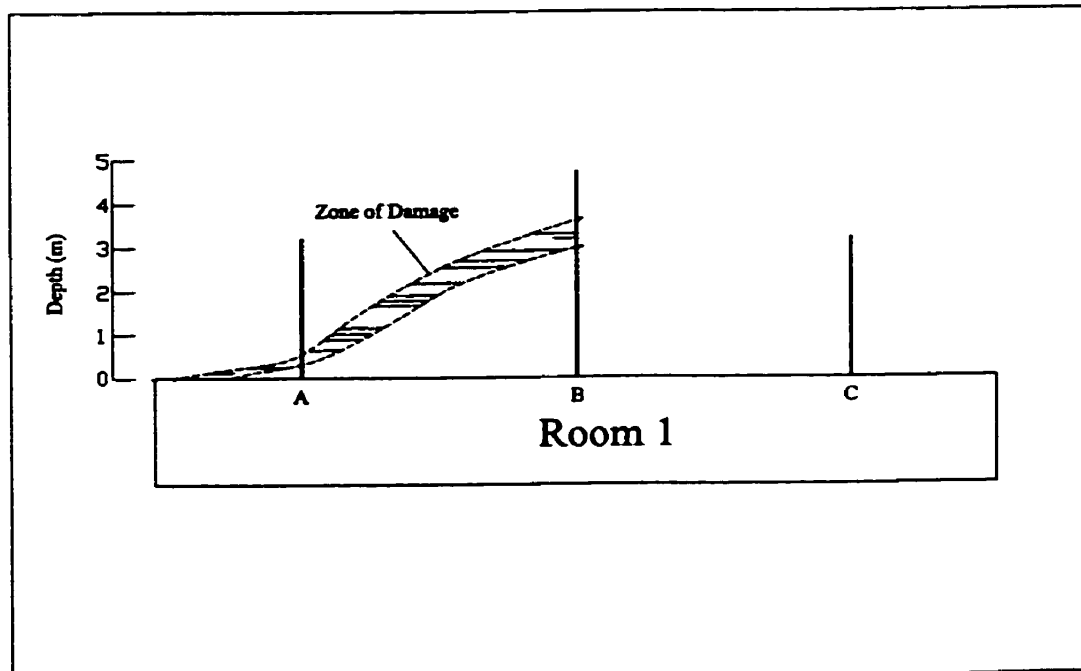


Figure 2.7 Mapping of cracking in the roof of Room 1 (The lines in the hatched zone of damage are not actual cracks)

boreholes A and B. No cracks were detected in borehole C during the two-month inspection.

The development and propagation of cracks in the roof of Room 3 was monitored for three weeks (Figure 2.9). Series of hairline cracks were formed at depths of 1.0m to 1.1m in the east-side borehole A, and two open cracks with widths up to 6 mm were observed at depths of 1.0m and 1.2m in the third week. Hairline cracks were observed at a depth of 3.0 m in the central borehole B. One hairline crack was observed at a depth of 1.2 m in the second week in the borehole C, and series of hairline cracks were encountered at depths from 1.2m to 2.3m in the third week.

Cracking was also monitored in observation boreholes along a travelway which was 2.5 m high and 16 m wide. Two monitoring boreholes were installed on the western roof of the travelway and 3 monitoring boreholes along the central line (Figure 2.10). Detailed mapping of cracks is shown in Figure 2.11. Cracks occurred at depths of approximately 0.3 m to 1.0 m in the west boreholes and at depths of 3.0 m to 3.8 m in the central boreholes. Open cracks were also observed in both the central and west boreholes.

It was also revealed that in the roof of these rooms, the rock mass damage was characterized by open fractures. These tension fractures were able to grow with elapse of time.

On the basis of these field observations, it can be concluded that damage zones with crack growth develop above the openings in a dome shape with the height of the apex being about 3.8 m.

2.3 Importance of Knowing Zone of Failure

An accurate prediction of the zone of failure around an underground opening is one of the most important components of underground design in mining as well as civil engineering tunneling. Where the safety of personnel is involved, the question of the stability of openings and the support needed to prevent collapse is of paramount importance. Investigations with respect to the stability of openings generally include the calculation of stress distributions around openings by theoretical analyses, deformation and convergence measurements, measurement/observation of fracture patterns and failure

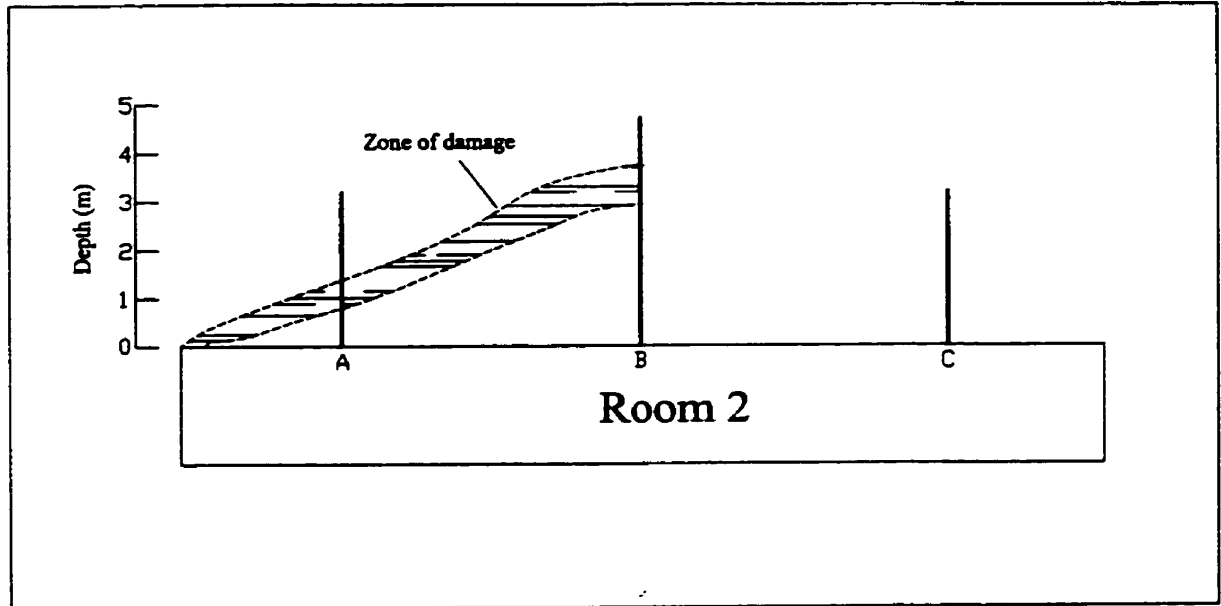


Figure 2.8 Mapping of cracking in the roof of Room 2 (The lines in the hatched zone of damage are not actual cracks)

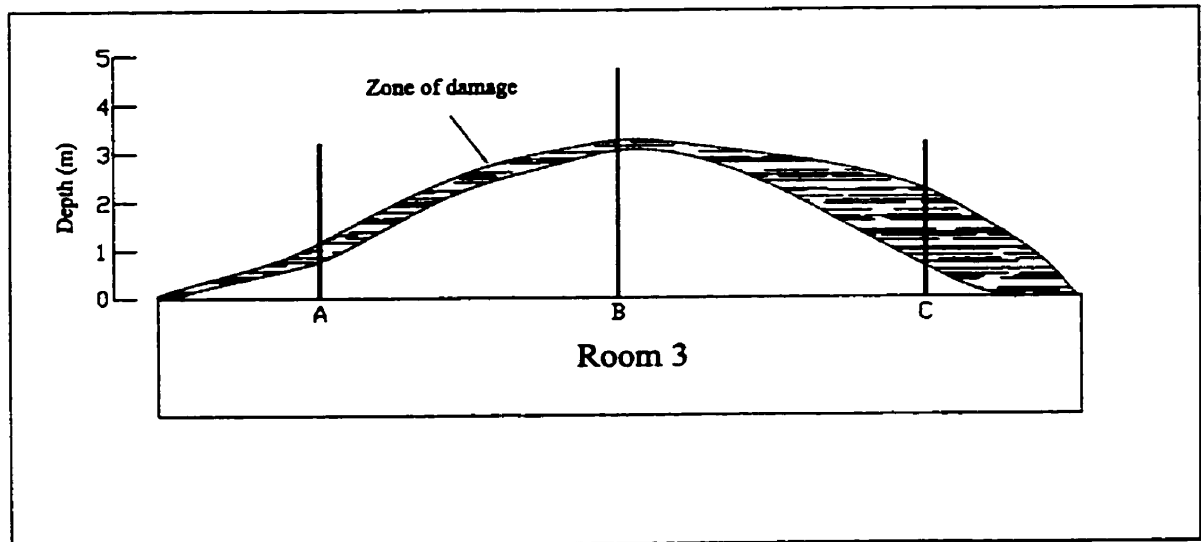


Figure 2.9 Mapping of cracking in the roof of Room 3 (The lines in the hatched zone of damage are not actual cracks)

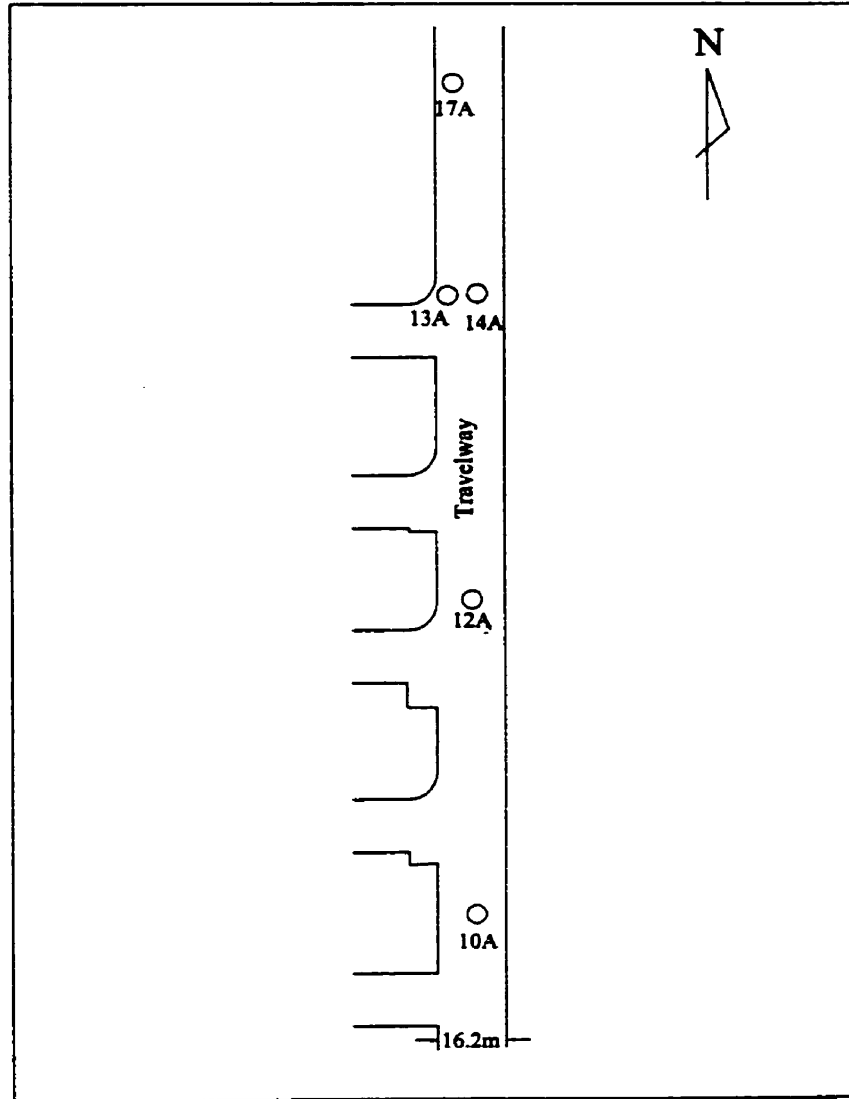


Figure 2.10 Layout of observation boreholes in the back of a travelway

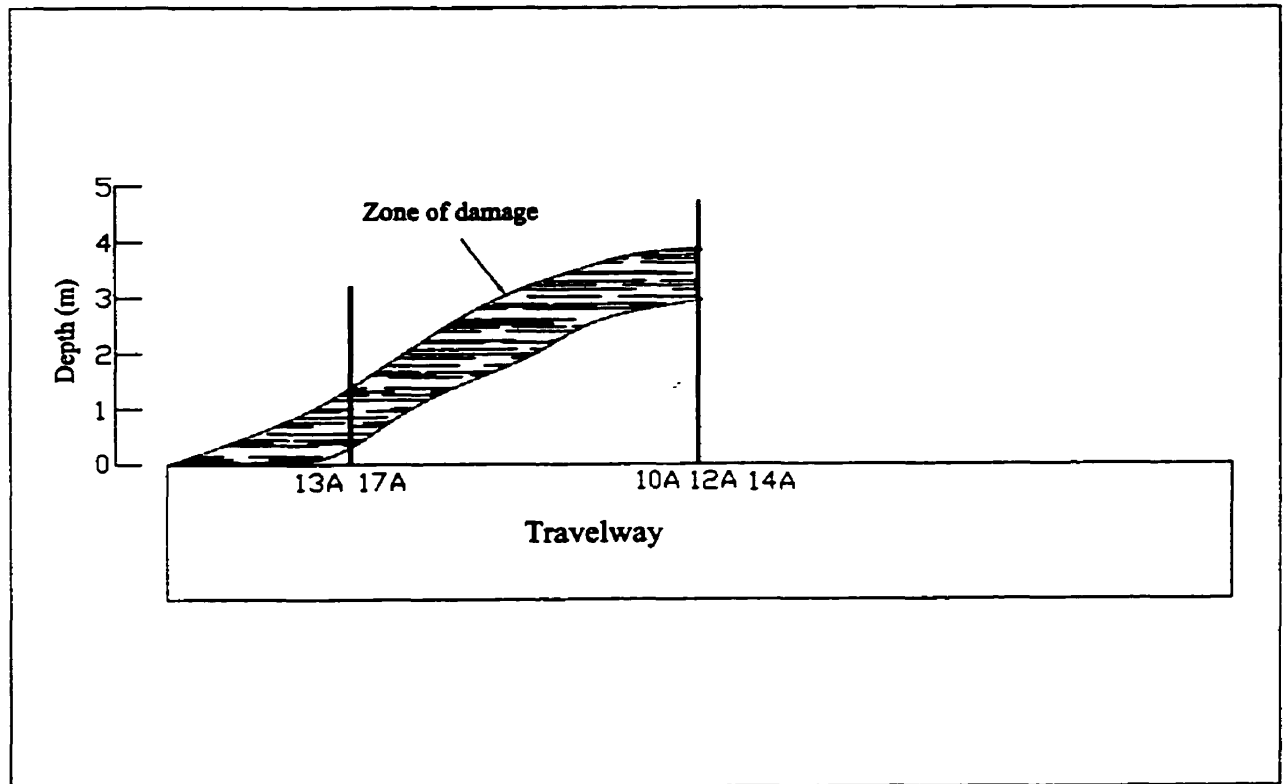


Figure 2.11 Mapping of cracking in the roof of Travelway (The lines in the hatched zone of damage are not actual cracks)

mechanisms based on field investigations, and physical modelling (Hoek and Brown 1980).

Knowledge of the extent of the failure zone is essential for support design. The main functions required of the tunnel support system can be deduced from a qualitative consideration of the process of fracturing. The initial stress raisers must be eliminated where possible and fracture propagation suppressed. The other function of support is to control the movement of the blocks, slabs or buckled fragments formed by fracture propagation around the periphery of the tunnel.

2.4 Roof Control Strategies in Saskatchewan Potash Mines

Stability of rooms in mining of Saskatchewan potash has been sought using a variety of methods based on stress-control principles. These methods can be grouped into 6 categories (Serata 1974) – stress relief technique, parallel room technique, time-control technique, compounded time-control technique, multiple-level technique, and large room technique. Among these, the stress relief technique has been used at the IMCC mine at Esterhazy and the Rocanville Division of the PCS. It is not intended to describe all these techniques in this thesis. For illustrative purposes, the stress relief technique is briefly described.

This method involves the following principles. Vertical normal stress peaks near the walls and horizontal normal stress peaks near the roof and the floor of an underground opening are postulated for elastic materials (Hoek and Brown 1980). A stress envelope around the mine opening, as shown in Figure 2.12, is then established by connecting these peaks (Baar 1971). It is assumed that creep is restricted to the interior of the theoretical stress envelope and that the envelope bounds the “effective” opening (Serata 1974).

Mining methods based on these principles have generated stability in most openings with relatively few rock mechanics problems (Duncan 1990). However, most of the mines have been producing for over 30 years and their underground workings now cover a considerable area with extraction ratios ranging from 30-55%. This has led to extensive

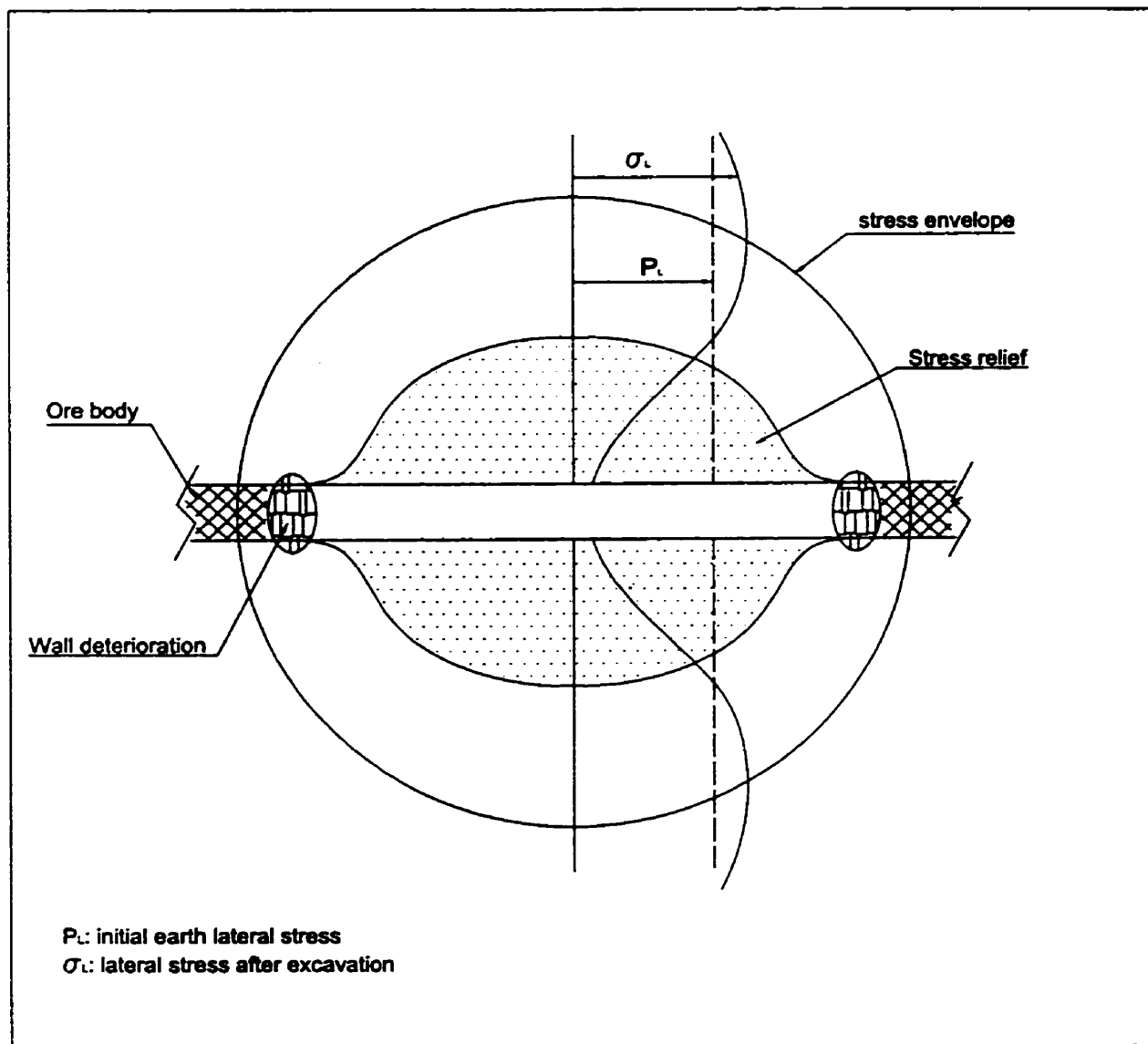


Figure 2.12 Formation of stress-relieved ground for stabilizing mine openings (after Serata 1974)

stress redistribution with stresses being transmitted higher into the roof strata. For example, the use of “yield pillars”, while providing in-room stability, may lead to stress redistributions that promote fractures in the overlying water-bearing limestone formation (Dawson Bay) and open pathways for water to enter the mine workings. Therefore, although it is essential to consider local failure around individual rooms it is also vital to consider the risk of failure on a wider scale than a single room.

2.5 The Properties of Salt Rock

In most literature, salt has been used as a general term to represent all evaporites such as potash, halite, anhydrite, and gypsum. They have many similar microstructural and deformational characteristics. A general knowledge of the behaviour of salt rock can be obtained from the well-documented laboratory studies of potash specimens conducted in the Geological Engineering Department of the University of Manitoba.

Uniaxial Compressive Strength

A typical stress-strain curve under uniaxial compressive testing of Rocanville potash is shown in Figure 2.13, and can be divided into three parts by two deflection points. The first deflection point on the stress-strain curves of potash (at about 5-8Mpa) occurs on both the lateral and the axial stress-strain curves. It represents a yield point where the predominantly “elastic” behaviour changes into “ductile” behaviour. The crack initiation point is probably located between 8 and 12 MPa where the trend of volumetric strain shows the first sign of reversal toward dilatancy. Between the yield and crack initiation points, ductile deformation takes place. A brittle mechanism seems to dominate the deformation process during the late phase of deformation. At stress levels represented by the broad top of the stress-volumetric-strain curve some of the microcracks grow to a size large enough to be observed by the naked eye. They follow suitably orientated cleavage planes inside crystals and grain boundaries between crystals. At peak strength and past the peak strength to about one-third of the way down the falling leg of the stress-strain

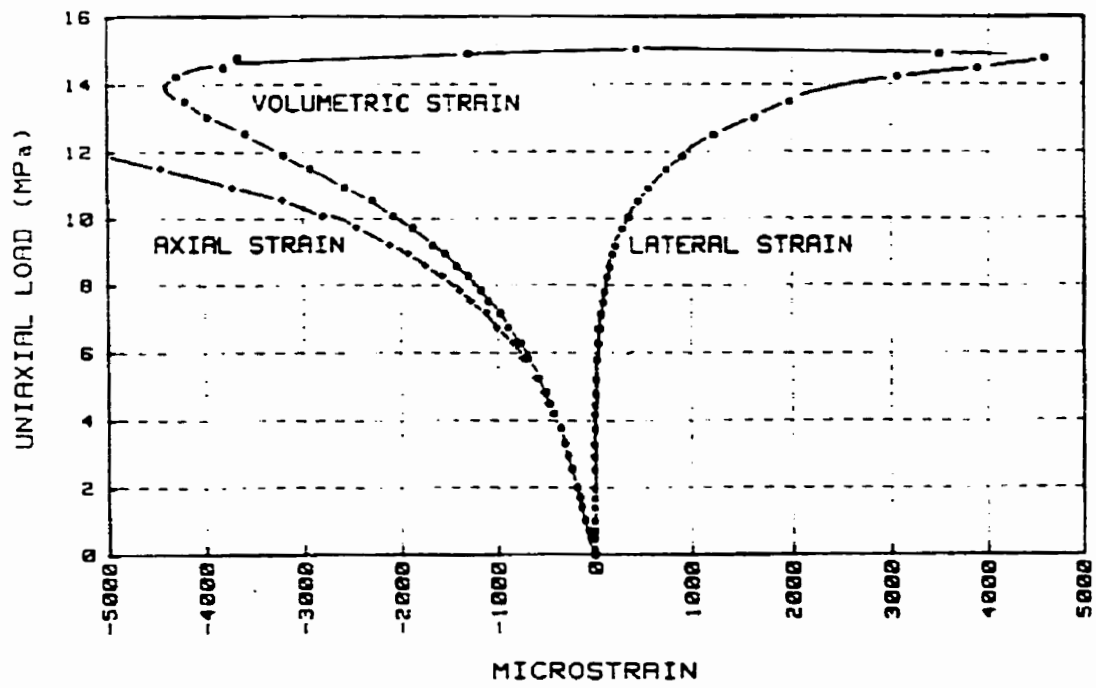


Figure 2.13 Stress-strain response of potash measured from axial and lateral clip-on gauges (after Duncan 1990)

curve, the tensile cracks grow and dilate without any sign of interaction between them. Only at lower stress levels can one see the buckling instability and the formation of the occasional shear zone (Lajtai and Duncan 1988). The “shear zone” is produced by the rotation of cleavage-bound slabs and not through simple translational or planar sliding.

The ultimate strengths from conventional uniaxial compression tests for the Esterhazy potash at a relatively fast constant strain rate (3-5 $\mu\epsilon/s$) vary between 15 and 18 MPa, which is lower than the strengths of 24 to 26 MPa of the neighboring Patience Lake potash. It is speculated that the large grain size relative to the specimen size of the Esterhazy potash has a substantial effect in reducing the strength (Duncan, 1990).

Triaxial Compressive Strength

Triaxial compressive tests at various confining pressures (0.5, 2, 5, 7 and 10 MPa) were conducted on the Patience Lake potash by Duncan (1990). A summary illustration of the principal stress relationships at the ductile yield point, point of volumetric strain reversal, and ultimate strength for a series of tests is shown in (Figure 2.14). From this plot it is possible to characterize three states of deformation for potash:

- 1) An initial state dominated by a large elastic component of deformation extending from the onset of deviatoric loading to the ductile yield stress line.
- 2) A pre-dilational state of deformation extending from the ductile yield stress line to the volumetric strain reversal line during which non-dilational structural mechanisms and solid body plastic mechanisms dominate the overall deformation of the potash.
- 3) A dilational state of deformation extending from the volume reversal line to the peak strength envelope during which structural dilation and brittle fracture begin to dominate all other mechanisms.

The peak strength envelope at confining pressures between 0 and 10 MPa and at a strain rate of 1.75 $\mu\epsilon/s$ indicates that the strength is more sensitive to confining pressure between the range 0-5 MPa than confining pressures above this. In order to

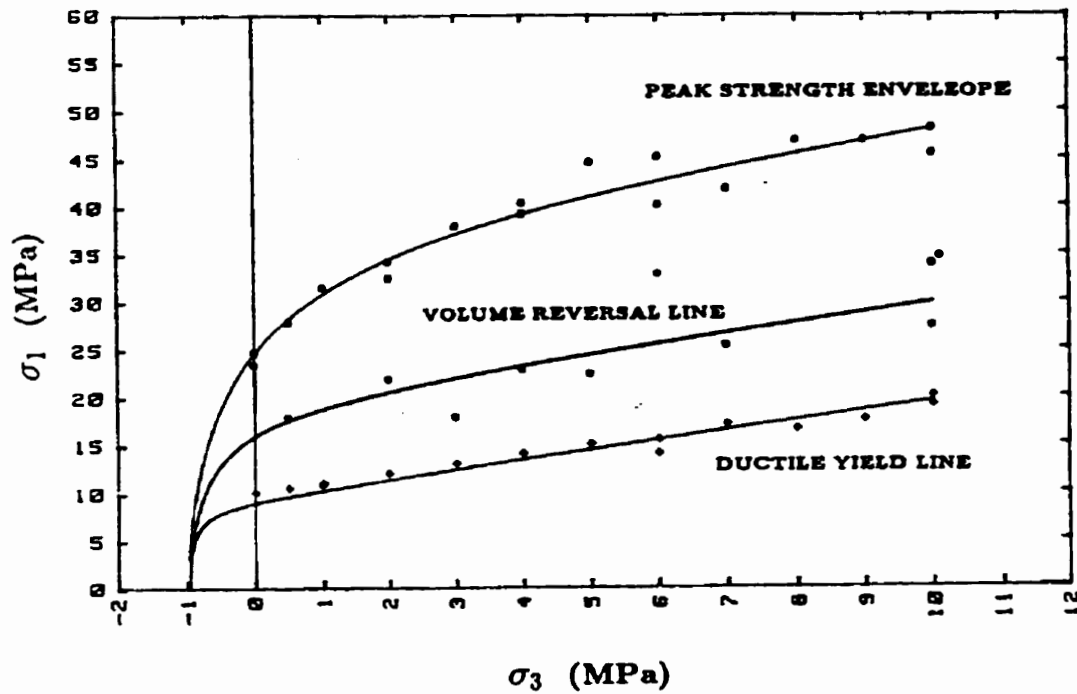


Figure 2.14 Summary illustration of the principal stress relationship at the ductile yield point, point of volume reversal and ultimate strength for Patience Lake potash tested at a strain rate of $1.75 \mu\text{E/s}$ (after Duncan 1990)

mathematically fit the strength versus confining pressure relationship, Duncan (1990) developed an empirical failure criterion based on the Hoek and Brown criterion:

$$\sigma_{1f} = \sigma_3 + (m_1 \sigma_c \sigma_3 + s \sigma_c^2)^{0.5} \left(1 + \frac{m_2 \sigma_3}{\sigma_c}\right)^{-0.5}$$

where σ_{1f} is the major principal stress at failure, σ_3 is the minor principal stress, σ_c is the uniaxial compressive strength, and constants $m_1 = 29.6166$, $m_2 = 11.65$, and $s = 1$.

The new criterion accounts for the lower sensitivity of strength to confining pressure at higher confining pressures, as well as the very low tensile strength of potash. By “anchoring” the uniaxial compressive and direct tensile strengths, the new criterion is able to describe the principal stress relationship at failure within the whole stress region.

In order to simulate more realistic loading paths induced by underground rock excavation, Chen (1993) conducted reverse loading triaxial tests. In the tests, each specimen was loaded hydrostatically to an isotropic compressive stress state of 30 MPa, a value slightly higher than the *in situ* stress in Saskatchewan potash mines. The specimens were compressed for a period of 24 hours. A deviatoric stress was then applied by unloading the confining pressure at a constant rate through time while keeping the axial stress at the original level (30MPa). The deviatoric stress versus axial, lateral and volumetric strain relationships are shown in Figure 2.15. The general characteristics of the stress-strain curves in reverse loading tests are similar to those obtained in conventional compression tests. With faster constant stress rates (60.0 MPa/h), the deviatoric stress at the point of volumetric reversal occurred at approximately 12 MPa, much lower than 28 MPa for the two slower stress rates (1.25-0.06 MPa/h). It is probable that the early low stress reversal of the volumetric strain curve is produced through various mechanisms of structural dilation such as grain boundary de-bonding, dilation, sliding and yielding at grain boundaries, cleavage planes, pre-existing discontinuities and in the insoluble component. These mechanisms are weak initially, but sufficient to reverse the volumetric deformation to dilation. Damage that ultimately leads to failure of potash requires the progressive fracture of the polycrystalline matrix (crystals) and evolves at higher deviatoric stresses, as indicated by the late-stage high-stress reversal of

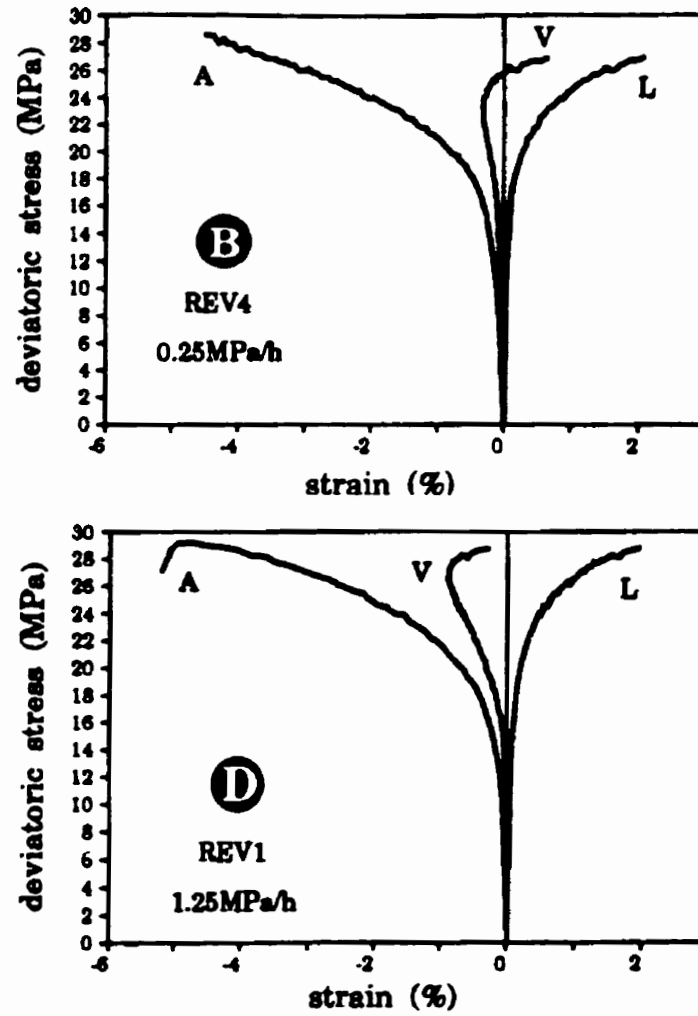


Figure 2.15 Stress-strain response under unloading triaxial tests (after Chen 1993)
(Symbols A, L, and V denote axial, lateral and volumetric strain respectively)

the volumetric strain curve under slower stress rates. It is concluded from the tests at these lower rates that brittle fracture was the cause of failure.

Long-term Strength

One way to interpret the long-term strength of rock is to consider the mobilized strength when the rock fails at an extremely slow strain rate. This long-term strength of salt rock was studied by uniaxially compressing intact salt rock to failure at an extremely slow constant strain rate (Duncan, 1990). Two Esterhazy potash samples were deformed at near constant strain rates in the range of 10^{-12} $\mu\epsilon/s$. Specimen CEA failed after 1221 days at a stress of 17.35 MPa and specimen CEB failed after 1036 days at a uniaxial compressive stress of 15 MPa. The average strength from the long term creep tests was 16 MPa, which is approximately 89% of the conventional uniaxial strength in the laboratory at a strain rate of 3 – 5 $\mu\epsilon/s$. Potash mining is not so slow as to induce these extremely slow strain rates in the rock in the immediate vicinity of an opening. For design purposes, the strength of salt rock could be adopted from the conventional laboratory uniaxial tests only after careful consideration of the field conditions and the strain rates induced by the mining processes at the mine.

Damage Criteria and Acoustic Emission Response

Acoustic emissions (AE) in polycrystalline rock originate as a result of dislocations, grain boundary movements, or initiation and propagation of fractures through and between mineral grains. The sudden release of stored elastic strain energy accompanying these processes generates an elastic stress wave which travels from the point of origin within the material to a boundary where it may be recorded as an acoustic event by a transducer (Hardy and Mowrey, 1976). Acoustic emission techniques have been used with some success in identifying microfracturing in brittle materials. Scholz (1968) found that characteristic AE patterns in rock correlated closely with stress-strain behaviour.

Examination of the acoustic emission response for Saskatchewan potash indicates that the onset of significant cracking begins at about 6 MPa or 0.25 σ_c (Eberhardt 1998)

(Figure 2.16), where sample deformation departs from linearity. This point was subsequently interpreted as being the crack initiation threshold (σ_{ci}). After the crack initiation point, stable crack propagation and coalescence continued until volumetric strain reversal occurred, thereby marking the crack damage threshold (Figure 2.17). The crack damage threshold, σ_{cd} , also marked an interval where the AE event count reached a relatively constant level. Figure 2.16 reveals that throughout stable crack propagation the number of detected events continuously increases. Once unstable crack propagation began (i.e. after the crack damage threshold is reached), the number of events peaked and remained constant until sample failure. The crack damage threshold, σ_{cd} , for the potash appeared at about 12 MPa or 53% of peak strength. By comparison to the crack damage threshold for typical brittle rock such as granite, which occurs at a higher percentage of peak strength, it seems that the ductile nature of the potash allows samples to slowly “yield” and sustain increasing load throughout a longer period of unstable crack propagation.

2.6 Selection of Damage Criteria for Numerical Modelling

Fracturing or stress-induced cracking of the intact rock produces damage around openings in massive rock. The damage may be subdivided into two zones: the microdamage zone and the macrodamage zone. The first zone represents crack (damage) initiation in the intact rock at a microscopic scale; the second represents zones where cracks (damage) propagate in an unstable manner until ultimate failure. These two zones are defined by three critical points: the damage initiation threshold (stable crack growth), the damage threshold, and failure. These characteristic parameters have been well documented for brittle rocks (Bieniawski 1967, Carter 1992, Martin 1993, Eberhardt 1998).

Castro (1996) assumed that rock mass damage occurs where the induced deviatoric stress exceeds the stress level for the onset of stable crack growth as measured in uniaxial compression tests of the intact rock, and that the discontinuities do not have a significant influence due to the high stress environment. A similar procedure is used in this thesis to predict roof damage in Saskatchewan potash mines. The following sections discuss the

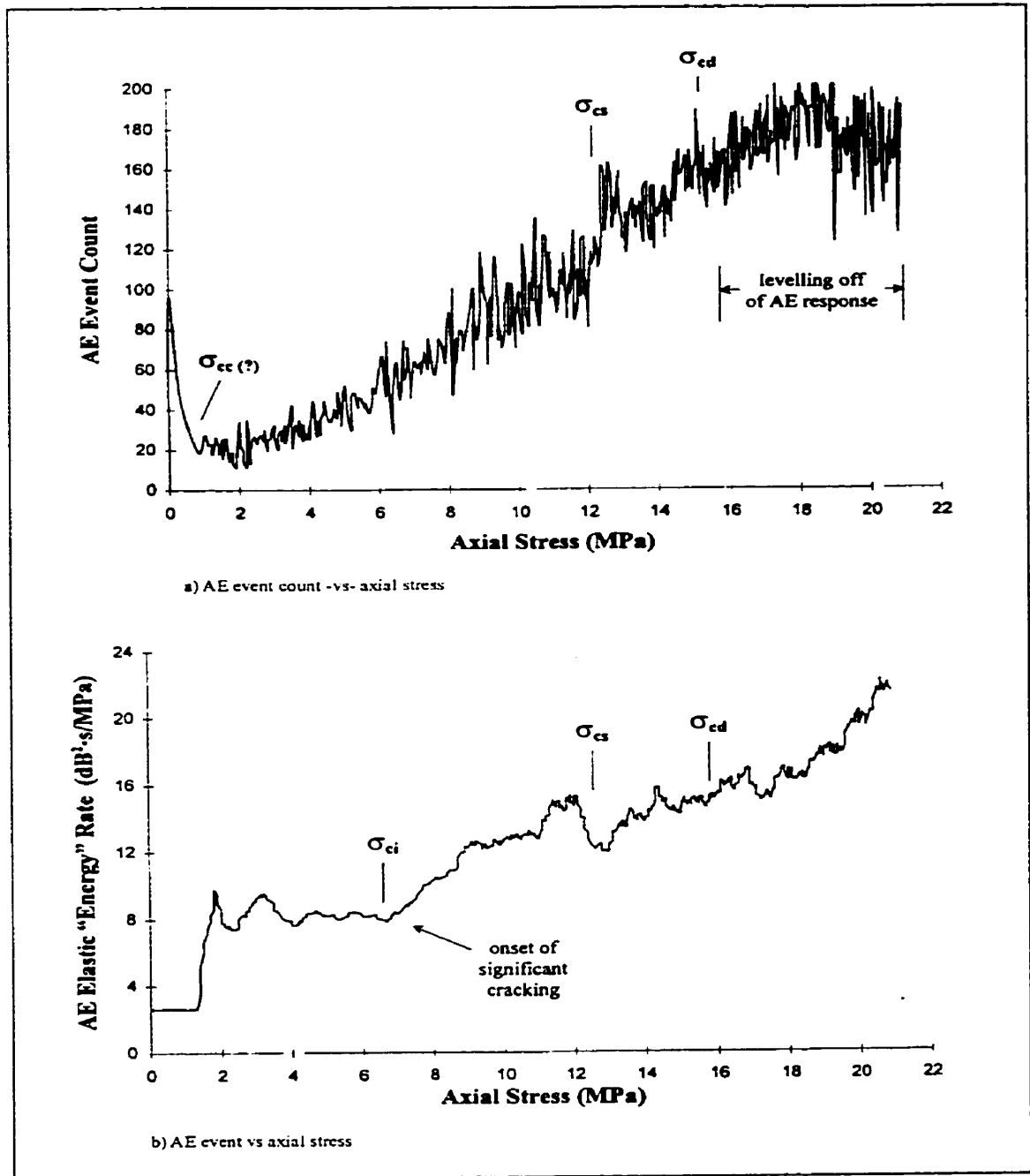


Figure 2.16 Plot of the AE event count and the AE event elastic impulse "energy" rate vs axial stress for a Saskatchewan sample (after Eberhardt 1998)

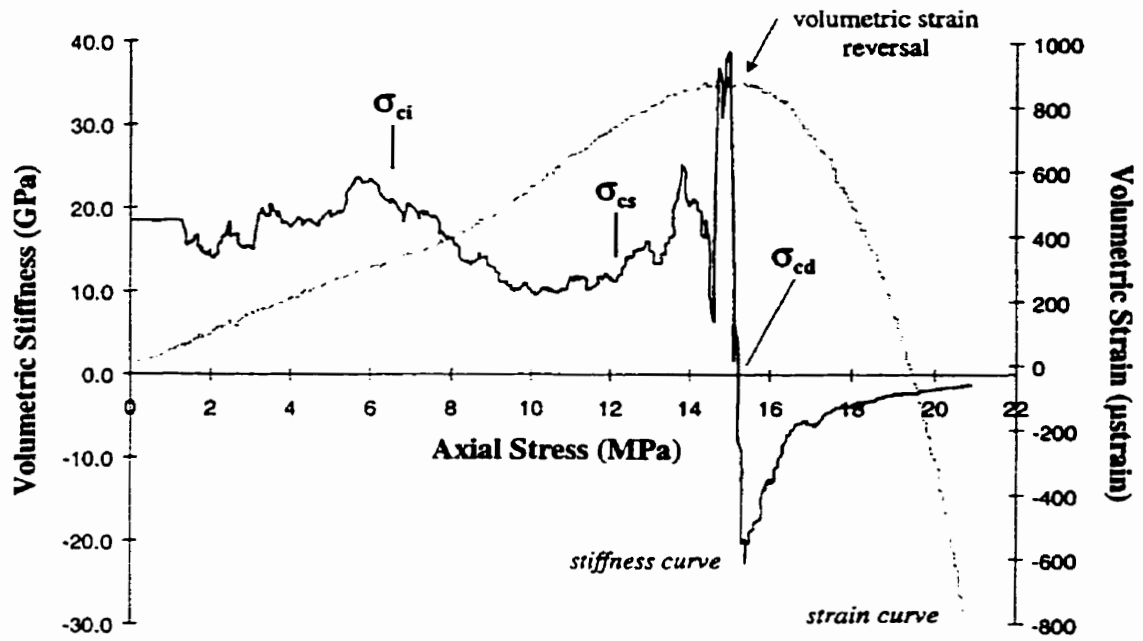


Figure 2.17 Plots of volumetric strain and stiffness vs axial stress for a Saskatchewan potash sample (after Eberhardt 1998)

choice of a damage criteria for salt rock for use in the numerical modelling described in subsequent chapter.

In the potash mines at Esterhazy most damage occurs near the excavations where little confining pressure exists. The uniaxial compression test or the triaxial compression test with low confining pressure should simulate such conditions in a reasonable manner.

Damage Initiation Threshold (σ_{DI})

Damage of rock starts with crack initiation. For a heterogeneous rock such as the coarse-grained salt rock at Esterhazy, there may be more than one crack initiation point (Duncan 1990). The crack initiation points for the crystals of halite and sylvite, the clay pods, and the grain boundaries are different (Figure 2.18). As would be expected, crystals are the stiffest elements and the grain boundaries are the least stiff. Grain boundaries account for most of the observed strain and for most of the dilation in potash rock. However, no significant crack propagation occurs until cracking of the crystals of halite and sylvite is initiated.

Examination of the acoustic emission response indicates that the onset of significant cracking begins at approximately 6 MPa, or $0.25\sigma_c$ (Eberhardt 1998) (Figure 2.16). The empirical damage initiation threshold for the salt rock mass, therefore, could be expressed as:

$$\sigma_1 - \sigma_3 = \sigma_{DI} \quad (1)$$

where σ_{DI} is taken as 7.5MPa, i.e. 0.25 uniaxial compressive strength (σ_c).

Crack initiation establishes the stress level at which some damage occurs. However, crack initiation without crack propagation is of no practical significance as the cracks are not continuous. The limiting stress at which unstable cracking is established in intact rock is of greater practical significance. Above it, failure is only a matter of time.

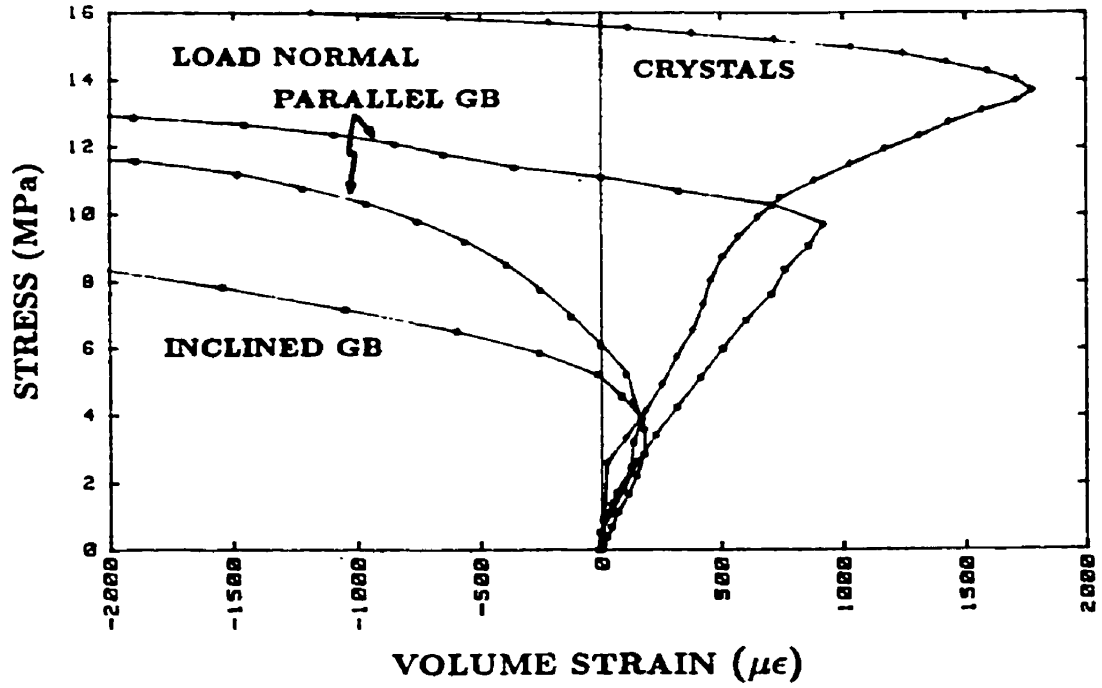


Figure 2.18 Stress-volume strain response of a Saskatchewan potash sample (after Duncan 1990)

Damage Growth Threshold (σ_{DG})

Determination of the damage growth stress threshold (σ_{DG}) is relatively straightforward from the stress-strain curves in the uniaxial compression tests. When the lateral strain surpasses the axial strain as the dominant component in the volumetric strain, the slope of the volumetric strain curve changes from a positive to a negative value, thus signifying volumetric strain reversal and the crack damage threshold.

Based on acoustic emission studies (Eberhardt 1998), after the damage initiation threshold is exceeded, stable crack propagation and coalescence occurs and continues until volumetric strain reversal. This point marks the crack damage threshold (Figure 2.17). The crack damage threshold for potash appears at 53% of peak strength.

From the analyses of the stress-strain relationship, acoustic emission response and the field observations in potash mines, an empirical damage growth threshold is expressed as follows:

$$\sigma_1 - \sigma_3 = \sigma_{DG} \quad (2)$$

where σ_{DG} is taken as 18MPa, i.e. 0.6 uniaxial compressive strength (σ_c).

The Critical Value for Failure (σ_f)

After the damage growth threshold is exceeded, unstable crack growth occurs and continues to the point where the numerous microcracks have coalesced and the rock mass can no longer sustain an increase in load. Ultimate failure then occurs. An empirical failure threshold is, therefore, expressed as follow:

$$\sigma_1 - \sigma_3 = \sigma_f \quad (3)$$

where σ_f is taken as 24 MPa, i.e. 0.8 short-term uniaxial compressive strength (σ_c), where 0.8 is a factor used to account for long-term strength (see Section 1.3).

The selection of the above damage criteria is primarily based on the laboratory uniaxial and triaxial compressive testing of potash samples near Esterhazy. However, these damage criteria are not solely location specific. As the stress-strain relationships of Saskatchewan potash samples delineate similar patterns, the proposed damage criteria could be applied to other mine sites.

The proposed Esterhazy empirical damage criteria can be derived from the Hoek-Brown criterion:

$$\sigma_1 = \sigma_3 + \sqrt{m\sigma_c\sigma_3 + s\sigma_c^2} \quad (4)$$

where σ_1 and σ_3 are the maximum and minimum principal stresses at failure respectively, and m and s are empirical constants. By assuming $m = 0$ and re-arranging the above formulae,

$$\sigma_1 - \sigma_3 = \sqrt{s}\sigma_c \quad (5)$$

which takes the same form as the proposed empirical damage criteria. For the Hoek-Brown failure criteria, it is implicitly assumed that the constants s and m are related to the cohesive and frictional strength components respectively. By ignoring the frictional strength by letting $m = 0$, the proposed empirical damage criterion, therefore, implies that the frictional strength component is not mobilized. It has been shown, in support of this implication, that the brittle failure process is controlled by the cohesion of the rock mass (Stacey 1981). Martin and Chandler (1994) showed, on the basis of damage-controlled laboratory tests, that the initiation and propagation of cracks as load increases reduces the intrinsic cohesion of the intact rock and that this reduction in cohesion occurs before the peak strength of the sample is reached.

The next chapter explores the application of Equations (2) and (3) in numerical simulations of the development of fracture and failure in a wide room in salt rock and compares the predictions with the crack measurements made in the mine with a borehole viewer.

Chapter 3 Numerical Simulation of the Damage Zones Using Phase² and InSight^{2D}

In this section two finite element programs are used to simulate the development of zones of damage and failure in the roofs of mining panels in the potash mines at Esterhazy, Saskatchewan. Phase² was selected because of its widespread availability and user friendliness. InSight^{2D} was adopted for this study because it is capable of modelling fracture initiation and propagation.

3.1 Numerical Modelling Using Phase²

The finite element code Phase² was developed by the Rock Engineering Group at the University of Toronto. It is a 2-dimensional finite element program for calculating stresses and displacements around underground openings. The code runs on IBM 386/486/Pentium or compatible personal computers. The results of analyses are shown in the Interpret menu and include principal stress contours, displacement contours, strength factor, and user data. The strength factor is calculated by dividing the rock strength (based on the given failure criteria) by the induced major principal stress at every point in the mesh. Both elastic and plastic models are available for definition of rock materials. In the case of elastic materials, the strength factor can be less than unity, indicating overstress. In addition, Phase² contains DXF file creation features for use with AutoCAD, thus allowing printing using AutoCAD's comprehensive set of printer drivers. For more new features the Phase² User's Manual can be referred to.

The following assumptions were made in applying Phase² to the Esterhazy potash mines:

- For initial, short term displacements, the salt rock behaves elastically and the elastic properties for the rock mass can be assumed equal to the values determined in the laboratory from intact salt rock samples;
- The material properties used in the case studies are shown in Table 3.1, and are based on laboratory data discussed earlier. It is noted that the uniaxial strengths in Table 3.1 are higher than values obtained from laboratory testing of the Esterhazy salt rock specimens discussed earlier. As those lower laboratory data are attributed to the grain-

size effect (Duncan 1990), the average uniaxial strength value is employed in the following studies.

Table 3.1 Material properties for salt and potash rock

Material	E(GPa)	ν	σ_c (MPa)
Salt	25	0.32	30
Potash	25	0.32	30

- The effect of the progressive and time-dependent development of damage zones which occurs in reality is assumed to be approximated by using the long term uniaxial compressive strength (i.e. the degraded strength) in the damage criterion.

The purpose of defining failure criterion parameters for an elastic material is to allow the calculation and the plotting of strength factors. Even though an elastic material in Phase² does not “fail”, use of the “failure” criteria allows determination of the degree of overstress at points throughout the rock mass.

Three damage/failure criteria were used: (a) Hoek-Brown failure criterion, (b) Duncan failure criterion, and (c) the proposed Esterhazy empirical damage criterion.

1) The Hoek-Brown failure criterion (empirical)

$$\sigma_{1f} = \sigma_3 + \sqrt{m\sigma_3\sigma_c + s\sigma_c^2}$$

Where $m = 4.7$, $s = 1.0$ according to Duncan's (1990) studies of Saskatchewan salt rocks, and $\sigma_c =$ unconfined compressive strength.

2) The Duncan failure criterion (empirical)

$$\sigma_{1f} = \sigma_3 + (m_1\sigma_c\sigma_3 + s\sigma_c^2)^{0.5} \left(1 + \frac{m_2\sigma_3}{\sigma_c}\right)^{-0.5}$$

where $m_1 = 29.6166$, $m_2 = 11.65$, $s = 1$

3) The proposed Esterhazy empirical damage criteria or thresholds are:

Damage initiation threshold: $\sigma_{DI} = \sigma_1 - \sigma_3 = 0.25 \sigma_c$

Damage growth threshold: $\sigma_{DG} = \sigma_1 - \sigma_3 = 0.6 \sigma_c$

Failure: $\sigma_f = \sigma_1 - \sigma_3 = 0.8 \sigma_c$

As crack initiation develops at the microscopic scale, it is not of practical interest. Therefore, prediction of the zone of damage initiation is not shown in the following model studies.

Case Model 1

The mesh shown in Figure 3.1 was constructed to simulate the loading conditions and the geometry for Esterhazy underground potash mining. The external boundary size is 100 m \times 26.5 m. The room size is 20 m \times 2.5 m, and is located in the centre of the mesh. A hydrostatic stress of 25 MPa is assumed. This initial field stress is applied prior to excavation and the system brought into equilibrium before excavating the opening.

The predicted region of failure using the Hoek-Brown failure criterion occurs around the corners of the opening and develops in the roof up to a height of 5 m as shown in Figure 3.2a. *In situ* observations (Figures 2.7-2.11) show that cracking does not reach as high as 5 m.

The Duncan failure criterion could not be employed for this model. A large tensile region with high tensile stress (i.e. large negative values of minor principal stress) occurs in the roof, which results in a numerical error due to the square root of a negative number in the Duncan failure criterion.

Application of the proposed Esterhazy empirical failure criterion (Equation 3) produces a large “failure” area in the roof as shown in Figure 3.2b. Compared to *in situ* crack mapping the predicted zone of damage is much larger.

A tensile zone in the central area in the back is revealed from σ_3 contours (Figure 3.3). Tensile cracks are not common at the roof surface in the mines, however. It is evident

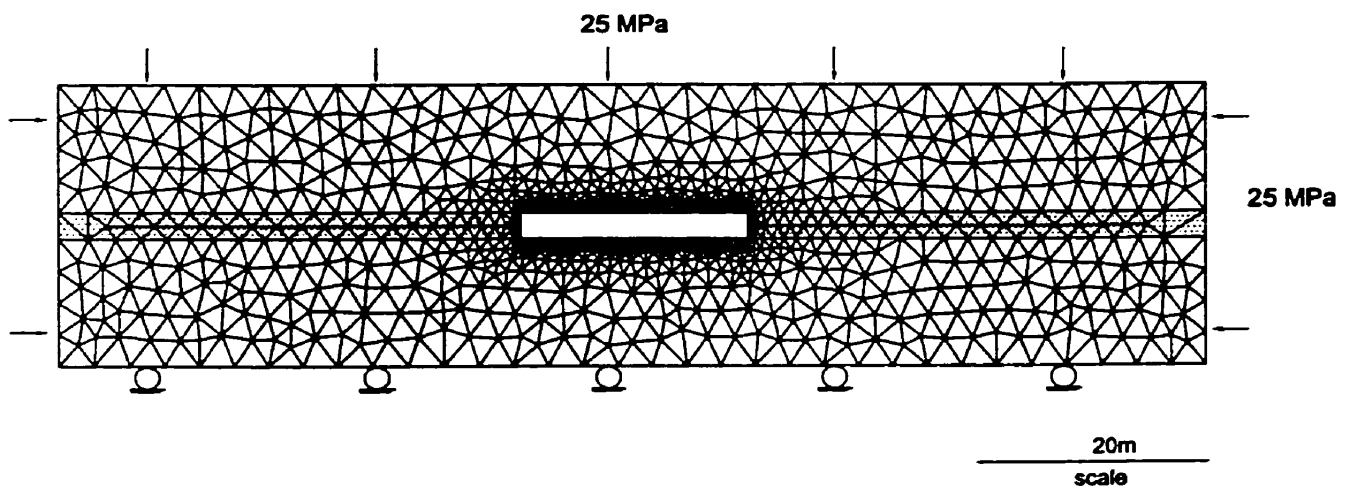


Figure 3.1 Finite element mesh for Case Model 1

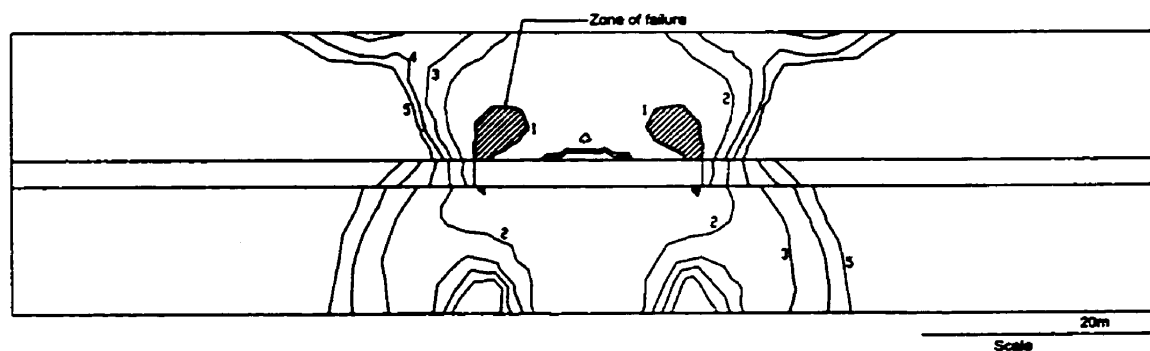


Figure 3.2a Contours of strength factor (Hoek-Brown failure criterion, $m=4.7$, $s=1$)

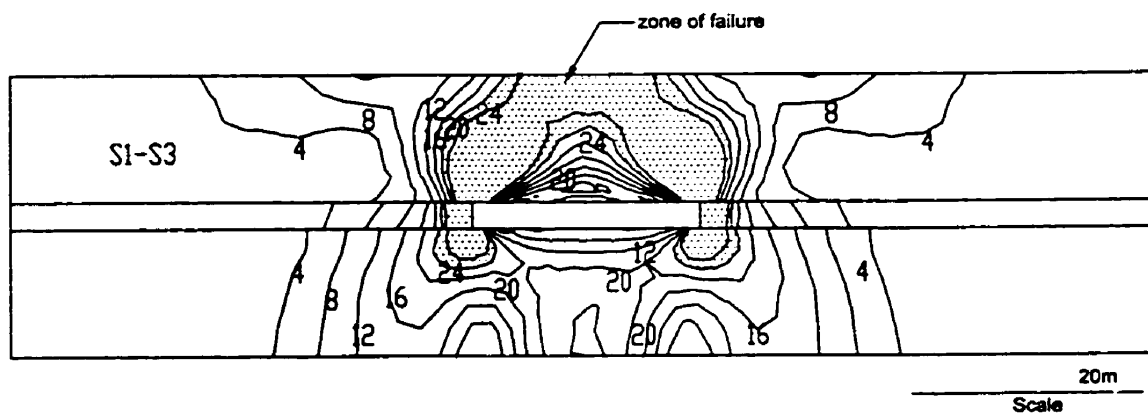


Figure 3.2b Contours of deviatoric stress (MPa) and zone of failure by the Esterhazy failure criterion (Equation 3)

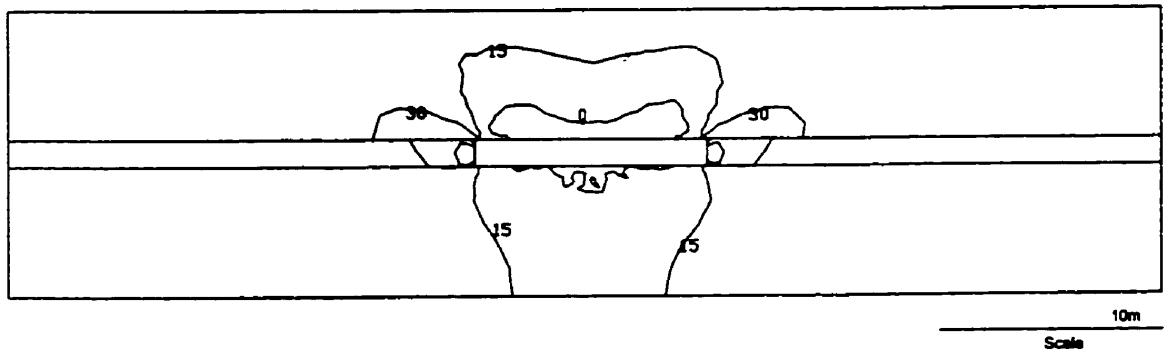


Figure 3.3 Contours of minimum principal stress σ_3 (MPa)

that the roof of 12.5 m in thickness in the model performs like a thick beam in these models since the external boundaries are not far enough from the opening.

Case Model 2

In order to eliminate the beam action, the vertical and horizontal dimensions of the external boundary were increased to 200 m (Figure 3.4). Figure 3.5 and Figure 3.6 show the σ_1 and σ_3 contours for this model. The major principal stress σ_1 is concentrated in the side walls and at the corners of the opening, and gradually reduces to the far field stress away from the opening (Figure 3.7). The central area in the roof and the floor are destressed, and small tension zones develop where σ_3 assumes negative values.

The Hoek-Brown Failure Criterion

The strength factor contours are shown in Figure 3.8 for the Hoek-Brown failure criterion with $m = 4.7$ and $s = 1.0$. Failure takes place only in the side walls of the underground opening.

According to laboratory triaxial compression tests conducted by Lajtai et al (1991), crack damage occurs at about 65% of the peak strength (Table 3.2). Thus, by keeping the values of m and s unchanged and by reducing only the unconfined compressive strength to 65%, the predicted damage zone changes to that shown in Figure 3.9a. The maximum predicted height of the damage zone in the roof is 1.7 m. Compared to the field observation data in Figures 2.7 to 2.11, the predicted zone of damage in the roof is smaller in the region above the side walls and the height of the zone of damage is lower as well.

Table 3.2 Saskatchewan potash strength (after Lajtai et al 1991)

Confining Pressure (MPa)	0	0.5	1	2	3	4	5	6	7	8	9	10
Crack Damage (MPa)	12.7	18	13	22	18	22	23	33	26	29	31	32
Peak Strength (MPa)	24.5	28	32	34	38	39.5	45	42.5	42	46	43	47

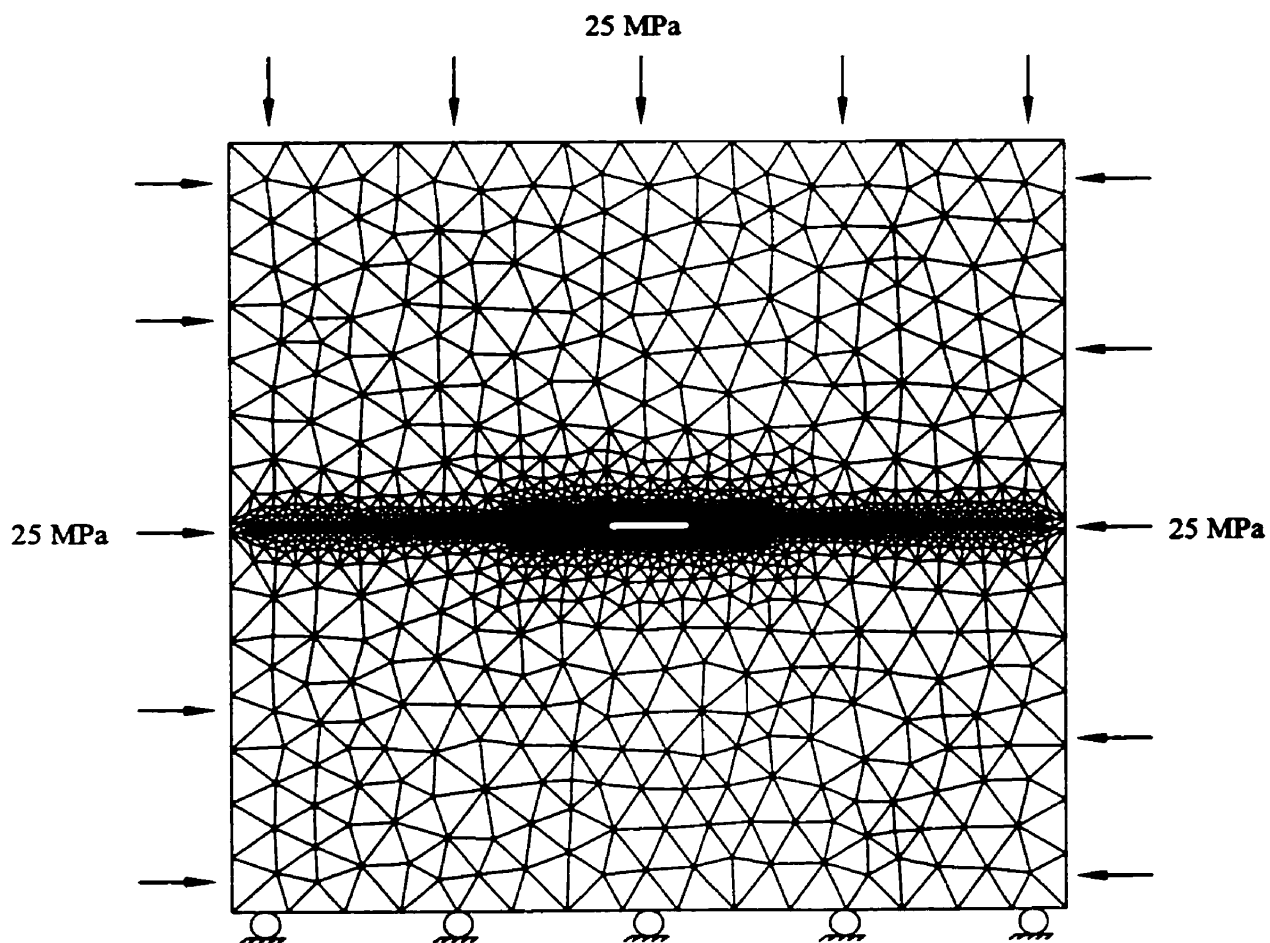


Figure 3.4 Finite element mesh for Case Model 2

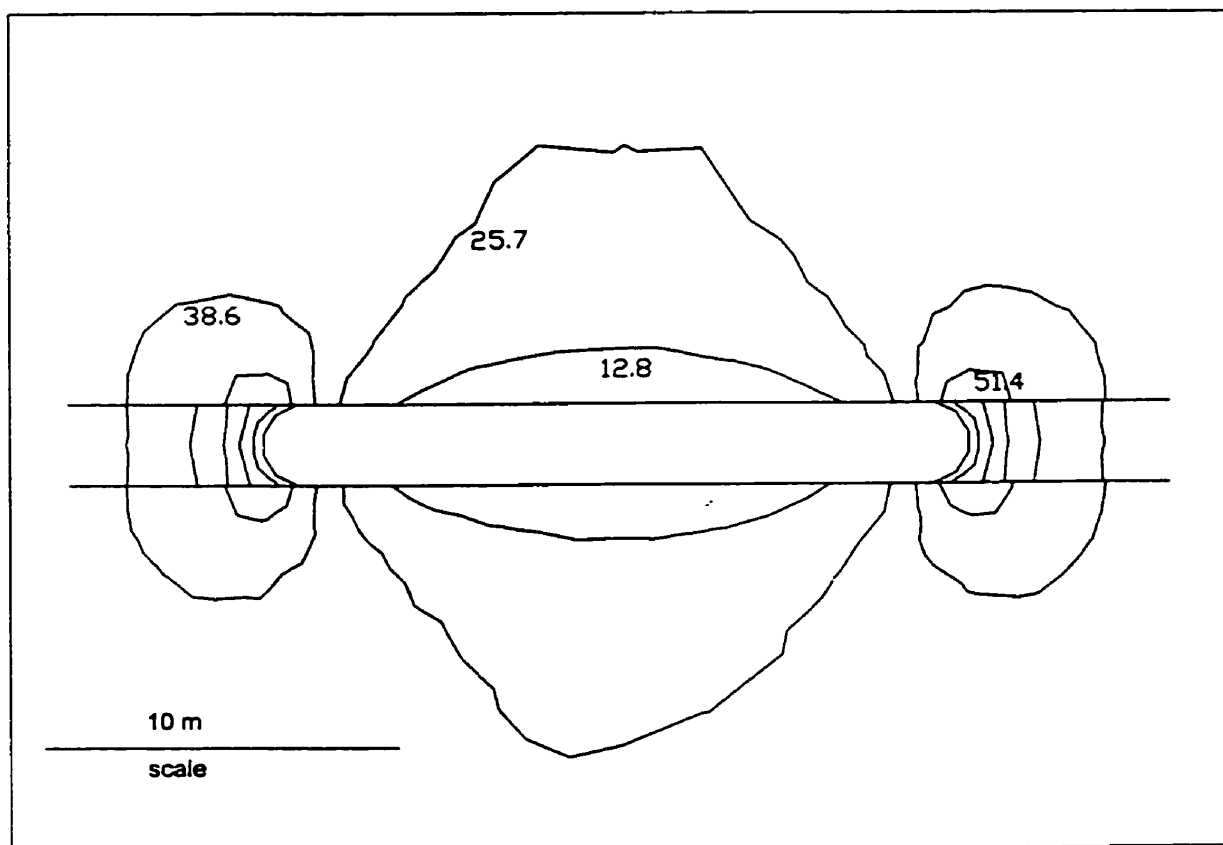


Figure 3.5 Contours of the major principal stress σ_1 (MPa)

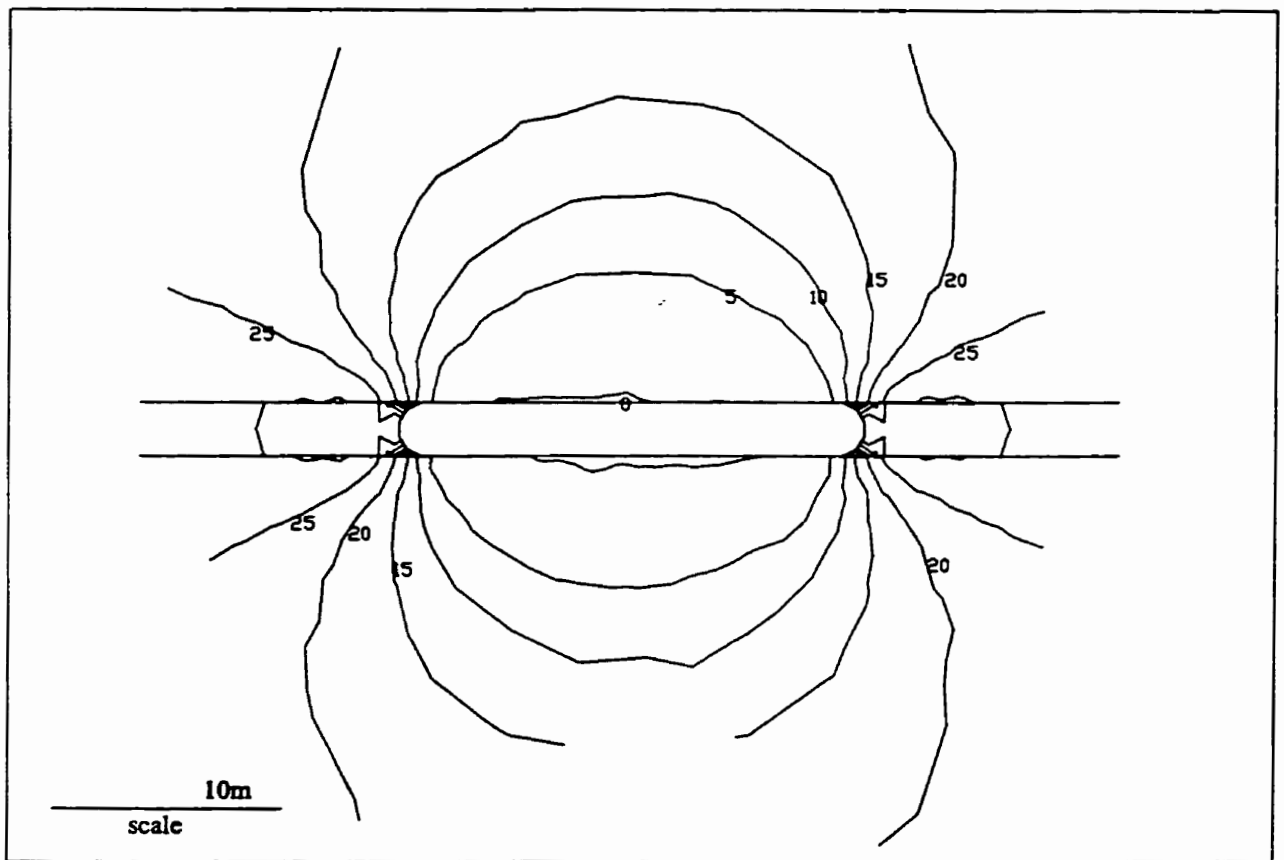


Figure 3.6 Contours of the minor principal stress σ_3 (units in MPa)

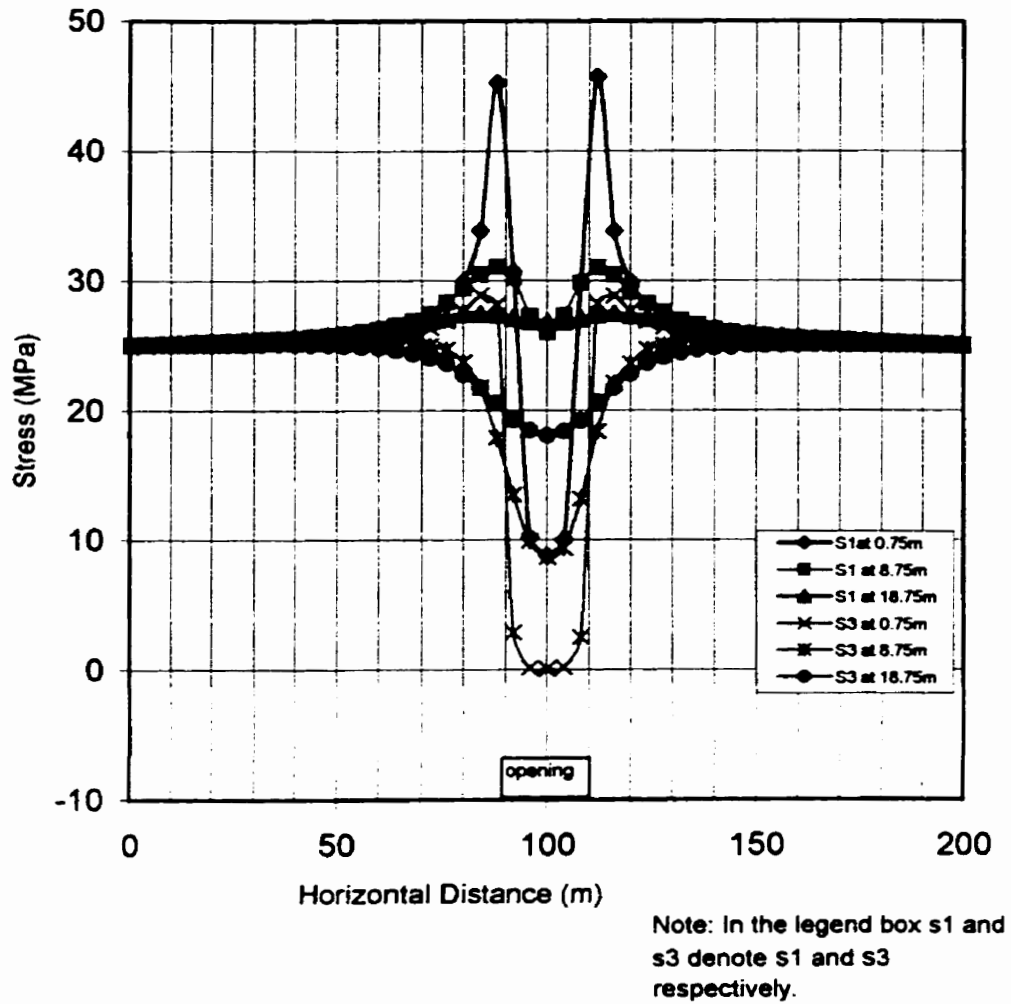


Figure 3.7 Principal stress distributions at different heights in the roof

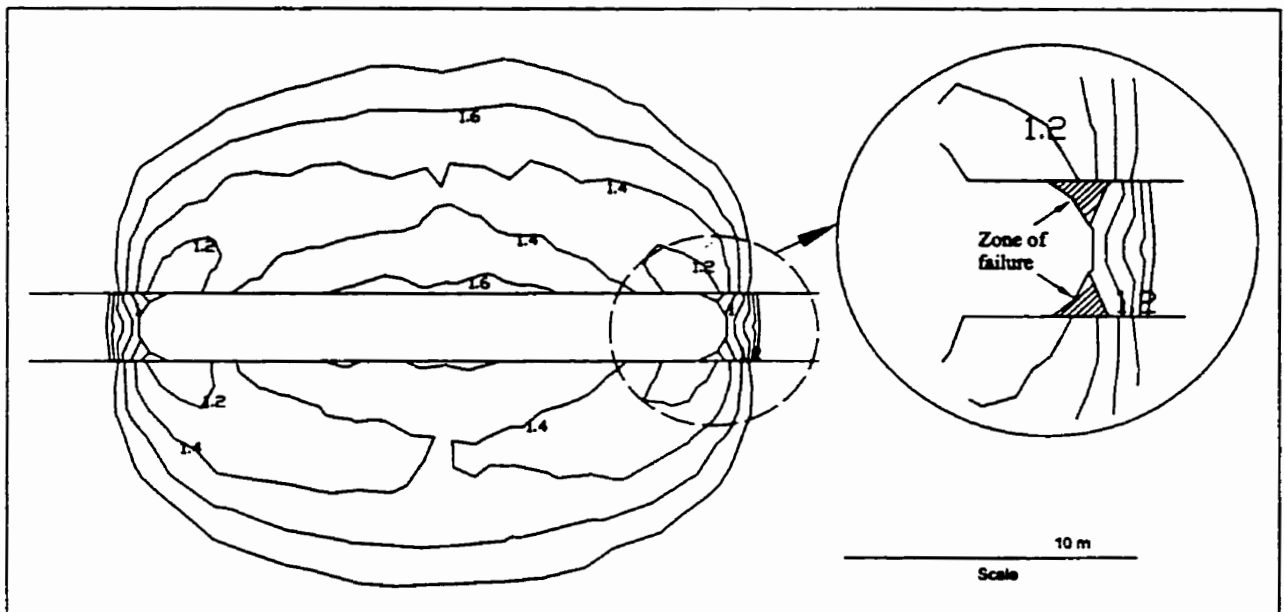


Figure 3.8 Contours of strength factor using the Hoek-Brown criterion ($m=4.7$, $s=1.0$)

If σ_c is reduced to 80% of the peak value as suggested in section 2.3.4 for the long-term strength, failure takes place in side walls and corners of the roof but over a much smaller area, as shown in Figure 3.9b.

The Duncan Failure Criterion

The Duncan failure criterion was also applied and predicted a failure zone only in the side walls of the opening (Figure 3.10).

If σ_c is degraded to 65% of the peak strength as recommended by Lajtai et al (1991), failure is predicted in the side walls and in the roof above the side walls to a height of 2.4 m, as shown in Figure 3.11a. If σ_c is reduced to 80% of the peak value, failure is predicted in the side walls and the corners of the roof or back (Figure 3.11b). Obviously, these results do not match the field observation data shown in Figures 2.7 to 2.11.

The Esterhazy Damage/Failure Criteria

The deviatoric stress contours are shown in Figure 3.12. According to the writer's empirical failure criterion (Equation 3), a failure zone with a height of 4 m appears above the abutments in the roof when the deviatoric stress ($\sigma_1 - \sigma_3$) exceeds 24 MPa (i.e. $0.8\sigma_c$). A dome-shaped zone of damage growth (Figure 3.13) occurs in the roof with a central height from 3.7 m to 6.8 m where ($\sigma_1 - \sigma_3$) exceeds 18 MPa (i.e. $0.6\sigma_c$) according to Equation 2. In this model the height of the lower boundary of the predicted damage growth zone coincides with what was observed by borehole camera in mining rooms, while the upper boundary is higher than any observed cracking.

Case Model 3

In order to study the effect of clay seams on the development of damage and failure in the roof, a finite element model incorporating a clay seam was constructed as shown in Figure 3.14. The height of the clay seam is 7 m above the opening according to the stratigraphy in Figure 2.2. As the clay seam is usually thin with a thickness ranging from

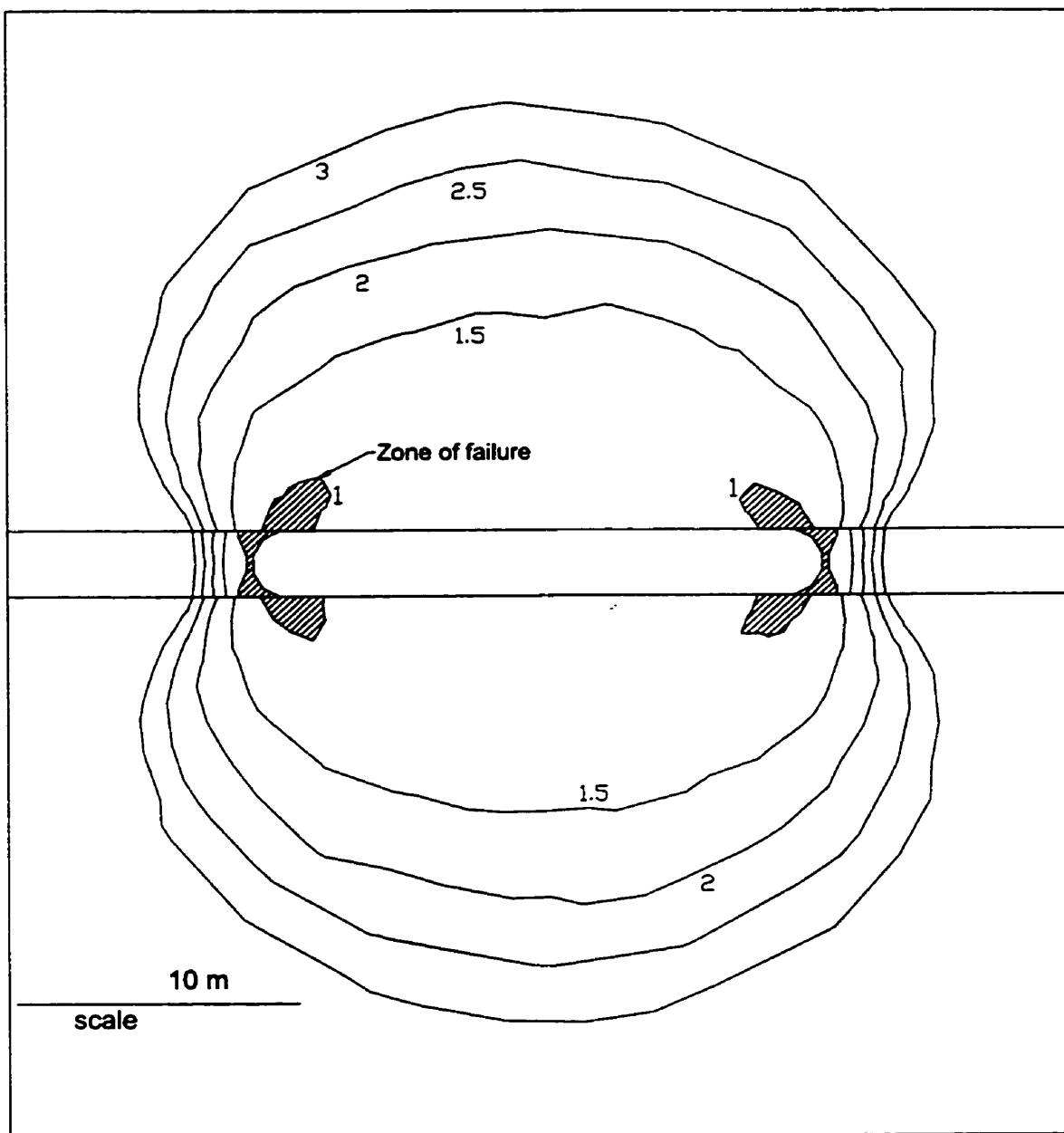


Figure 3.9a Contours of strength factor and predicted zone of failure for Hoek-Brown criterion ($m=4.7$, $s=1$, σ_c reduced to 65%)

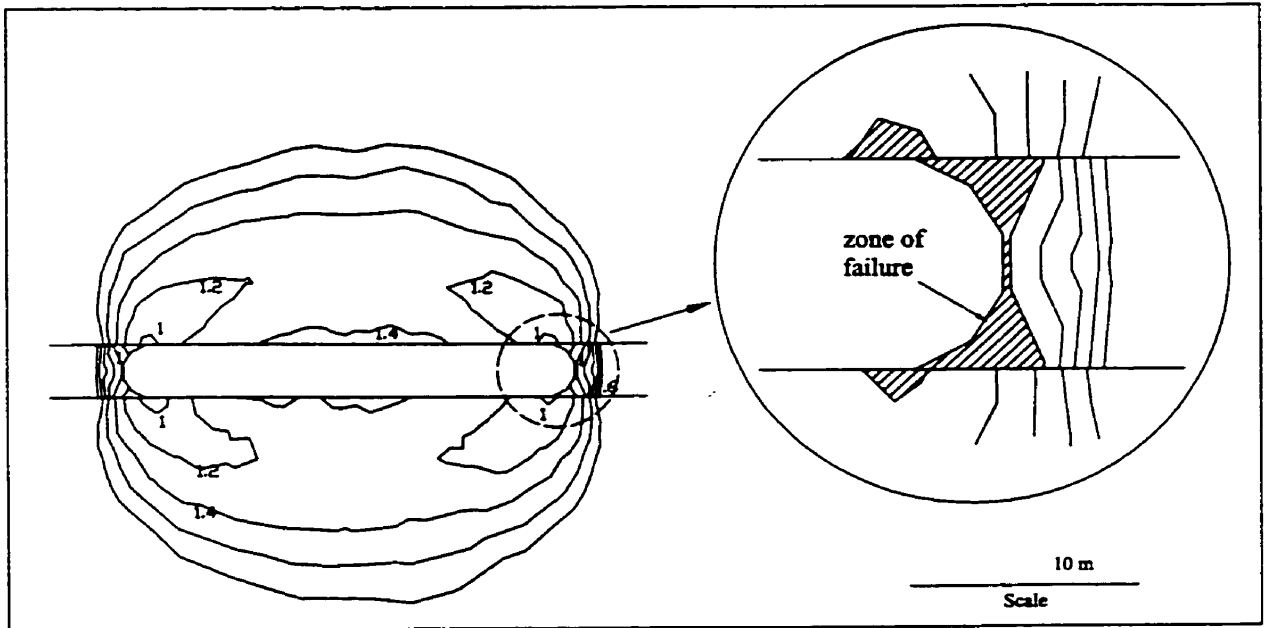


Figure 3.9b Contours of strength factor and zone of failure for Hoek-Brown failure criterion (σ_c reduced to 80%)

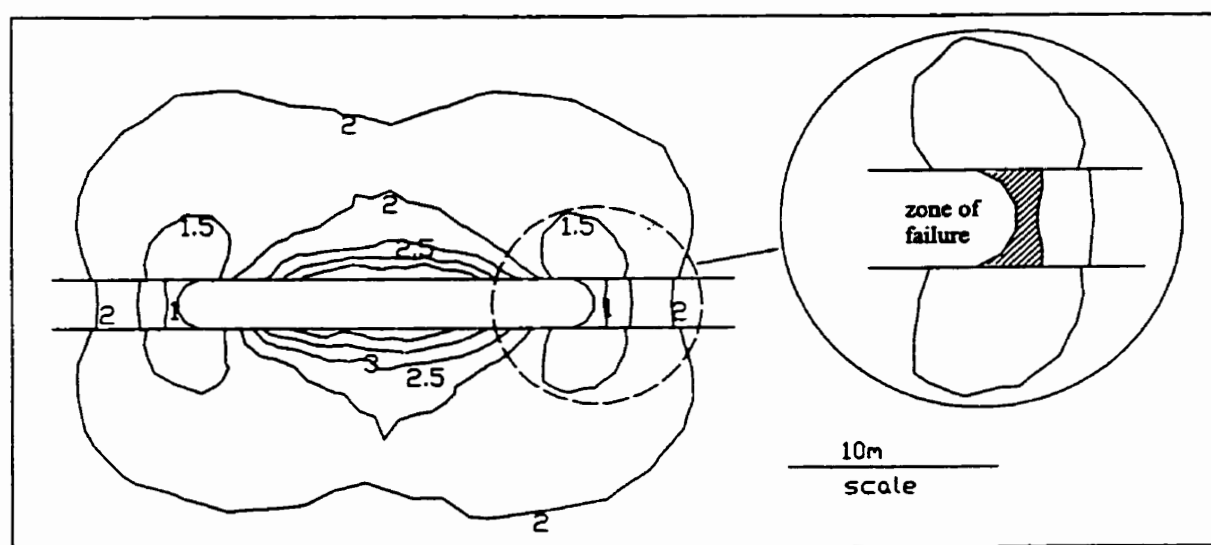


Figure 3.10 Contours of strength factor and zone of failure for Duncan failure criterion

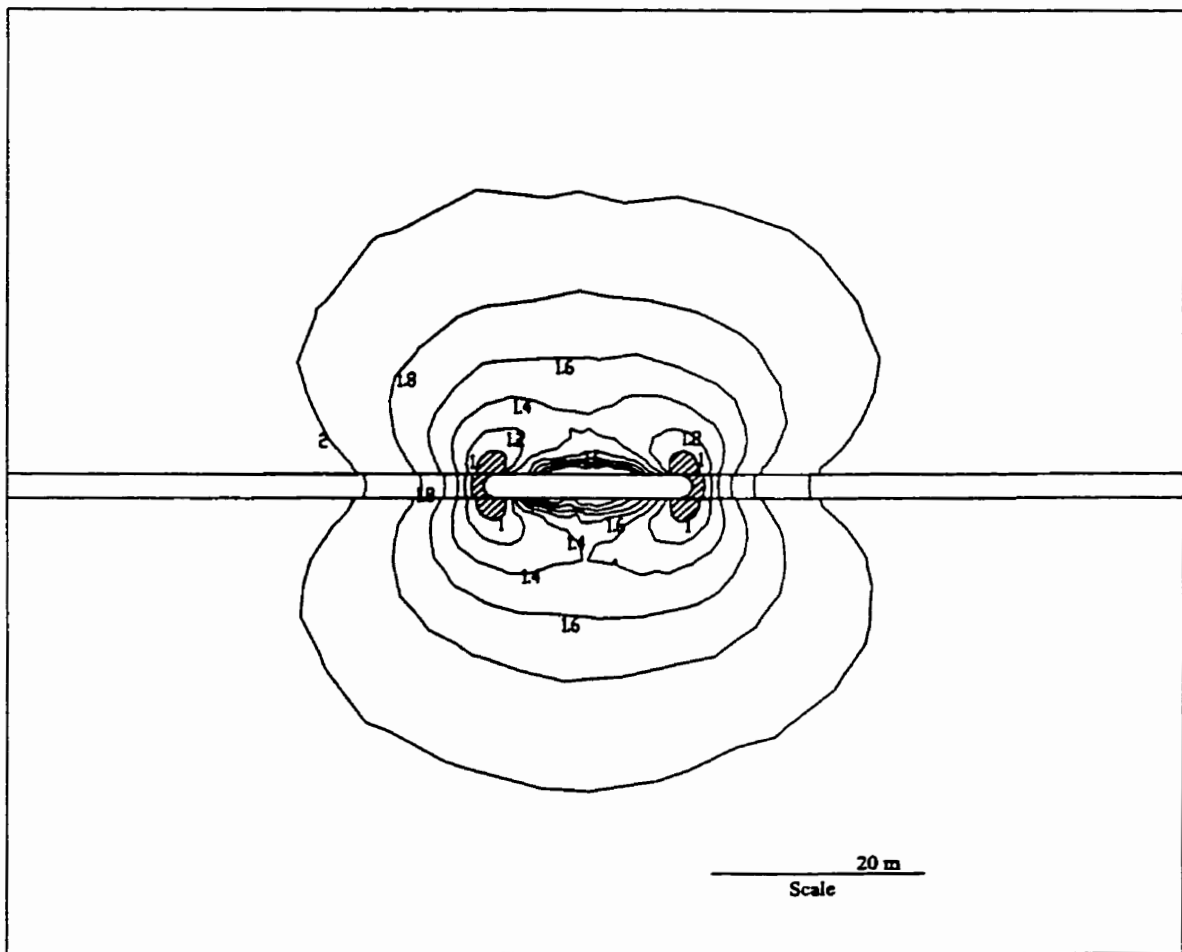


Figure 3.11a Contours of strength factor for modified Duncan failure criterion (σ_c reduced to 65%)

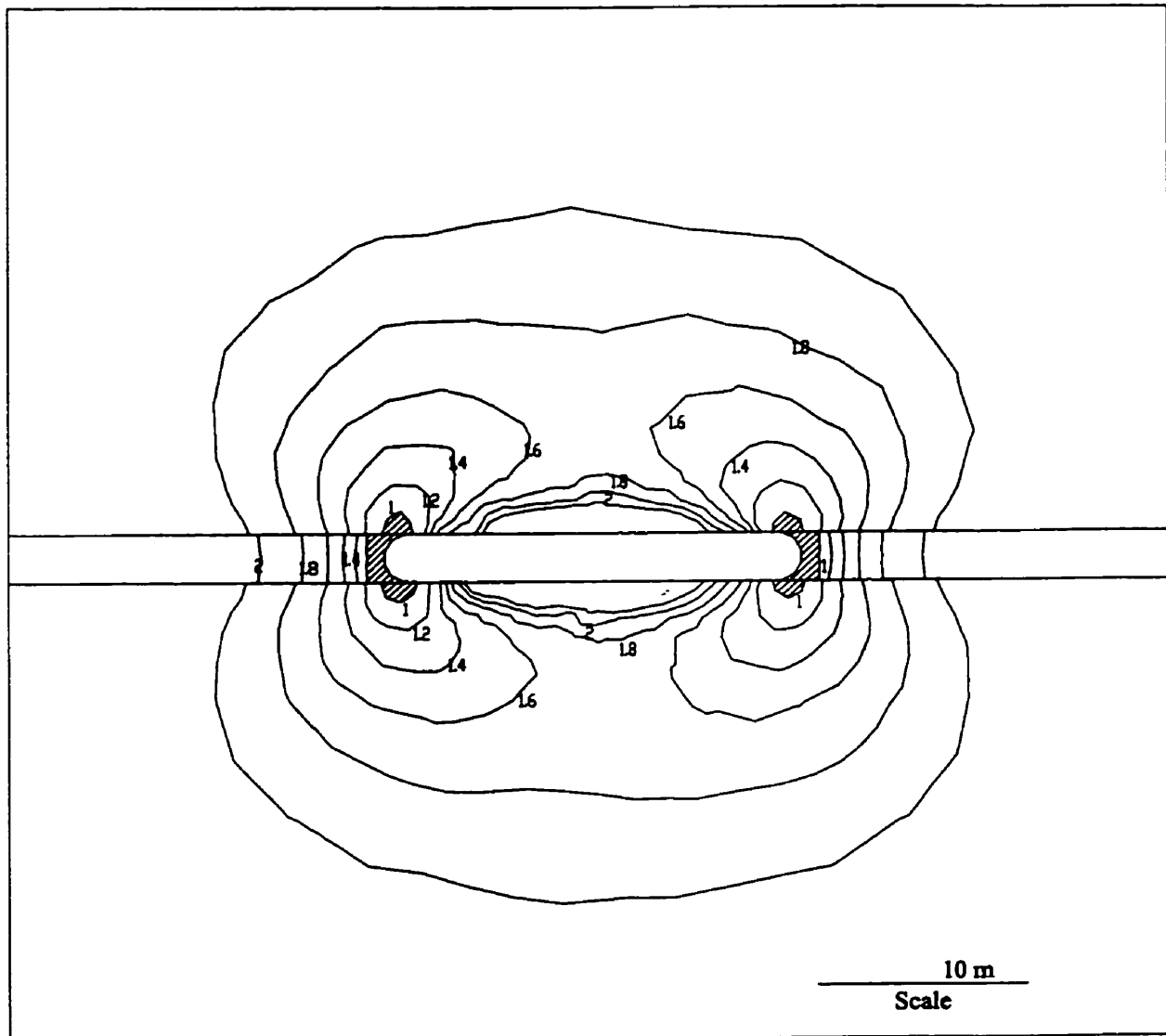


Figure 3.11b Contours of strength factor for modified Duncan failure criterion (σ_c reduced to 80%)

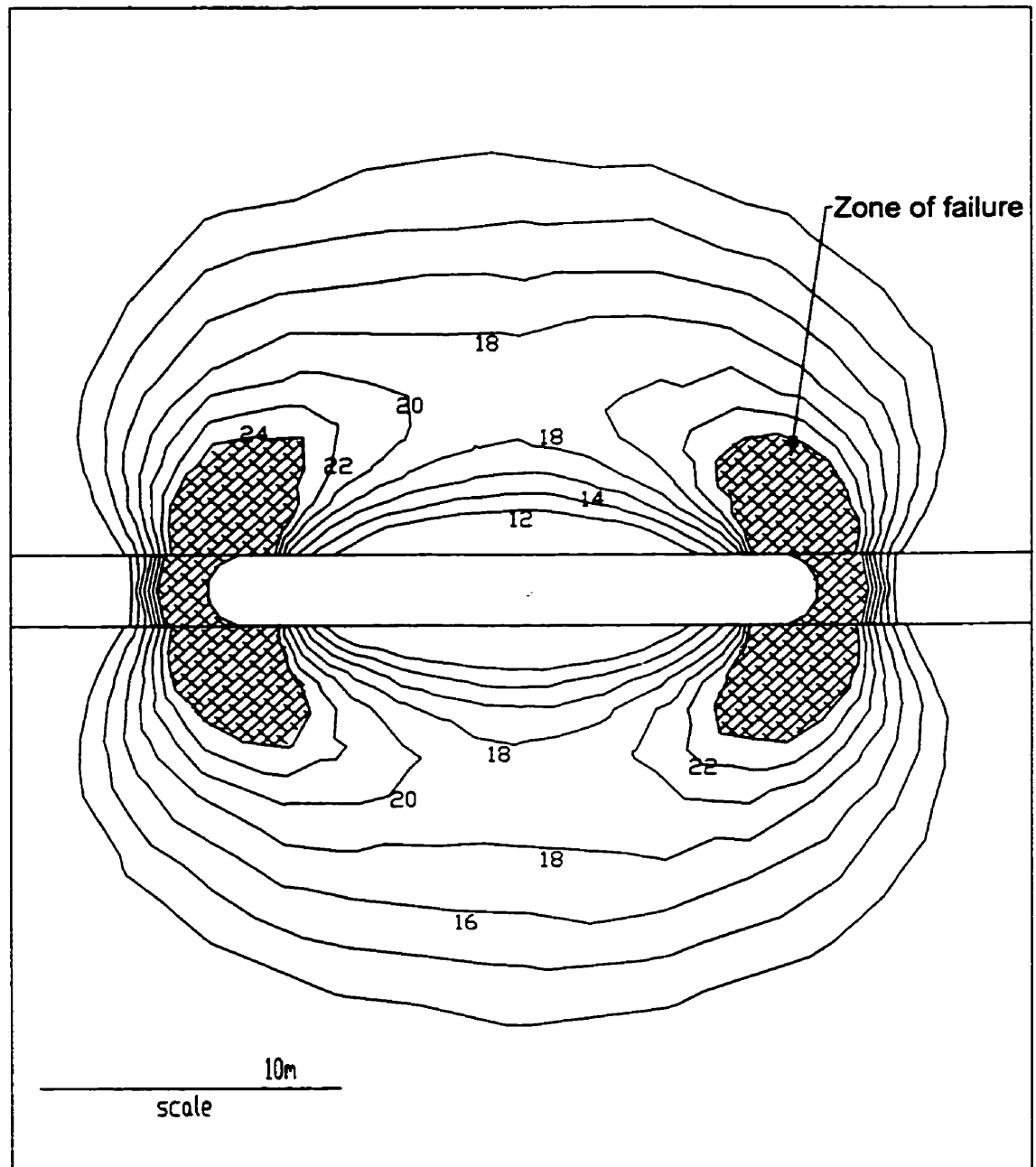


Figure 3.12 Contours of deviatoric stress and zone of failure (units in MPa)

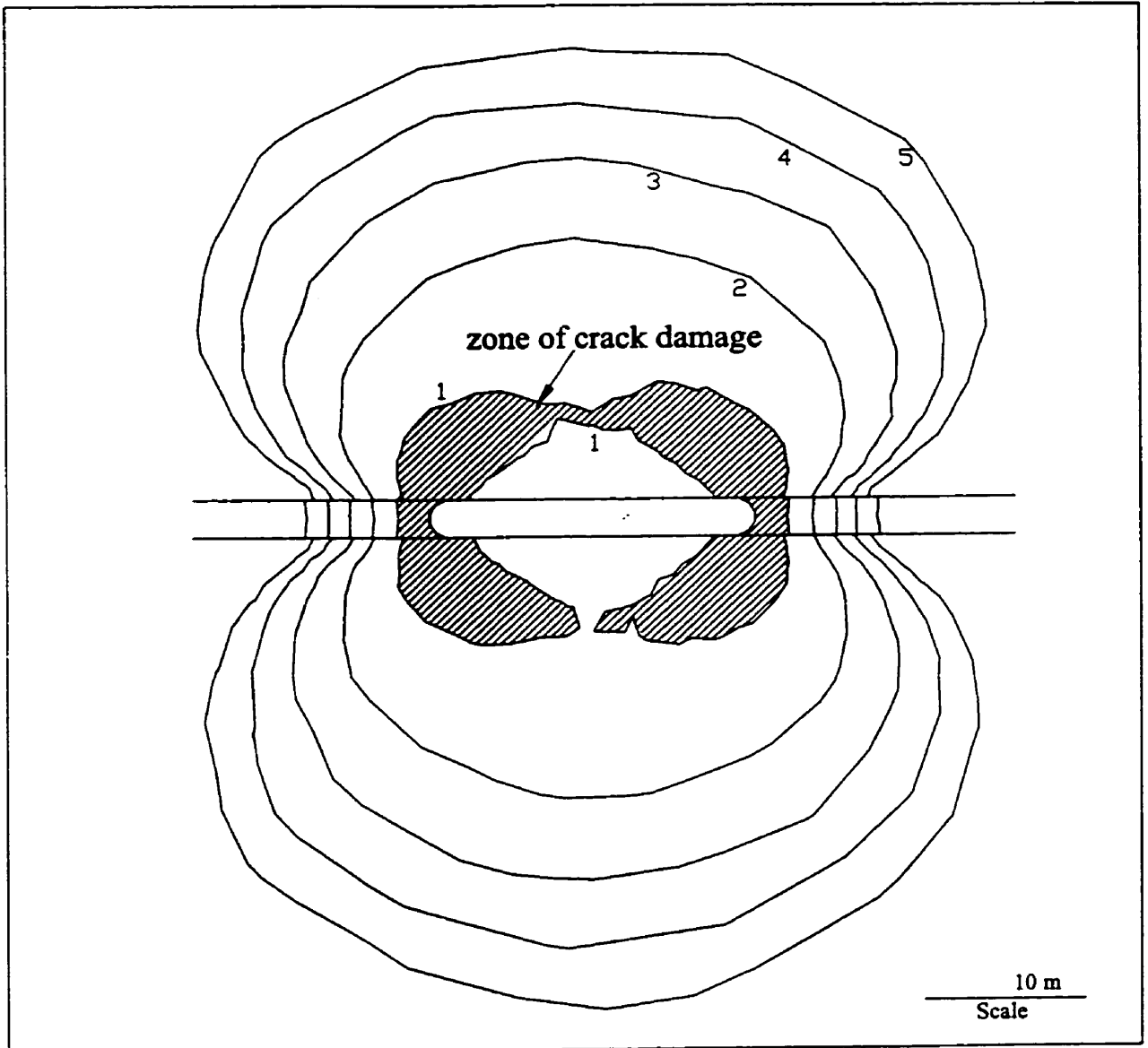


Figure 3.13 Contours of strength factor and zone of damage growth for the proposed Esterhazy damage criteria

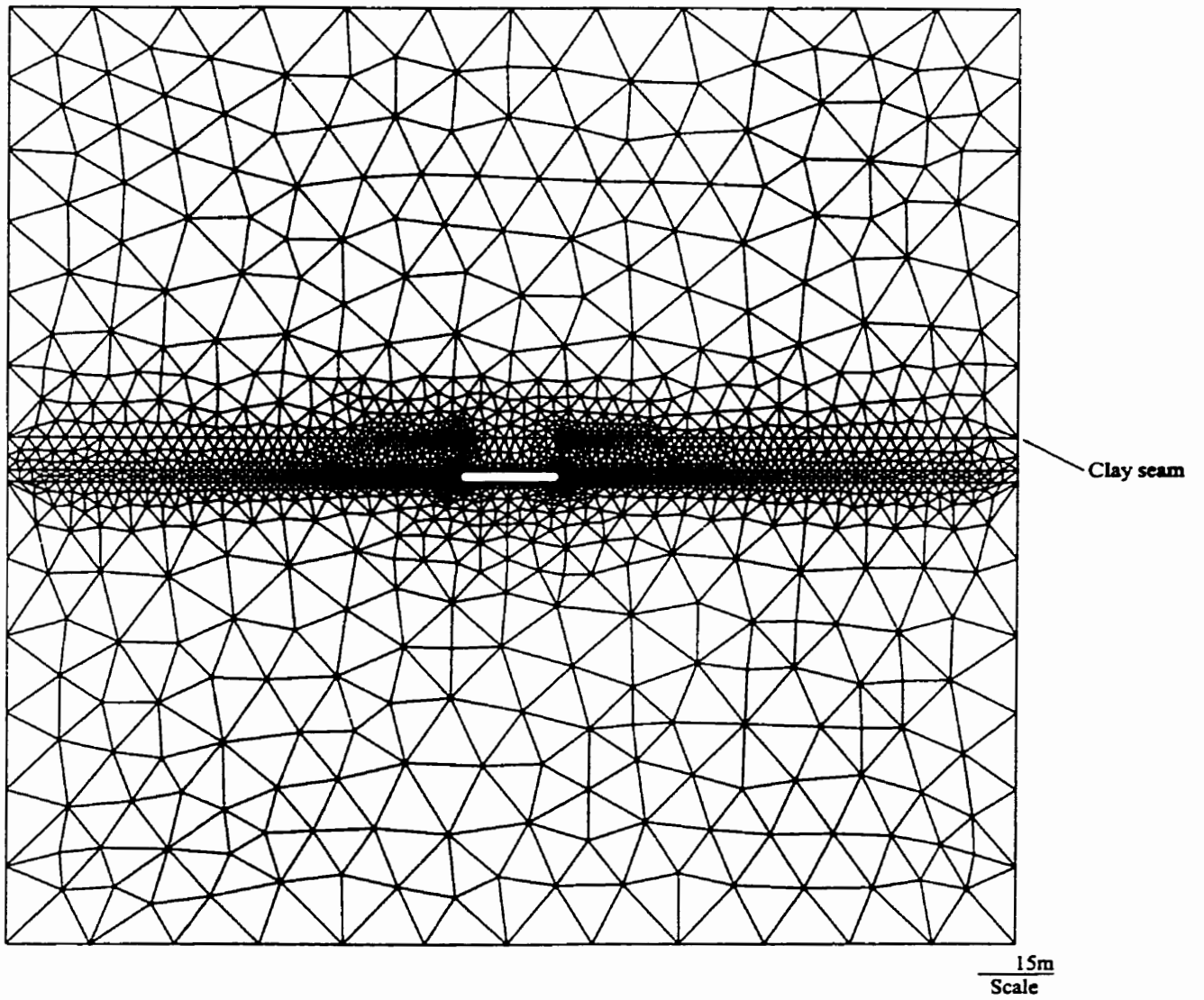


Figure 3.14 Finite element mesh for Case Model 3 for incorporating a clay seam

several centimeters up to 10 cm and the strength parameters were not investigated, the seam was treated as a joint with parameters:

Normal stiffness, 250 GPa/m

Shear stiffness, 101 GPa/m

Aperture, 10 cm

Cohesion, 0 MPa

Tensile strength, 0 MPa

Friction angle, 25°

The large value for the normal stiffness and the small value for the shear stiffness reflect typical joint stiffness behaviour.

Overall, the pattern of the principal stresses is similar to that of Case Model 2 except that stresses are perturbed along the clay seam (Figure 3.15). Failure occurs in the walls according to the Hoek-Brown failure and the Duncan failure criteria (Figures 3.16a and 3.16b).

The zone of failure according to the proposed Esterhazy failure criterion (Equation 3) can be deduced from the distributions of deviatoric stress (Figure 3.17). The shape and height of the zone are almost the same as those of Case Model 2 in Figure 3.12. The upper boundary of the contour of deviatoric stress 18MPa is, however, arrested by the clay seam, which implies that the zone of damage would proceed along the clay seam according to the proposed Esterhazy damage criterion (Equation 2). Nevertheless, no significant change of the deviatoric stress is observed compared to Case Model 2.

Horizontal slipping along the clay seam is noted with a maximum offset of 0.7mm (Figure 3.18). Horizontal slip along the clay seam does not appreciably change the principal stress distributions. It could be, therefore, concluded that the zones of damage in the back are little affected by the clay seam at a height of 7 m above the opening.

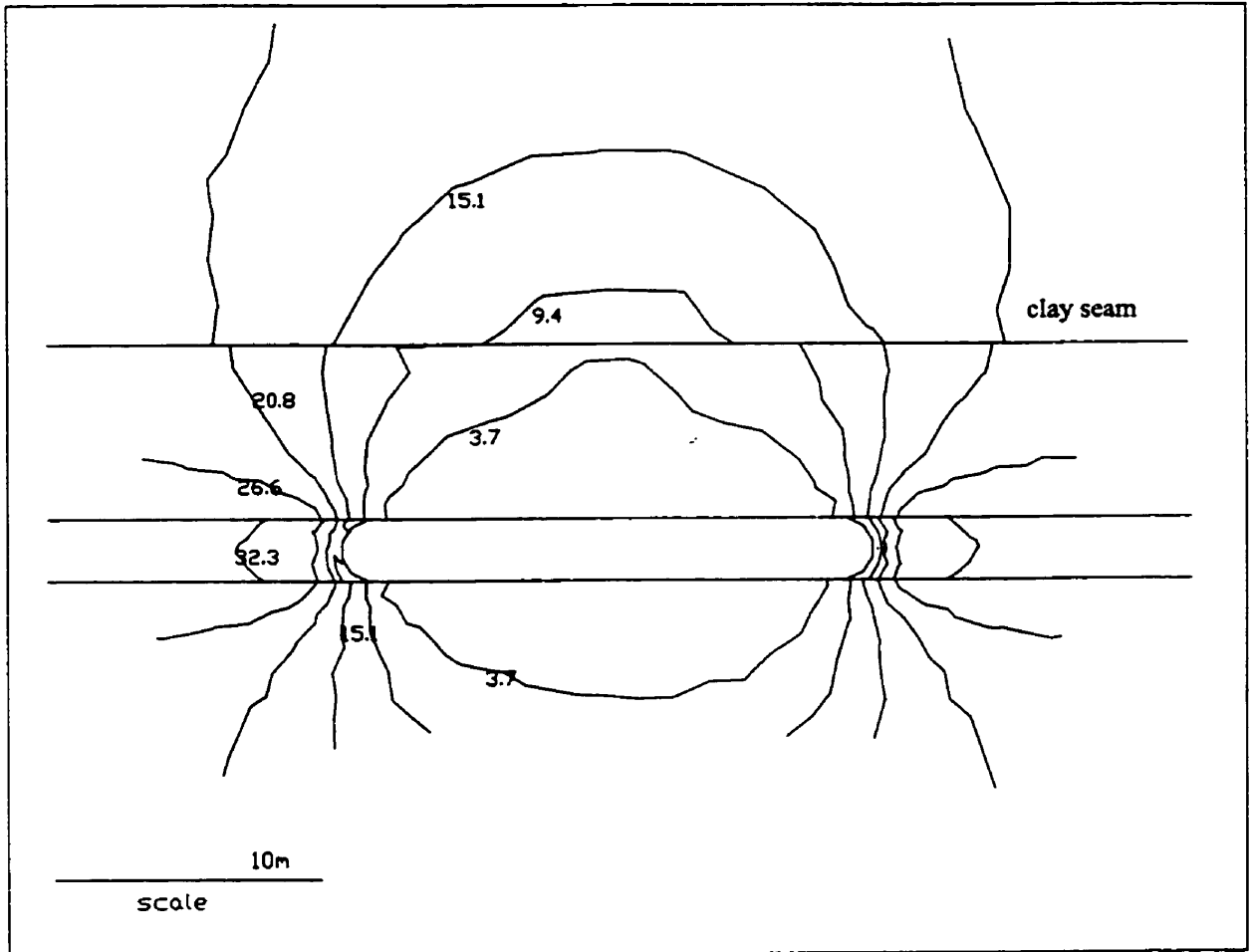


Figure 3.15 Contours of minor principal stress σ , (MPa)

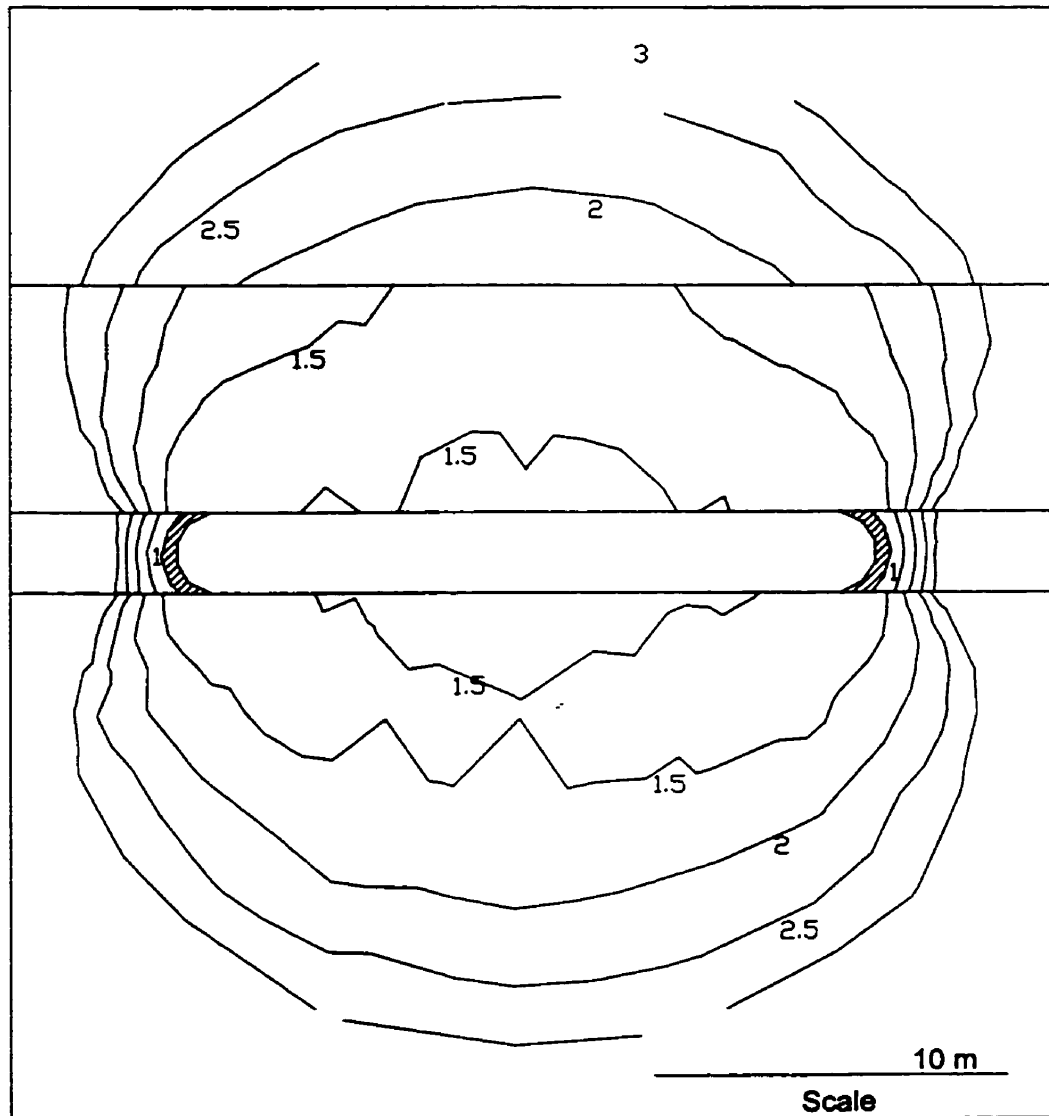


Figure 3.16a Contours of strength factor and zone of failure for the Hoek-Brown criterion ($m=4.7$, $s=1$)

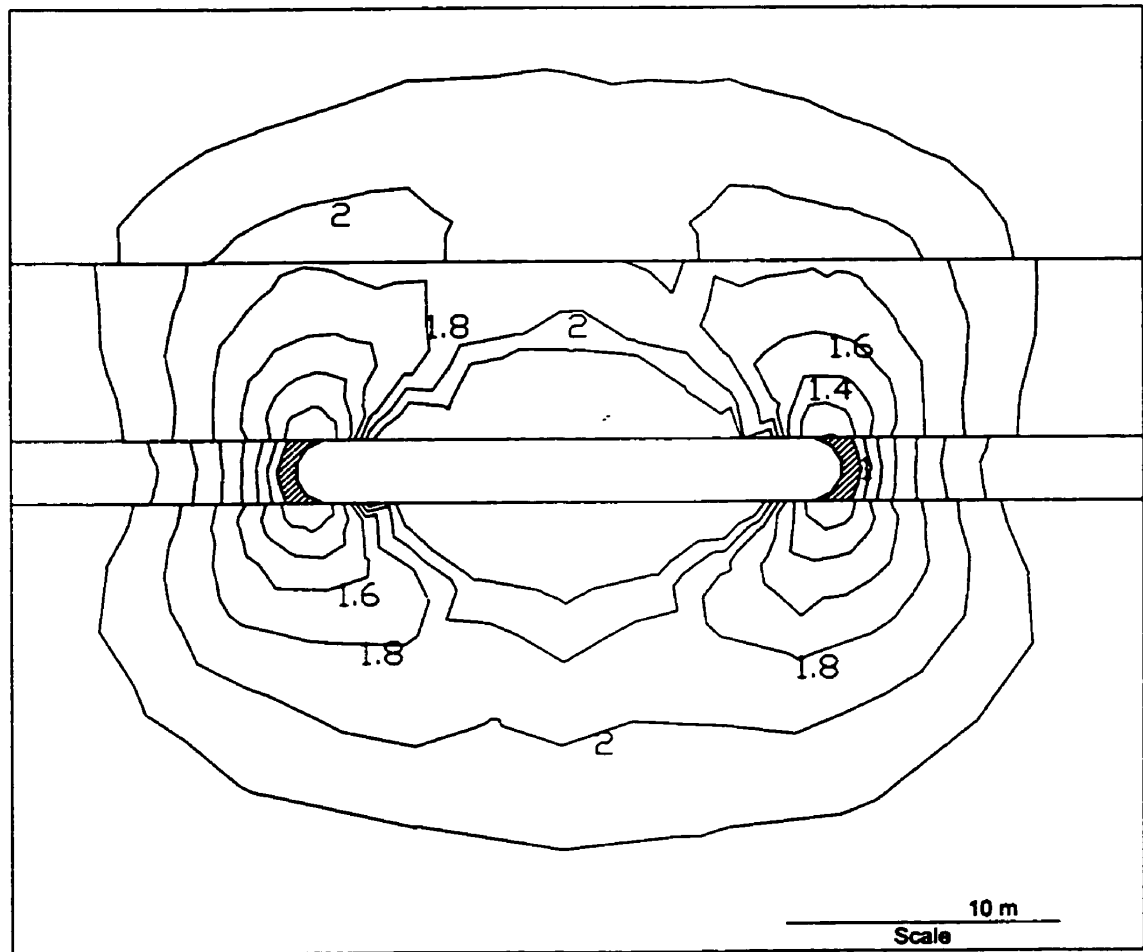


Figure 3.16b Contours of strength factor and zone of failure for the Duncan failure criterion

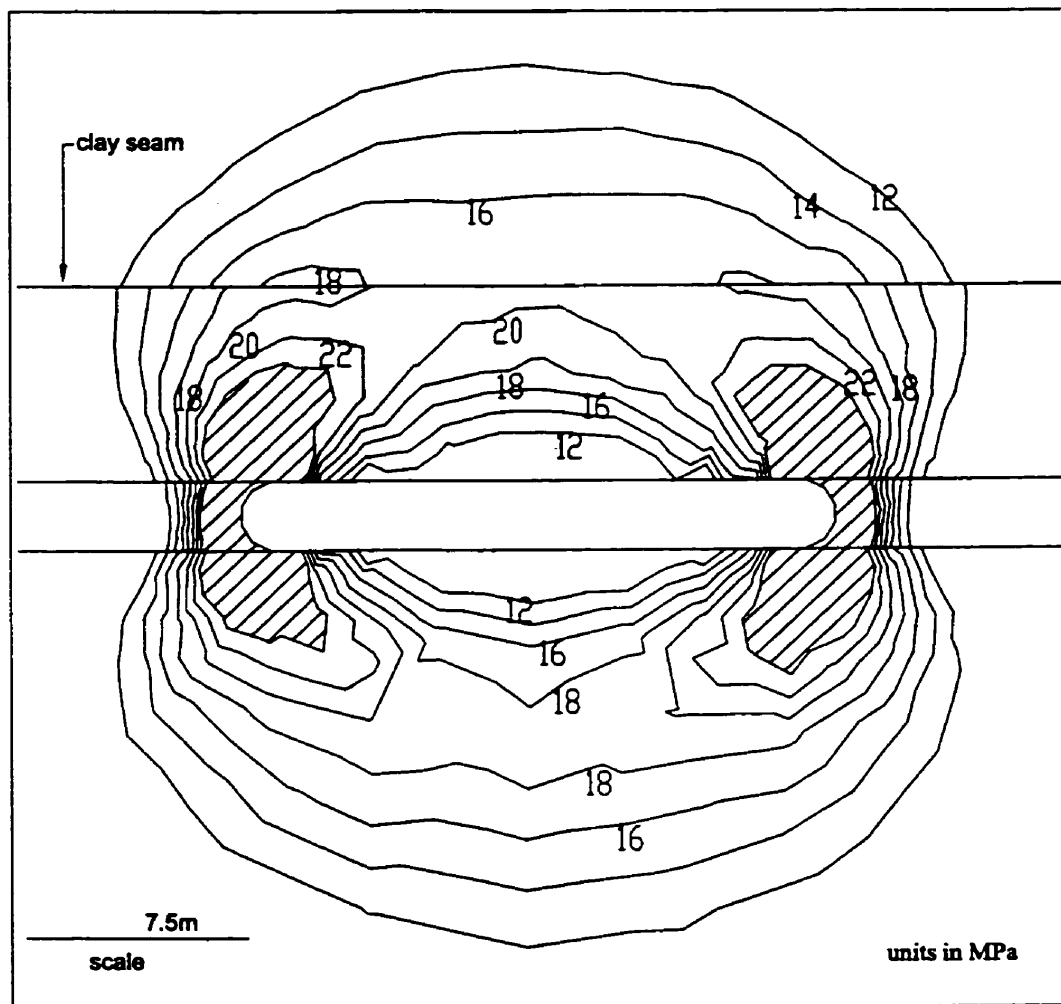


Figure 3.17 Contours of deviatoric stress and zone of failure for the Esterhazy failure criterion (Equation 3)

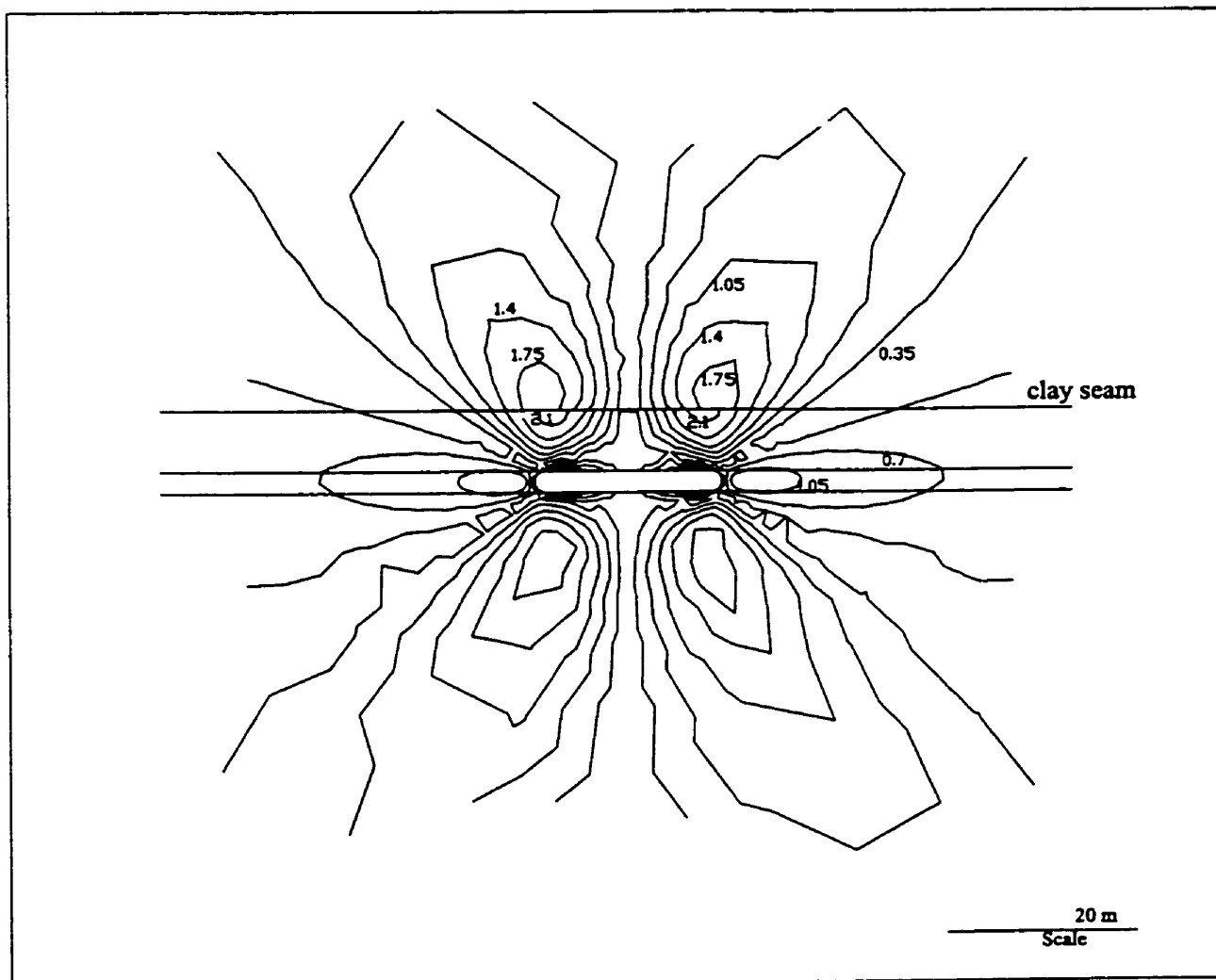


Figure 3.18 Contours of horizontal displacement (mm)

3.2 Discussion

The modelling studies show that neither the Hoek-Brown criterion nor the Duncan empirical criterion is able to simulate the failure zones for the potash openings as measured *in situ* by borehole camera. Some improvement was achieved by reducing peak strength values.

The Esterhazy empirical damage criteria predicted an arch-shaped zone spanning the immediate roof, a geometry which is reflected by the *in situ* measurements. The extent of the region of damage is, however, larger than that measured *in situ*. The upper boundary of the predicted zone is also higher than the observed damage zone (Figure 3.13) but the lower boundary of the predicted damage growth zone coincides with the height at which cracks were observed *in situ*.

The discrepancy between predicted and observed damage/failure zones may be attributed to a number of factors, including:

- 1) Salt rocks are assumed to behave elastically in the above model studies, which is valid for a short time frame. However, salt rocks creep and increase their ductility with increase in confining pressure. Stress redistribution due to creep was not considered.
- 2) Strength reduction below a short-term peak measurement is a tool for establishing long-term strength. However, the use of long-term strength in a model cannot “simulate” the ductility/creep of salt rock.
- 3) Damage/failure criteria were selected from the laboratory test data on intact salt rock samples, which may not reflect the characteristics of *in situ* salt rock mass.
- 4) During the advance of mining openings, the rock behind the face may be damaged and its strength considerably degraded. The reduction of rock mass strength in the above modelling process provides only a reasonable approximation to the problem. It assumes that the rock strength everywhere around openings has been damaged. Clearly, the most extensive damage only occurs in limited areas around the opening, i.e. areas of maximum tangential stress concentrations (Martin 1993). Thus the strength around the openings will vary from a maximum value

(undamaged) to a minimum value (maximum damage). Therefore, the implication of the reduction of salt rock strength in the preceding continuum modelling studies would yield an overestimated zone of failure/damage.

- 5) In the mining environment the creation and orientation of fractures is probably influenced by clay seams as demonstrated in Figure 2.4.
- 6) Failure in the roof is progressive as demonstrated from borehole camera observation at different times, while Phase² modelling did not simulate progressive failure. Alternatively, the progressive failure can be simulated by reducing the moduli or by removing the rock material within the contour where the safety factor equals 1. This procedure progresses step after step until a final excavated shape of the opening is achieved. However, this method tends to produce an oversized zone of failure. For example, in an attempt to simulate the progressive nature of spalling process for a circular opening, stability was achieved when a notch of failure reached a depth of about 2-times radius from the centre of the opening (Zheng et al 1989). This problem arises from using a 2-dimensional model to simulate a 3-dimensional failure process (Martin 1993).

The simplicity of use of Phase² makes it an attractive tool and if appropriate criteria are selected it can provide an initial indication of the potential for damage or failure. The inability, however, to model crack propagation is a major drawback. For this reason, the next phase of the research involved the application of a model that does simulate progressive cracking.

3.3 Discrete Fracture Modelling Using InSight^{2D}

The borehole camera observations revealed a progressive development of discrete, localized cracks rather than pervasive, ubiquitous crack damage throughout a volume of rock. Initiation and propagation of discrete cracks causes local stress redistribution. Thus, to simulate progressive, discrete fracturing, a finite element code which is able to model discrete fractures and stress redistribution is required. A new finite element program,

InSight^{2D}, can accomplish this goal by employing crack propagation criteria and a means of following crack growth.

InSight^{2D} was developed at the University of Manitoba (Dzik et al. 1994) and runs on a 486 IBM compatible personal computer. It assumes linear elasticity and has the capability of handling multiple material types and assigning specific material properties to each finite element. Various failure criteria are available within InSight^{2D} for computing factors of safety. The program also incorporates an empirical compressive crack model (i.e. the finite-width crack model) developed at the University of Manitoba (Lajtai et al, 1990). With this model a propagating crack is represented by an open ellipse which is oriented parallel to the maximum compressive stress. Using a simple minimum principal stress criterion ($\sigma_3 \leq T_0$), unstable fracture propagation should commence at the moment the induced tensile stress reaches the value of the tensile strength T_0 . In order to minimize the size effect on crack nucleation, the “point stress” at the fracture-tip-process zone is replaced with an “average stress” using a stress averaging technique.

A safety factor in terms of the ratio of material strength to the induced stress at the crack tip is defined by the Uniaxial Strength Ratio (USR). The USR criterion is derived through the Rocker function (Johnston, 1985; Carter et al., 1991) which describes material strength, σ_{1f} , as a function of its uniaxial compressive, σ_c , and uniaxial tensile, σ_t , strengths:

$$\sigma_{1f} = \sigma_c \left(1 - \frac{\sigma_3}{\sigma_t}\right)^R$$

where R is a fitting constant. The USR is then defined as:

$$SF = \sigma_{1f} / \sigma_1$$

where σ_1 is the major principal stress (induced).

A complete discussion of the merits of this crack modelling approach is given by Carter (1992).

Laboratory tests discussed in Section 2.3 reveal that ultimate failure in laboratory testing is reached through a complicated process of crack initiation, propagation and coalescence. Further, a significant degradation of cohesive strength is noted as cracks begin to form and interact. Using InSight^{2D}, analysis of crack behaviour in a compressive stress field has progressed from the simple case of a single crack, to en echelon arrays of cracks, to multiple random crack arrays (Eberhardt, 1998). No studies, however, have used this program to examine crack initiation and propagation in mine roofs and prediction of the size of the developing instability.

In this thesis, the first model simulates single crack propagation in salt rock under uniaxial compression, followed by modelling under biaxial compression with a low confining pressure. These two conditions simulate the stress conditions near the underground openings. In the final model, the full mine opening at the Esterhazy mines is simulated and discrete fracture development in the roof is modelled.

Case Model 1 – Uniaxial Compression

Near underground openings the rock mass is subject to a stress state at or close to uniaxial compression. Thus a block model containing an elliptical crack under uniaxial compression is used to simulate this mining condition. The size of the model is 0.1 by 0.2 m. An initial elliptical crack of 5mm by 0.5 mm is created (Figure 3.19). The properties of salt rock assumed for this model were as follows:

Young's modulus E , 25 GPa

Poisson ratio ν , 0.32

Uniaxial compressive strength σ_c , 30 MPa

Tensile strength T_0 , 1.7 MPa

Rocker function R , 0.34

Plane stress conditions were employed in this model. The external stress imposed in the long-axial direction of the elliptical opening was gradually increased until failure occurred around the tip of the elliptical opening.

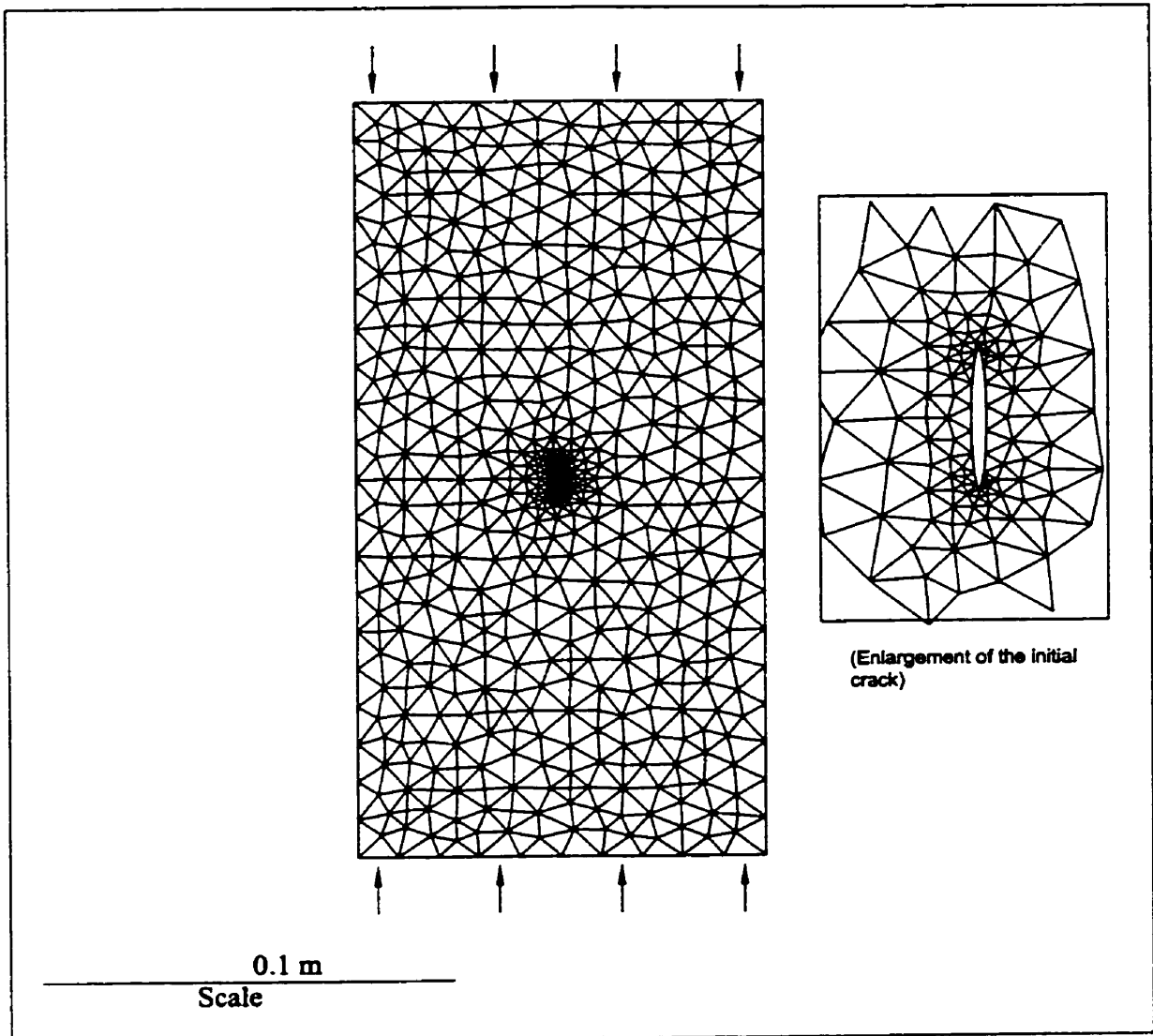


Figure 3.19 Finite element mesh of block under uniaxial compression

When the axial stress reached 18 MPa, a region with a safety factor (USR) less than unity was generated at the tip and a crack initiated (Figure 3.20). In addition, from the σ_3 contour (Figure 3.21) a tensile zone with $\sigma_3 < -1.0$ forms around the crack tip. It thus implies that the tensile stress exceeds the tensile strength at the tips and the crack tips will propagate.

The results from this analysis are comparable to the preceding analysis (Section 2.5) using the proposed Esterhazy damage criteria, i.e. damage of the rock mass in the roof of the potash mining rooms propagates when the deviatoric stress exceeds 18 MPa.

Case Model 2 – Triaxial Compression

In the mining environment, confining pressure increases from the room towards the interior of the rock mass. In order to simulate this condition for the Esterhazy mines, a small confining pressure was imposed on the block model by adding 0.5 MPa in the σ_3 and σ_2 (out-of-plane) directions (Figure 3.22). Both the applied out-of-plane stress and the intermediate principal stress were identical so as to avoid crack propagation in the out-of-plane direction. The maximum principal stress (axial) was increased until failure was predicted at the initial crack tip.

With the addition of this confinement to the block model, results show that when σ_1 increased to 40 MPa, a tensile zone ($\sigma_3 < -1.0$) formed around the crack tip (Figure 3.23). Compared to the uniaxial condition the stress level for crack initiation under triaxial loading is much higher.

Case Model 3 – Mine Opening

The mine opening used in the Phase² study was also adopted here. The tabular opening has a size of 20 m × 2.5 m, and the dimension of the external boundaries is 200 m × 200 m (Figure 3.24). An initial hydrostatic stress of 25 MPa was applied to the model.

Failure initiated at the upper corners of the opening (using the Rocker criterion) (Figure 3.25). An open crack of 1.7m in length was then inserted at the corners of the opening along the direction of σ_1 (Figure 3.26) and the model was run again. The new run

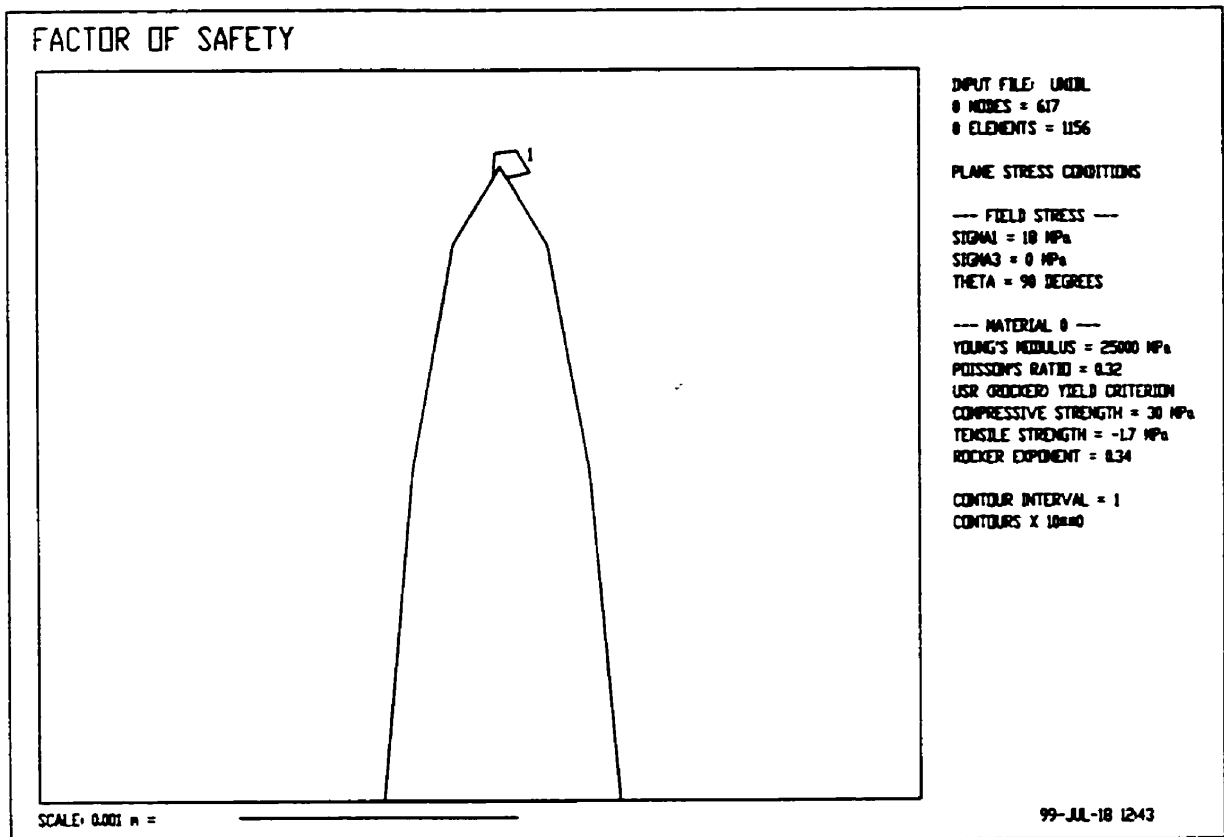


Figure 3.20 Factor of safety around the crack tip

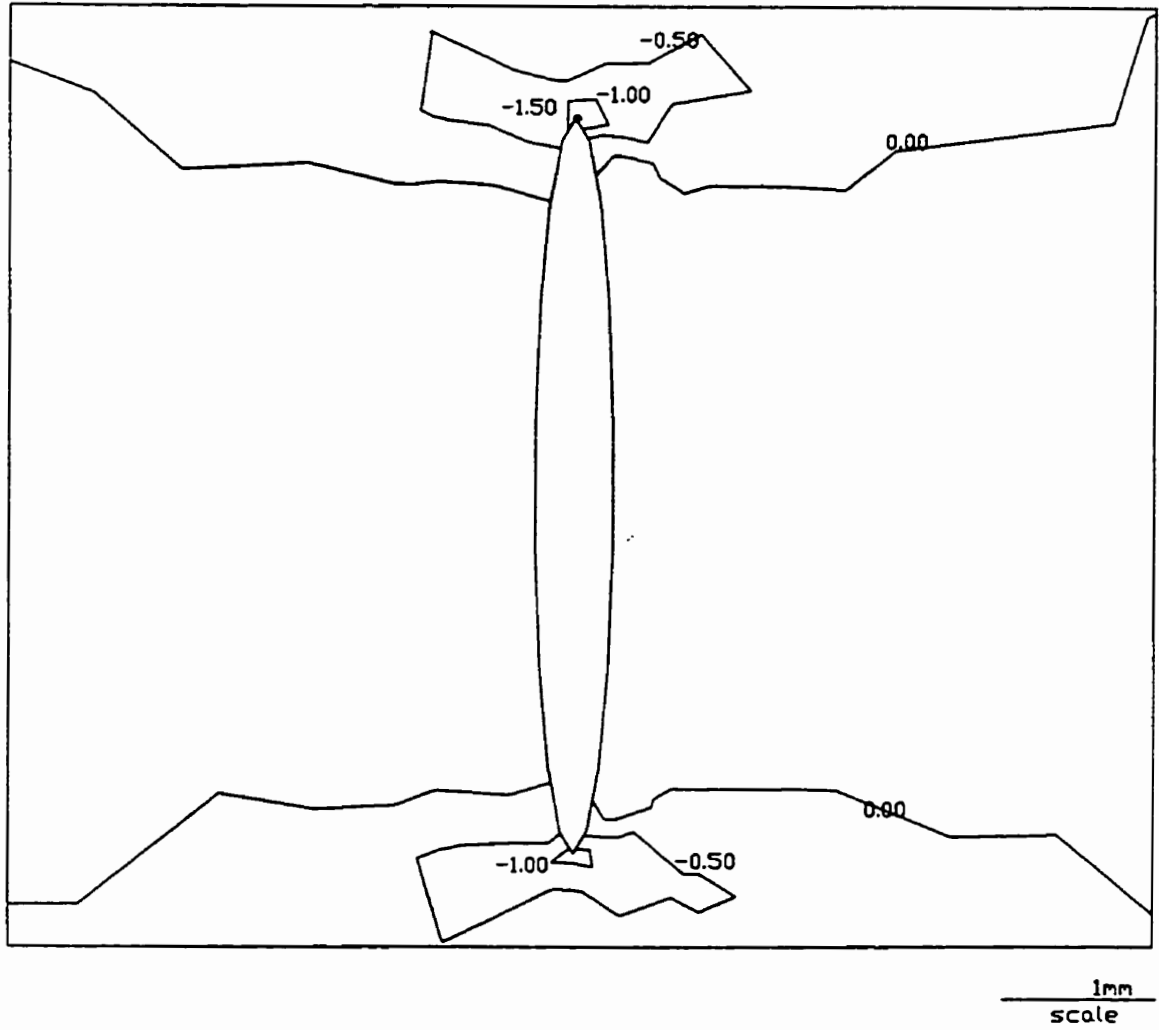


Figure 3.21 Contours of minimum principal stress (MPa)

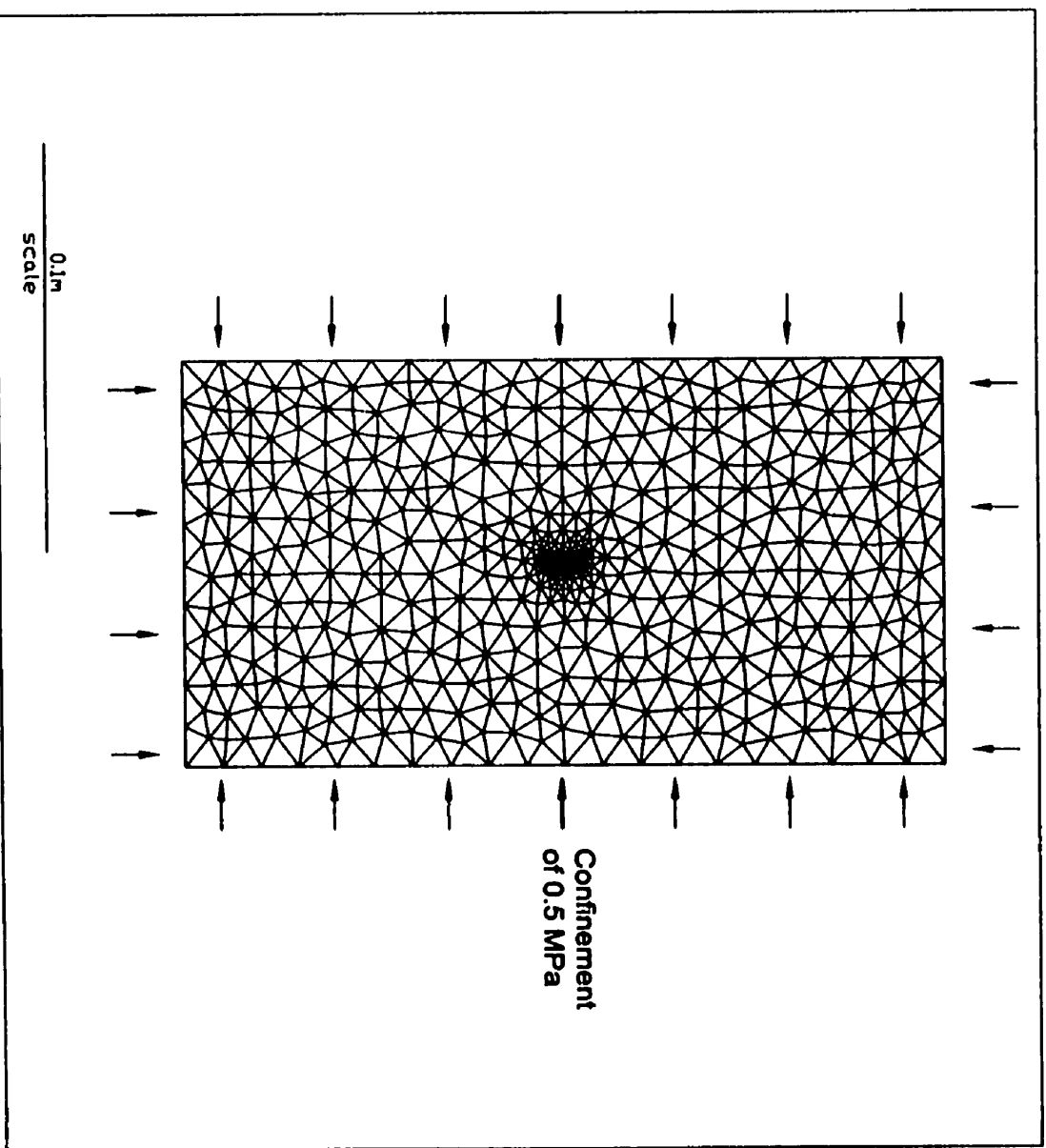


Figure 3.22 Finite element mesh of block under biaxial compression

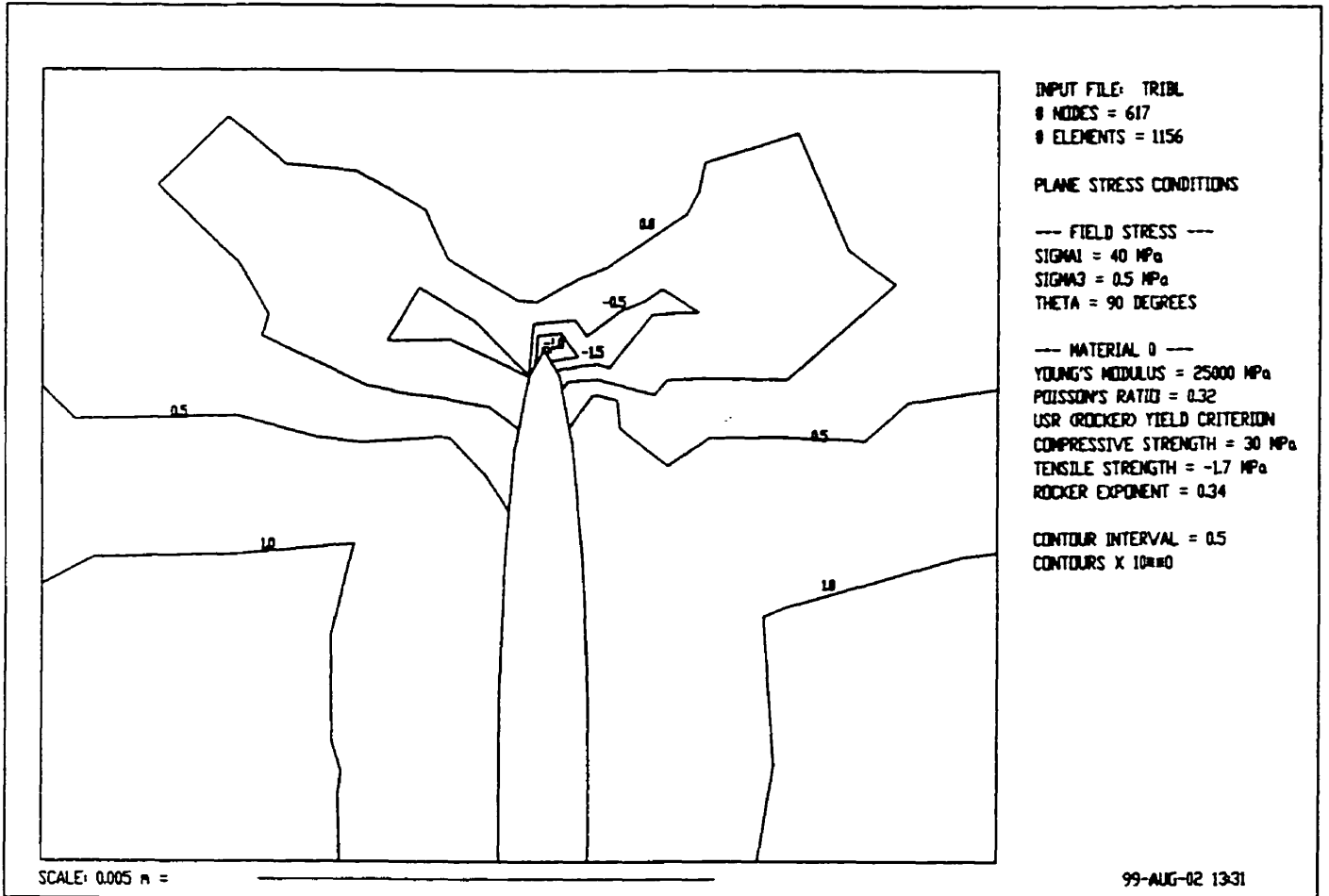


Figure 3.23 Contours of minimum principal stress

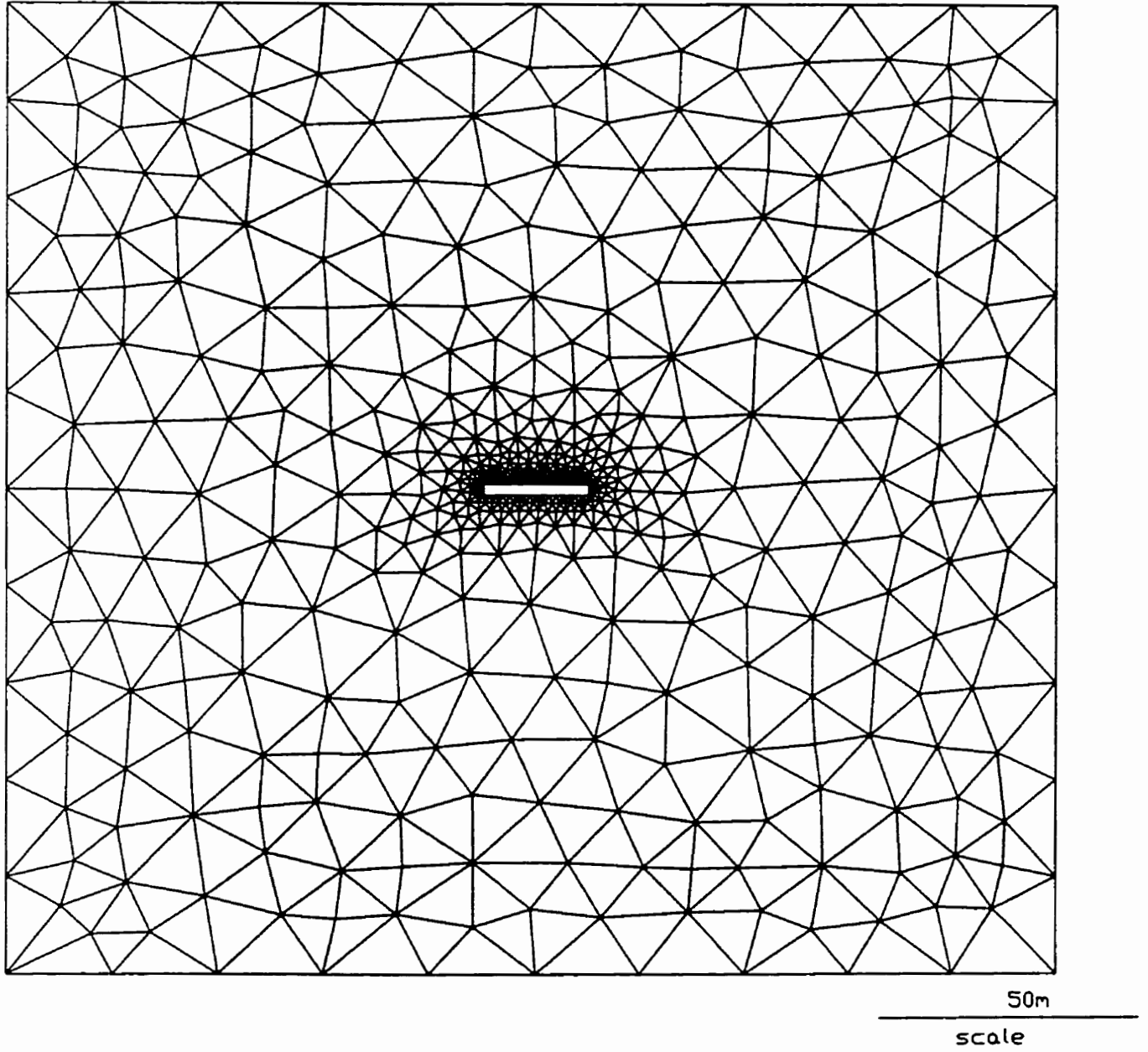


Figure 3.24 Finite element mesh for a tabular opening

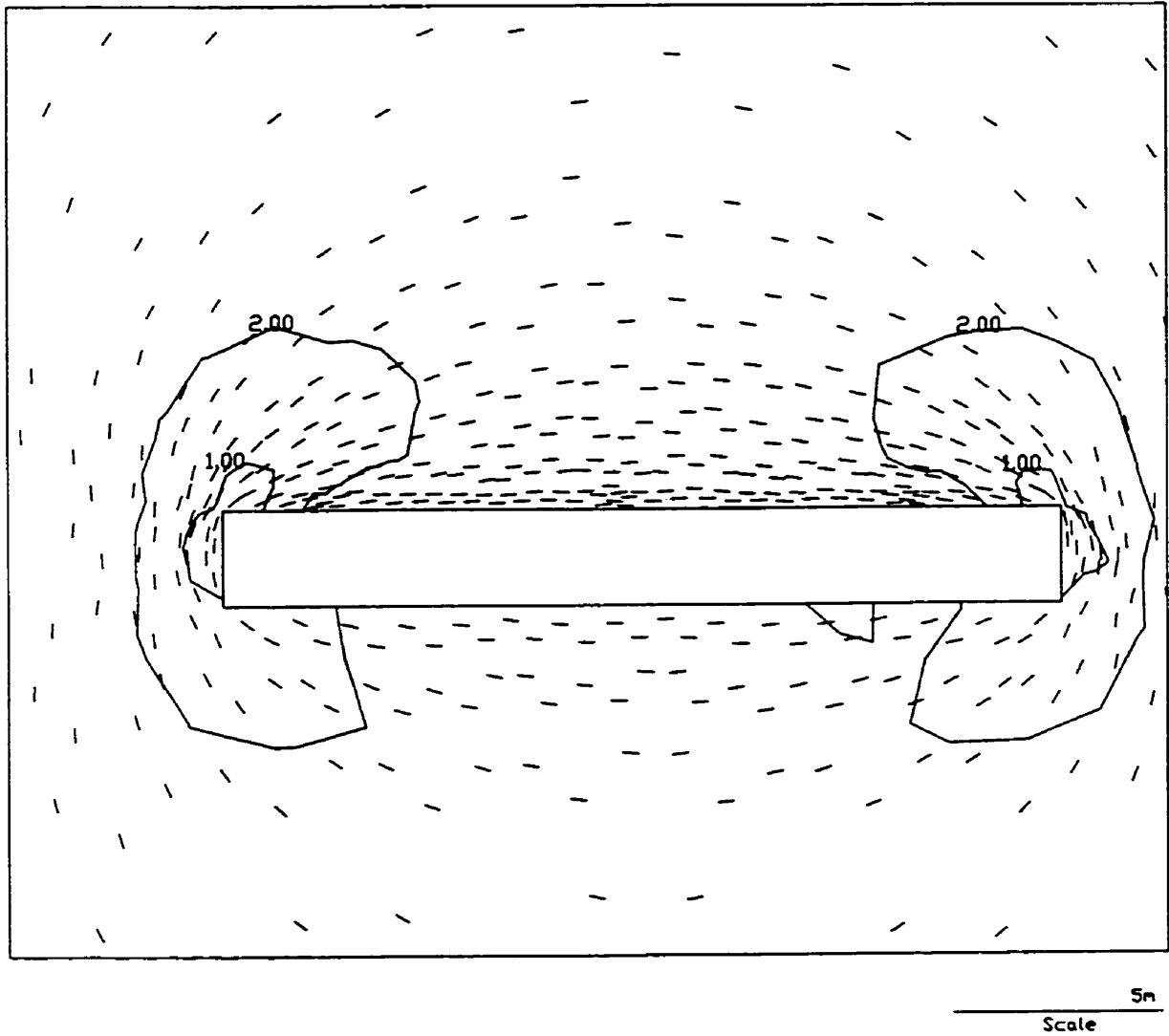


Figure 3.25 Contours of safety factor (USR yield criterion, $R=0.34$; the dash lines represent σ_1 directions)

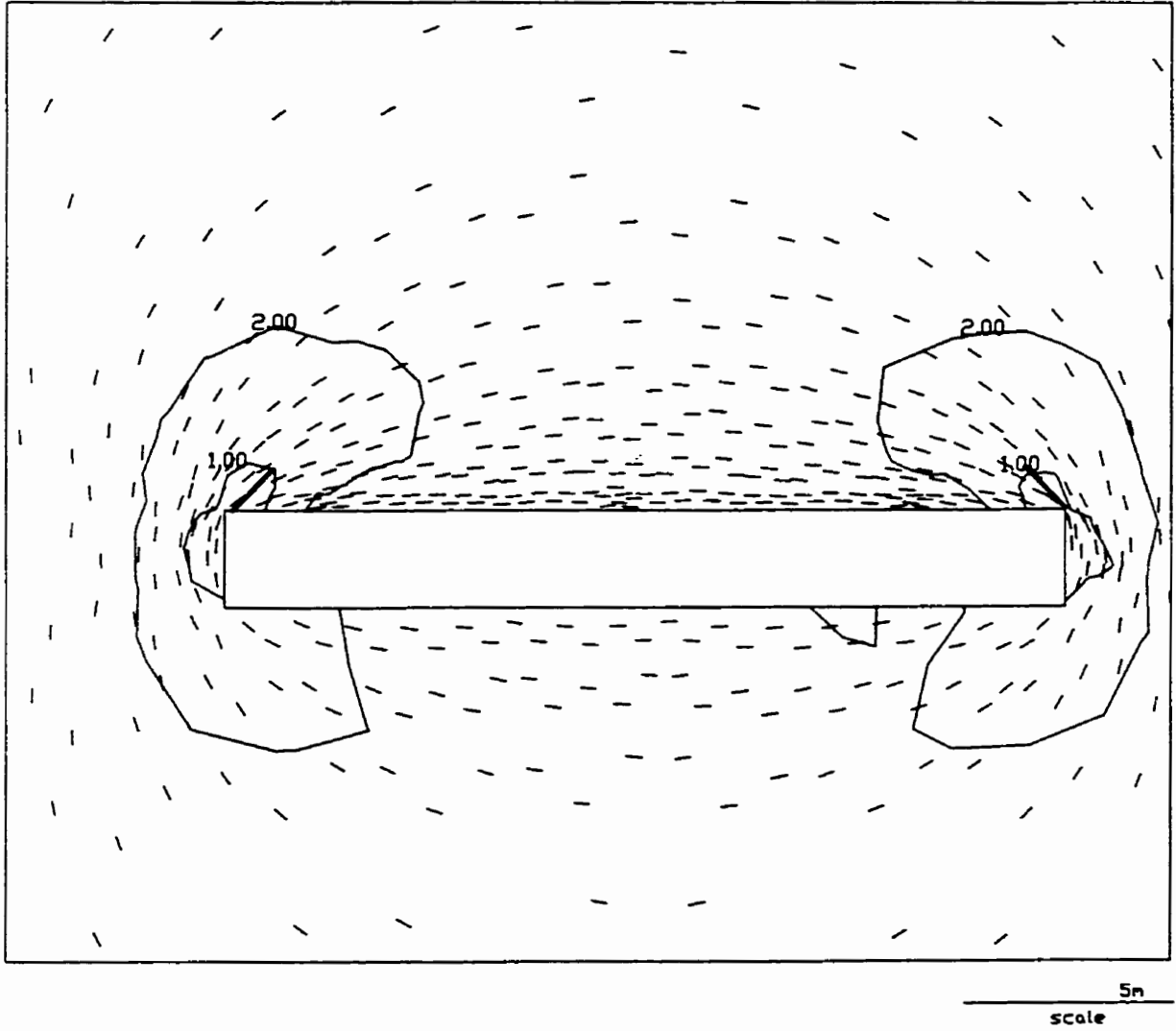


Figure 3.26 Introducing cracks in the failure region along σ_1 direction

predicted that the tensile stress around the crack is larger than the tensile strength of 1.7 MPa (Figure 3.27), which means that the crack will propagate further. A second crack was then introduced at the first crack tip and oriented in the σ_1 direction (Figure 3.28). Again, the safety factor around the tip of the second crack was still less than one (Figure 3.29a), and the tensile stress around the tip of the second crack was larger than the tensile strength 1.7Mpa (Figure 3.29b). The crack would therefore propagate further horizontally by following the σ_1 direction (Figure 3.29c). However, creation of the third crack and running the program could not continue as numerical errors occurred during the calculation procedure of the program InSight^{2D} for this next step and results were erroneous. Nevertheless, it was demonstrated that the initiation of discrete cracks above the edges of the opening induced a redistribution of stresses which led to progressive crack growth. Within the region beneath the crack the values of σ_3 are nearly zero or negative due to the effect of stress shielding by the cracks. This low stress zone is of a dome shape with a height of about 3.0 m above the opening and is under approximately uniaxial compression or tension.

The complete shape of cracking had the simulation been able to continue can be deduced by following a path along the σ_1 direction as shown in Figure 3.30. Compared to the *in situ* crack observation by borehole camera (Figures 2.7-2.11), the predicted zone of cracking matches the field data in both shape and size quite closely.

3.4 Discussion

These studies of discrete crack propagation using InSight^{2D} provide a much more satisfactory agreement with *in situ* observations than the stress-strength approach using Phase².

The complete propagation of the crack across the roof was not simulated because of the occurrence of numerical errors within the program. This difficulty may arise because, with the stresses compressive, a shear mode of failure might develop. A shear mode stress intensity factor, however, is not incorporated in InSight^{2D}. In addition, the damage/failure processes are more complicated than the ones simulated by this model. For example, additional cracks can develop by stepping off (en echelon) from the initial

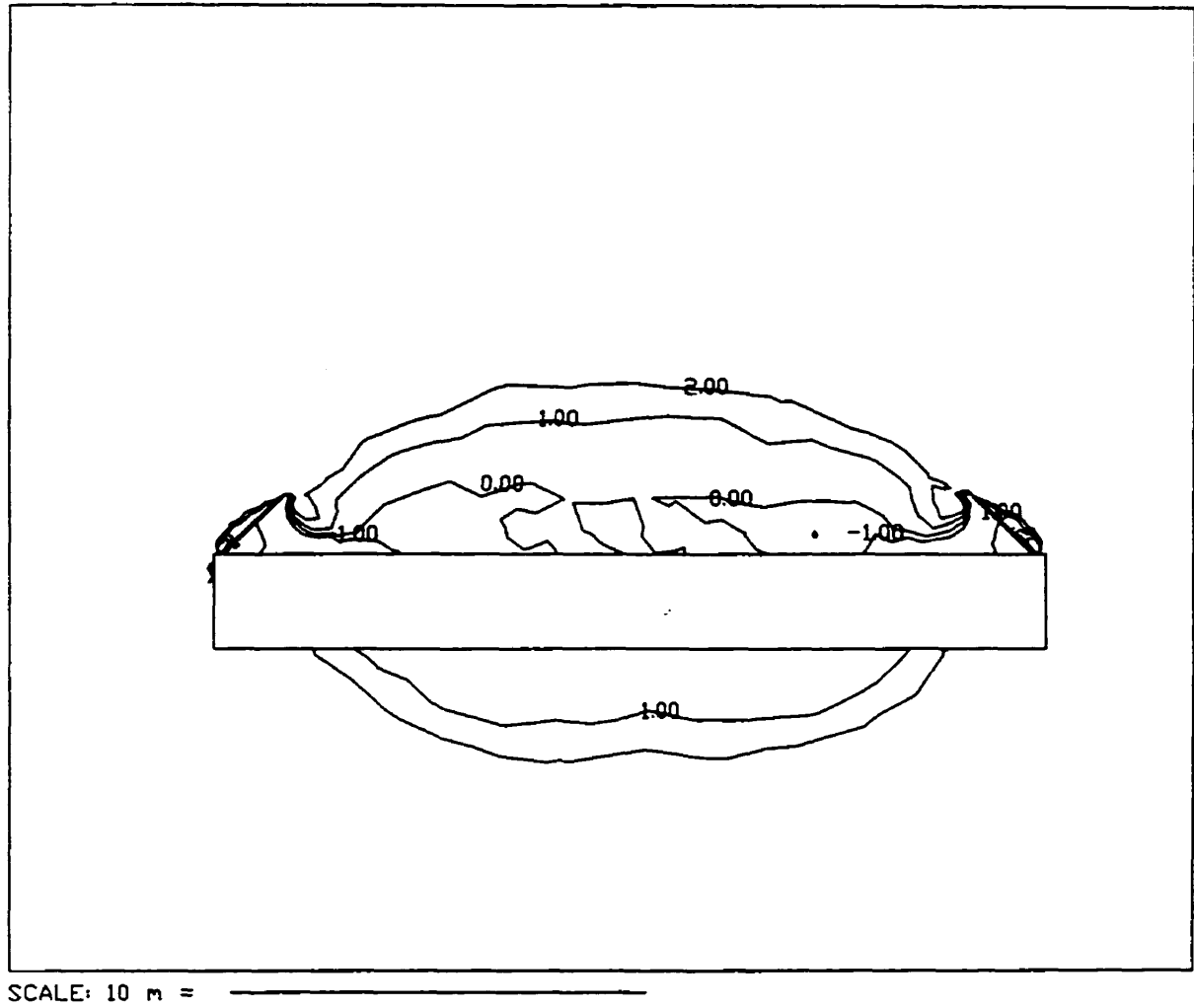


Figure 3.27 Contours of minimum principal stress (units in MPa)

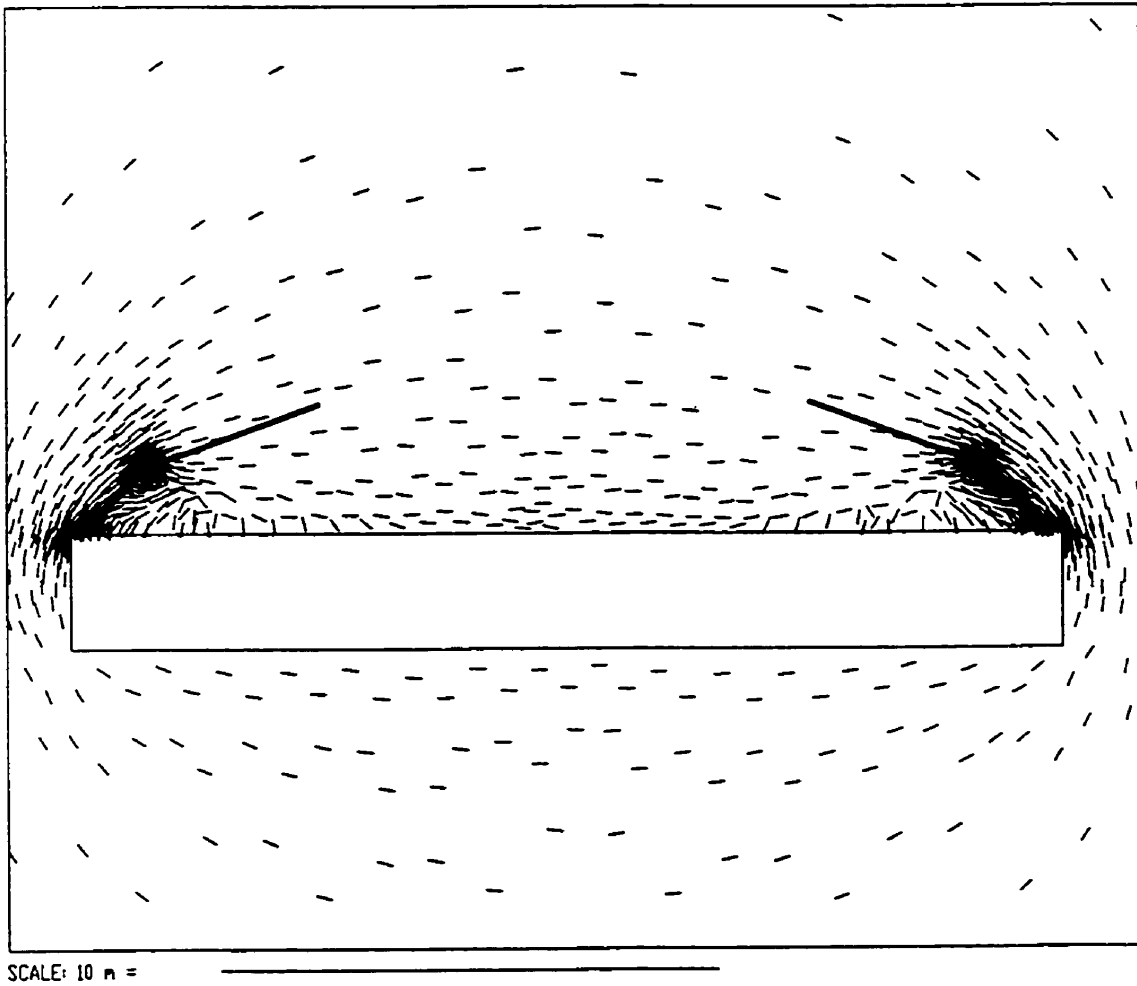


Figure 3.28 Introduction of the second cracks along the α_1 direction

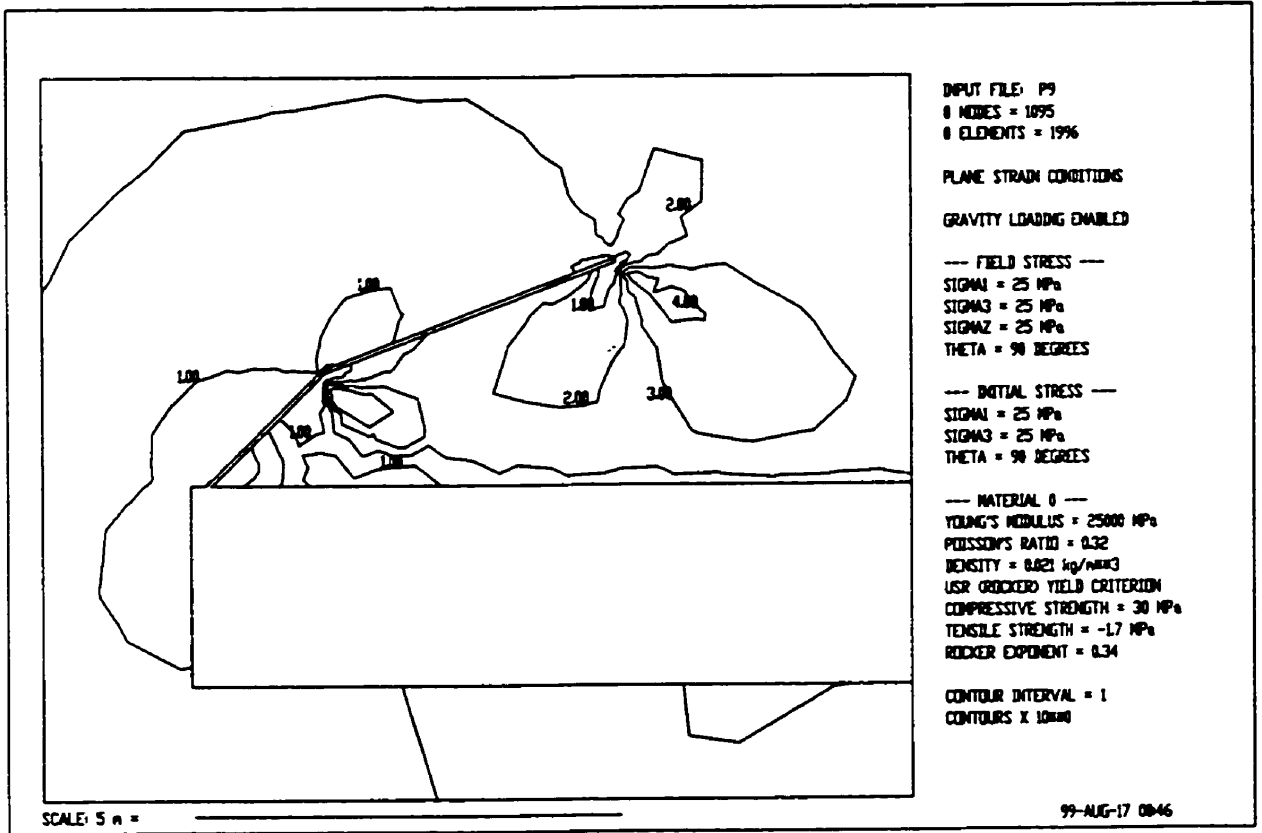


Figure 3.29a Contours of safety factor

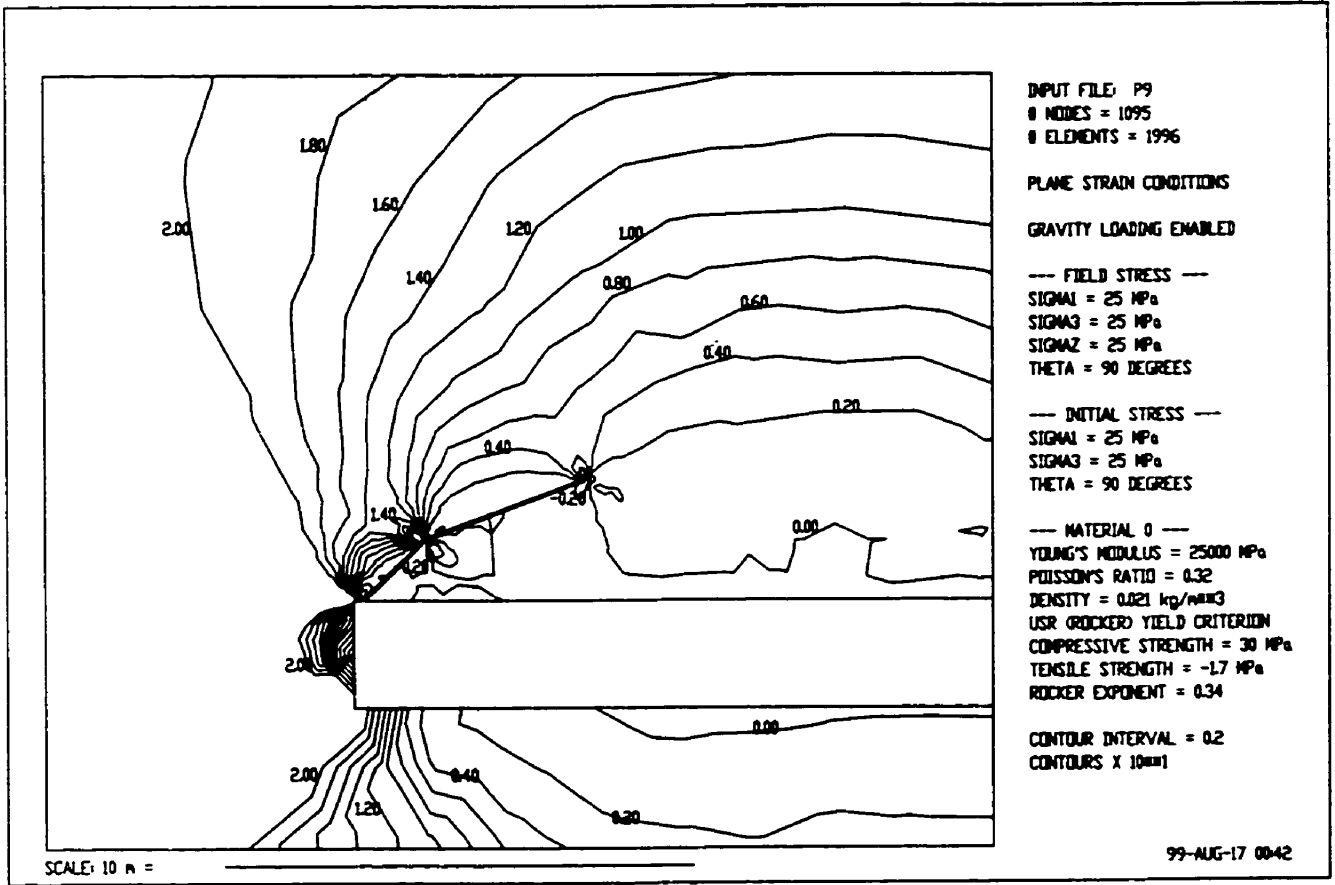


Figure 3.29b Contours of minimum principal stress (units in 10MPa)

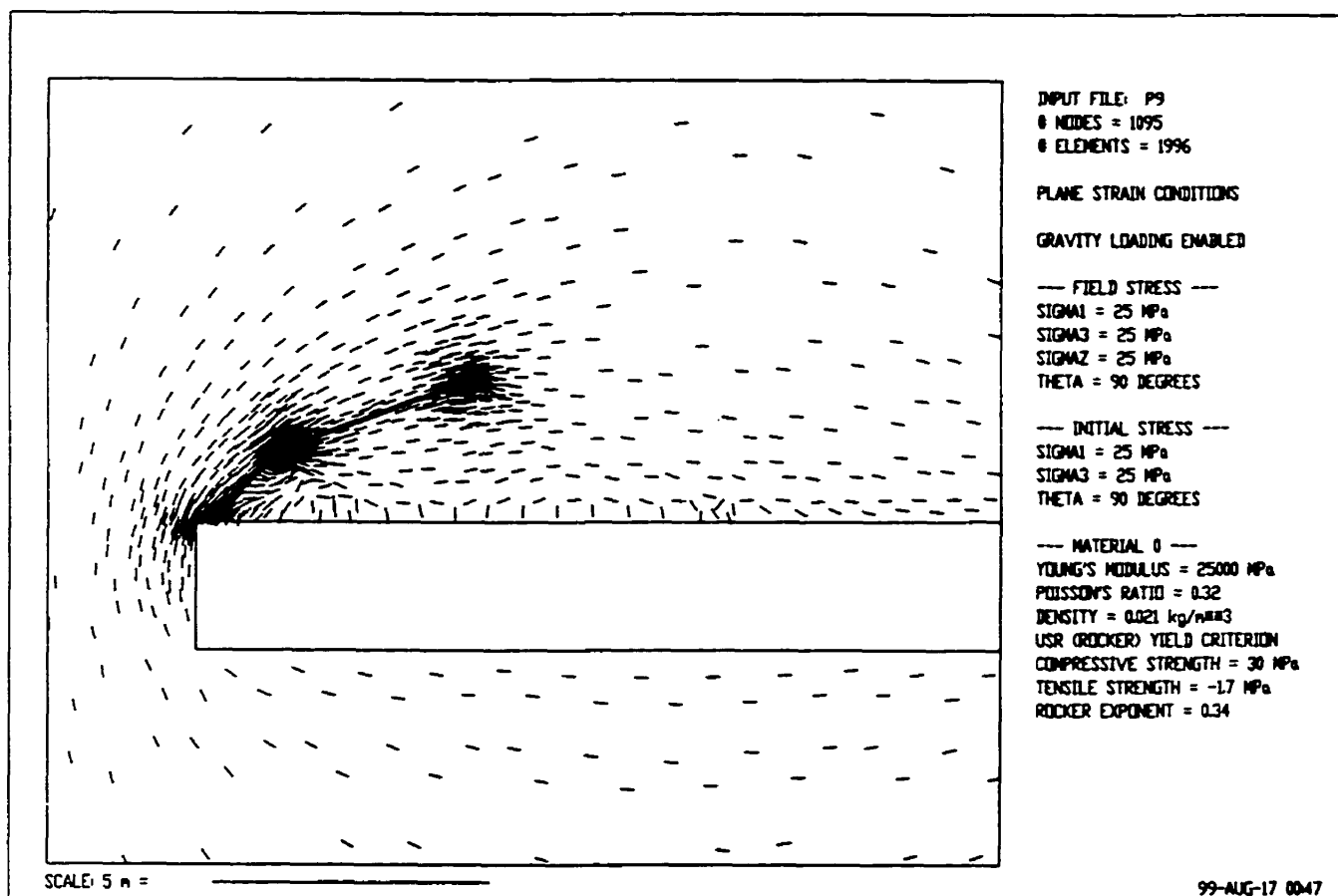


Figure 3.29c Trajectories of the maximum principal stress after the second crack is inserted

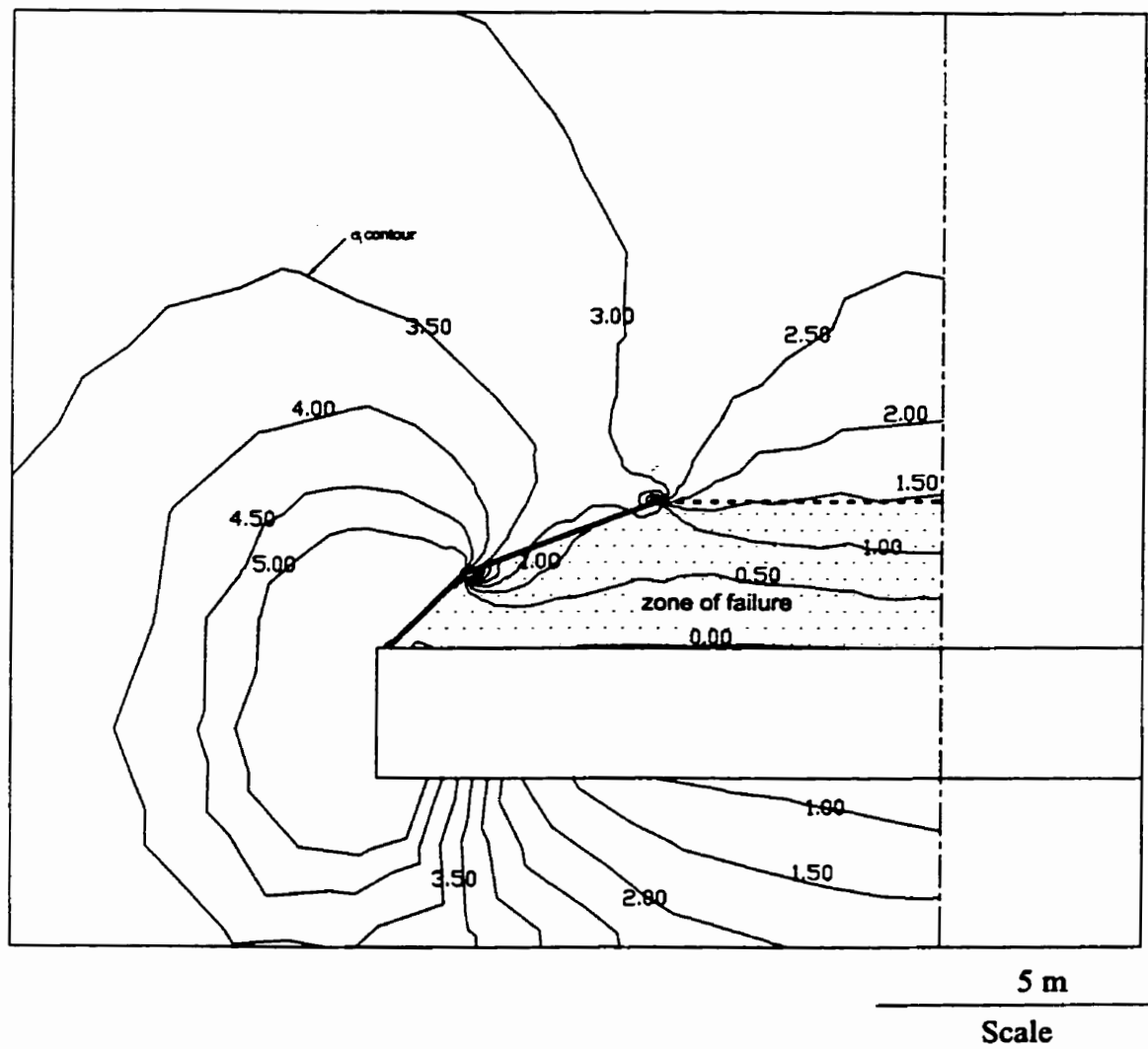


Figure 3.30 Deduced ultimate zone of failure

crack. The field observations indicate the presence of several cracks at different heights above the excavation.

As noted in Section 2.2, clay seams with a very small or zero tensile strength are a sedimentary feature in potash mines in Saskatchewan (Figure 2.4b). Propagation of cracks through the salt back from the edges of the opening might ultimately intersect a clay seam depending on the height of occurrence of the seam. The fracture would then follow along the clay seam (Figure 3.31).

3.5 Conclusions

Numerical modelling of the zones of damage/failure in the roof of an underground opening in a potash mine has been conducted. It was found that the proposed Esterhazy damage criterion is superior to the Hoek-Brown failure criterion and the Duncan failure criterion in that it can predict the zone of damage to some degree. Progressive failure, however, cannot be explicitly modelled. Modelling with InSight^{2D} overcomes this limitation in that discrete cracks can be simulated. The simulations predicted the growth of a dome shaped crack with initiation at the corners of the roof, and the height of the loosened zone of rock quite closely matched *in situ* measurements of cracks in potash mine roofs near Esterhazy, Saskatchewan.

None of the approaches agree perfectly with *in situ* observations. Possible reasons include:

1) Size Effect

The Esterhazy salt rock consists of coarse crystal grains. The strength parameters obtained from the laboratory testing may not represent the *in situ* salt rock mass due to the grain-size effect.

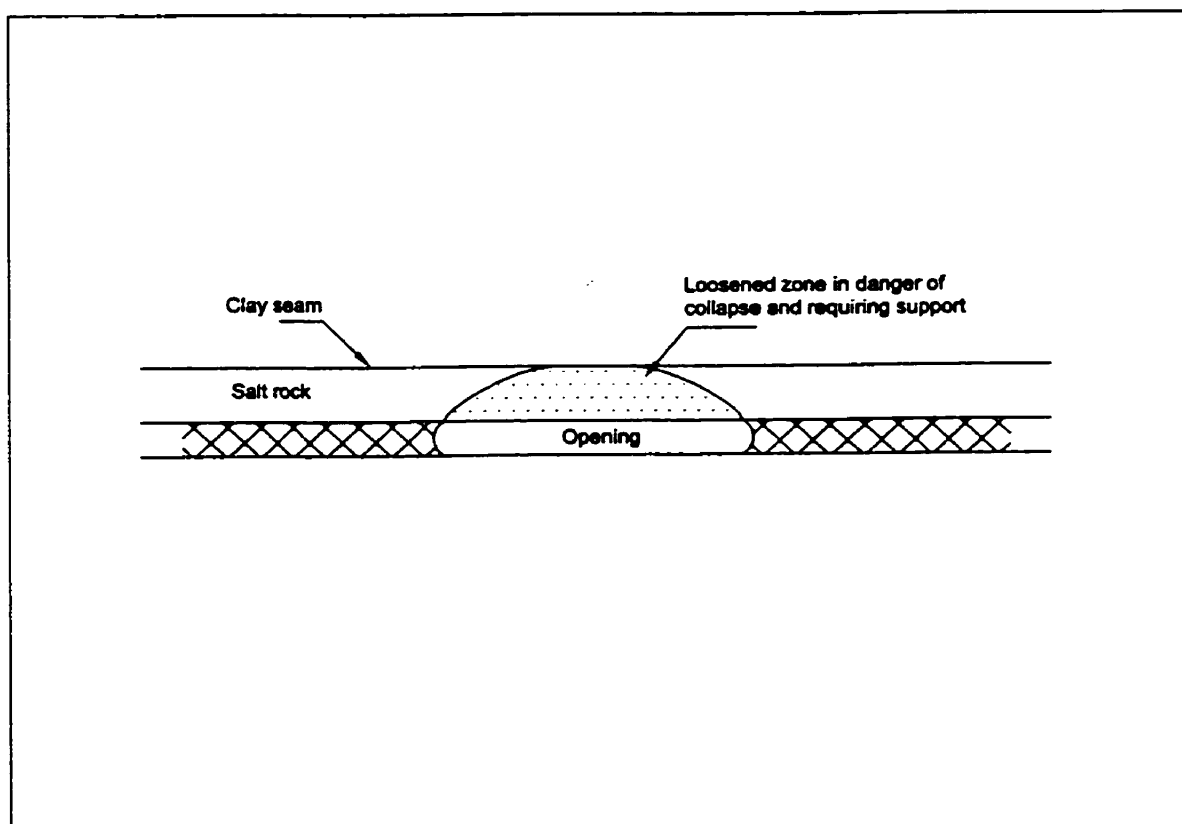


Figure 3.31 Conceptual sketch of the loosened zone in the roof

2) Loading Rate Effect

Studies of the behaviour of potash rock from the reverse loading triaxial tests by Chen (1993) show that potash behaviour under a reverse loading path is strongly rate dependent, reflected by the dependence of the initial deformational moduli, the ductile yield point, and post-peak behaviour on the rate at which the deviatoric stress was loaded to the specimen. The initial axial deformation moduli range from 29 GPa at the fastest stress rate to 12 GPa at the lowest stress rate. Lower stress rates correspond to higher ductility and higher stress rates correspond to lower ductility and greater brittleness. The discrepancy between the predictions and the field observations may arise partly from the selection of appropriate elastic constants and the critical points in the stress-strain curves that define the damage parameters.

3) Creep

Creep is an important phenomenon in potash mines. The numerical analyses in this study all assumed an elastic brittle behaviour, i.e. immediate, short term response.

4) Far Field Stresses

Since there are no measured *in situ* stresses available for the Esterhazy mines, the far-field stresses in the numerical models were assumed to be hydrostatic and equal to the overburden pressure. This is a reasonable assumption but it could be challenged.

5) Rock Mass Heterogeneity

The models have all assumed a uniform set of mechanical properties. In reality, the materials *in situ* vary in properties from point to point. Thus a crack may be stopped by stronger material and a new crack develop at a different location. This kind of multiple crack propagation which is seen in the field is very difficult to simulate numerically.

In closing this chapter, the height of the zone of “loosening” in the potash mine is predicted by a simple rock mass classification method. The RMR rating for the salt rock is 82 based on both field observations and laboratory testing. Therefore, the rock-load height is 3.2 m according to Unal’s (1983) empirical equation based on measurements from coal mines:

$$h_t = \left[\frac{100 - RMR}{100} \right] B$$

where B is the width of the underground opening. This agrees remarkably with field observations.

PART III JOINTED ROCK

Chapter 4 Stability of a Layered Roof

4.1 Introduction

Rock failure in massive rock, as described in the previous chapters, is governed by intact rock mass strength and stress levels. Also, in non-massive rock, planes of weakness such as joints, faults or other interfaces between different rock layers may not contribute much to failure in deep underground openings in conditions of high far field stresses. The movement along these weakness planes may be prohibited because discrete blocks intersected by the weakness interfaces have little kinematic freedom to allow translation and rotation. In contrast, failure of jointed rock masses around shallow openings is controlled by joints or other weakness planes, and stress levels are seldom of sufficient magnitude to fail the intact rock. Thus, a stress-strength analysis is no longer valid for such cases.

The prediction of the behaviour of jointed rock masses is a complex geomechanical problem. The rock mass may be jointed due to geological processes or by fractures induced by excavation. The engineer needs to determine whether the rock mass is stable or not, and if not, where the failure is likely to take place and its size. One widespread form of jointed rock mass is sedimentary strata which are dissected by cross-joints that intersect the bedding planes at large angles. The joints typically are confined within each bed (i.e. the joints are discontinuous and limited in length to the thickness of the bed) and are usually more closely spaced in thin beds than in thick beds.

The design of openings in horizontally layered sedimentary strata has traditionally been based on concepts of continuous elastic solid mechanics. Linear elastic beam theory assumes that the rock in the immediate roof behaves as a series of continuous beams or plates loaded by their own weight. The roof span is then designed for a specified allowable tensile strength of the rock. However, observations show that roof strata,

although cracked transversely, resist bending moments larger than those evaluated by linear elastic analysis (Economopoulos et al, 1994). Thus, discontinuous beam models were developed, of which the voussoir beam theory is the most important. It recognizes that in a horizontally confined situation the ultimate strength of a voussoir beam is larger than the modulus of rupture as predicted by classical beam theory. The beam, which is fractured vertically by zero tensile strength joints, may be able to carry its own weight by arching. The term “arching” refers to the process by which fractured rock becomes self-supporting by the development of a compression zone above an opening and by load transfer to the abutments on each side.

Four possible failure modes (Figure 4.1) for a single bed were proposed by Sterling (1980) based on physical modelling studies of the voussoir beam mechanism:

- (1) shear sliding along the vertical joints at the abutment
- (2) snapping through without localized failure of the beam material
- (3) crushing in high stress areas, snap through
- (4) diagonal cracking across the constituent blocks

Physical models consisting of horizontal roof layers with vertical, rough cross-joints were built by Stimpson (1989). For the particular opening geometry (rectangular) and boundary conditions (no lateral constraints) used, the ultimate collapse was by a mechanism of 2-hinge failure, in which a central portion of the roof displaces vertically by pivoting about two hinges (Figure 4.2). This collapse mechanism develops by progressive crushing at two pivot points on each hinge block as the central roof block displaces vertically. Crushing is assumed to occur when the uniaxial compressive strength of the material is reached at the pivot points. Crushing occurs initially at the top of the beam and then progresses vertically downwards as horizontal thrusts are redistributed. Sudden collapse occurs when the sense of rotation of the moments generated by the horizontal thrust reverses, i.e. stabilizing moments become destabilizing moments. Stimpson (1989) developed a mathematical model of this mechanism.

Although analytical solutions have been achieved and important insights thereby gained into the stability of jointed beams, they are unable to handle complex geological

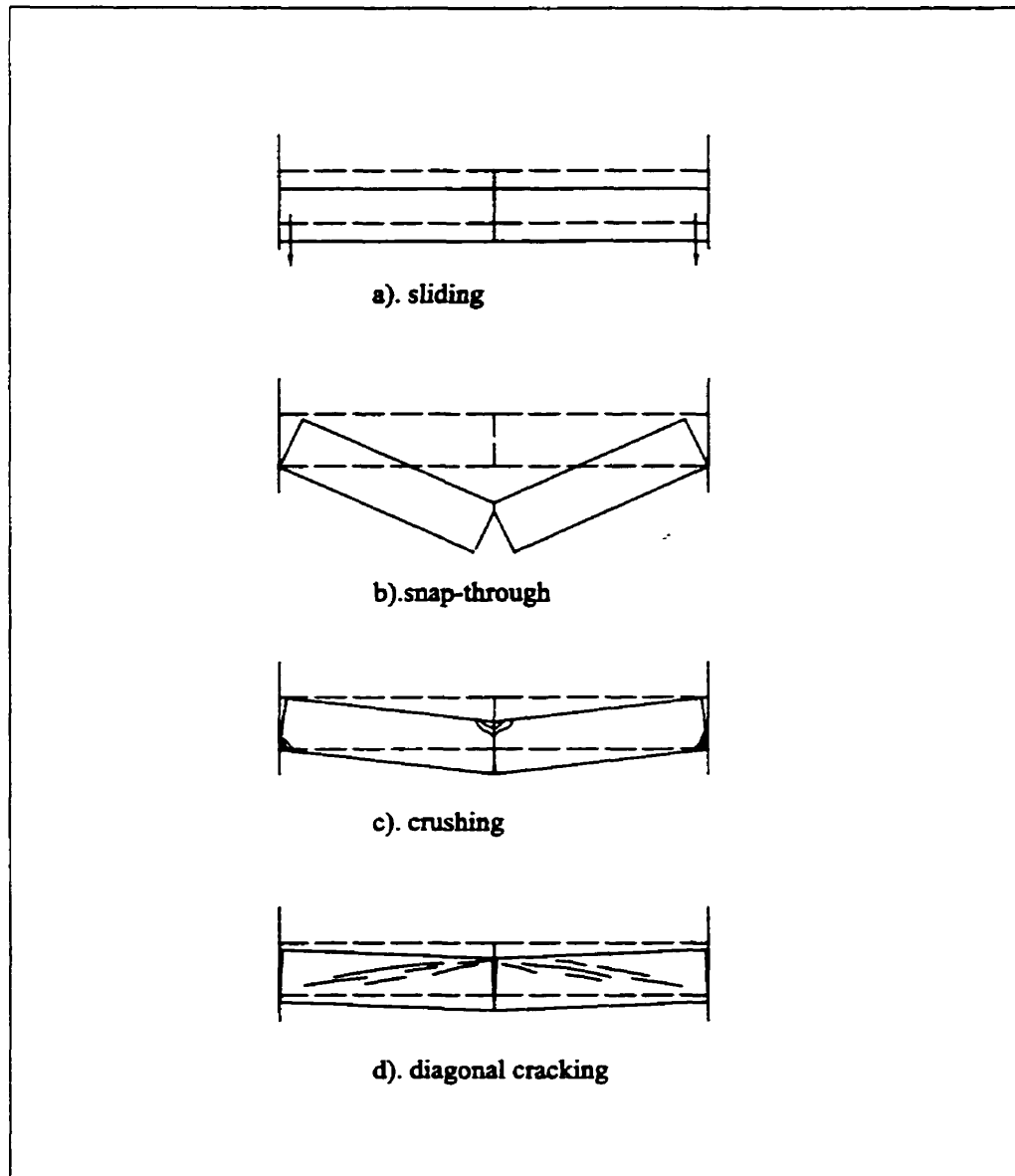


Figure 4.1 Four failure modes of voussoir beams
(after Sterling, 1980)

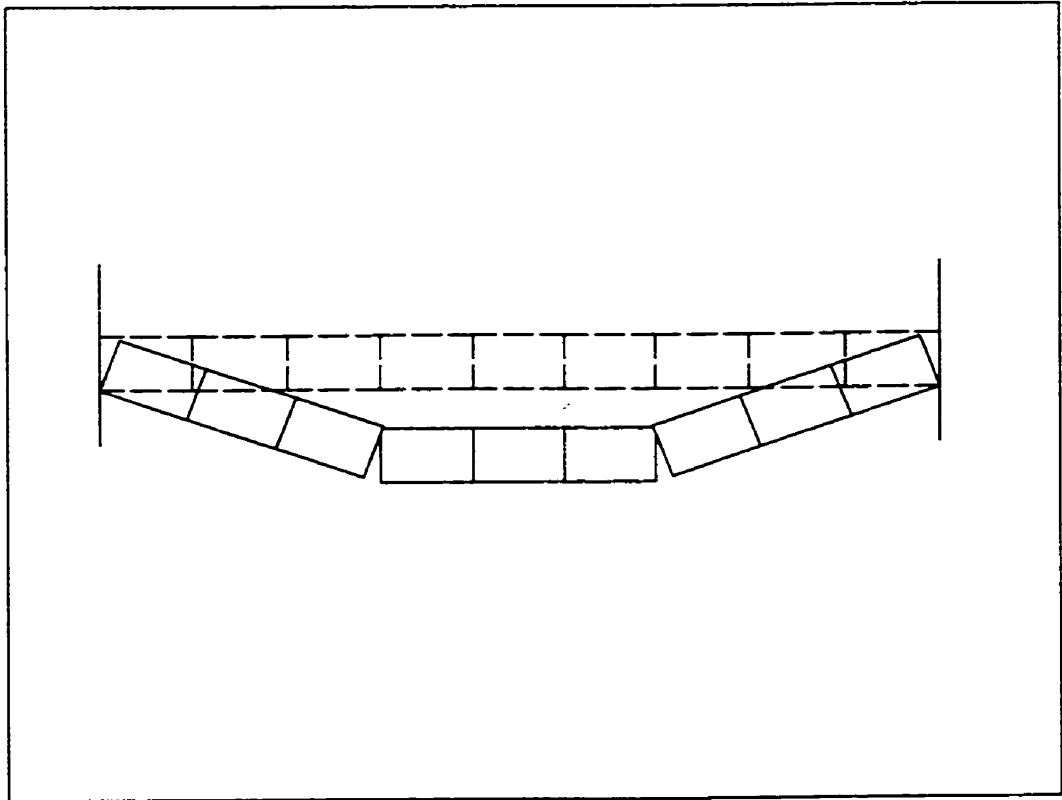


Figure 4.2 Two-hinge failure model (after Stimpson 1989)

conditions. What is needed is a method which can simulate and model large displacements (i.e. separation of bedded layers/joints and detachment of rock blocks from the rock mass). The distinct element method (UDEC) is such a tool and can be used to determine and analyze failure mechanisms and to conduct stability analyses. Because the behaviour of a jointed rock mass is highly sensitive to the locations, orientations and mechanical properties of the joints, the distinct element method is valuable for studying the sensitivity of failure mechanisms to these characteristics. This paper describes studies of the deformation and collapse of layered strata with joints using UDEC.

4.2 The UDEC Model

There are three main approaches to modelling a jointed rock mass with numerical methods (Desai and Giod, 1990). One approach consists of a direct numerical procedure in which joints and intact material are modelled explicitly. In the second, jointing is included implicitly in an “equivalent continuum” model; joint spacing is assumed to be small compared with system dimensions. Finally, generalized continuum formulations retain the length scale of jointing in the model.

The direct explicit technique is the key feature of the universal distinct element code (UDEC). It is ideally suited to modelling a jointed rock mass where the deformation mechanisms are dominated by block separation, rotation and slip, and where large relative motions may occur.

The advantages of the explicit technique are simple numerical realization and the relatively small amount of computer memory needed. However, the limitations imposed on the time step for computational stability may result in large computation times. Nonetheless, the explicit integration technique is the more favored method for modelling progressive failure of blocky rock mass.

With UDEC, blocks may be modelled as either rigid or deformable materials. Deformable blocks are subdivided into a mesh of finite elements, with each element behaving according to prescribed linear or nonlinear stress-strain constitutive relationships. The relative motions of the blocks along discontinuities are also governed by prescribed linear or nonlinear force-displacement relationships (springs) for

movement in both the normal and shear directions (Itasca 1996). UDEC uses time-marching, finite-difference schemes to solve the force equations of motion in the system.

4.3 Simulation Using Rigid Block Models

UDEC was applied to the problem of the stability of a rectangular opening excavated in a rock mass comprised of horizontal layers of equal thickness intersected by equally spaced vertical cross-joints.

Sensitivity studies were conducted on these model geometries to determine the effects on failure modes of spacing of joints, the span of the underground openings, dimensions of block, and the friction angle of the block surface. The following parameters were kept constant except as otherwise indicated:

Density of material: 2800 kg/m^3

Normal stiffness of joints: $4 \times 10^9 \text{ N/m}$

Shear stiffness of joints: $4 \times 10^9 \text{ N/m}$

Friction angle of joints: 40°

The blocks along the vertical abutments and along the base of the model were fixed in both horizontal and vertical directions.

Generally, the kinematic degrees of freedom for the rigid blocks include translation and rotation and it is noted that displacements of rock blocks are localized near the opening. In some of the simulations, large displacements of blocks in the roof led to ultimate collapse. In other models stable arching developed above the opening.

Effect of Joint Spacing

The effect of joint spacing was studied by keeping the thickness of the layers constant while changing the spacing of the vertical joints. With widely spaced vertical joints relative to span, the roof layers fail by shear failure along vertical joints at the abutments

(Figure 4.3a). With more closely-spaced joints, the roof fails by buckling and layer separation in an upwards progression from the opening (Figure 4.3b).

Effect of Opening Span

The effect of span was studied by continuously changing the span of the opening while keeping the size of blocks unchanged in a series of computer simulations.

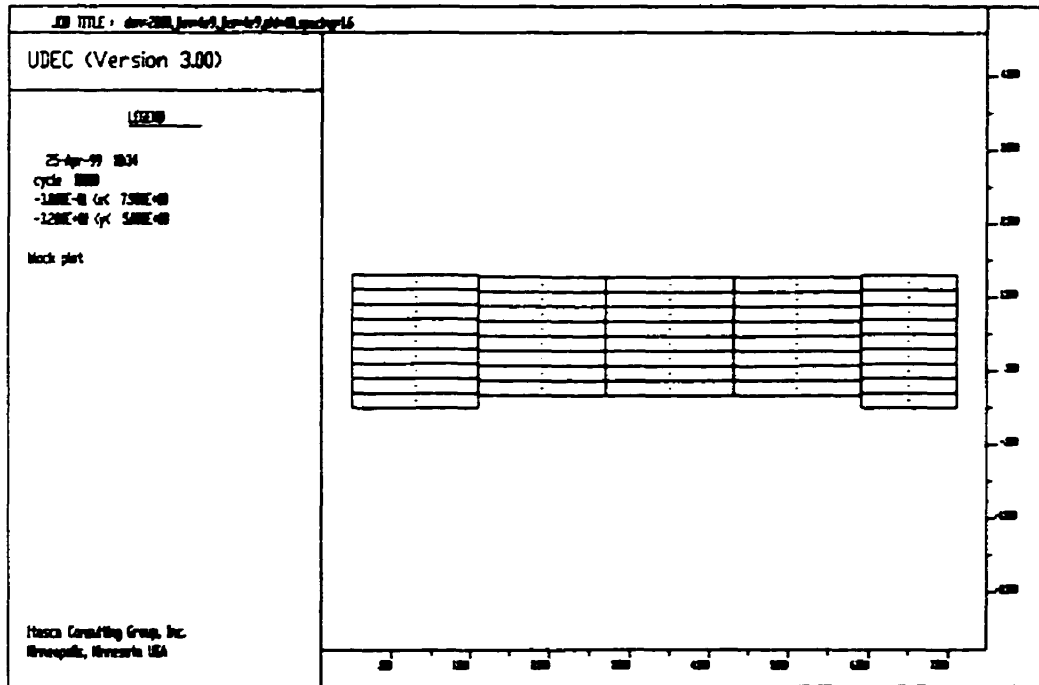
When the span is small, the roof fails by shear along the abutments (Figure 4.4a). With increasing span, rotation of blocks, layer separation, in addition to shear along joints, is observed. The rock mass in the roof eventually develops an arching mechanism, and the roof becomes self-stabilized (Figure 4.4b). When the span is large, the movement of layers is mainly by rotation. The roof ultimately fails in buckling by development of hinges at the middle of the roof and at the abutments (Figure 4.4c).

Effect of Friction Angle

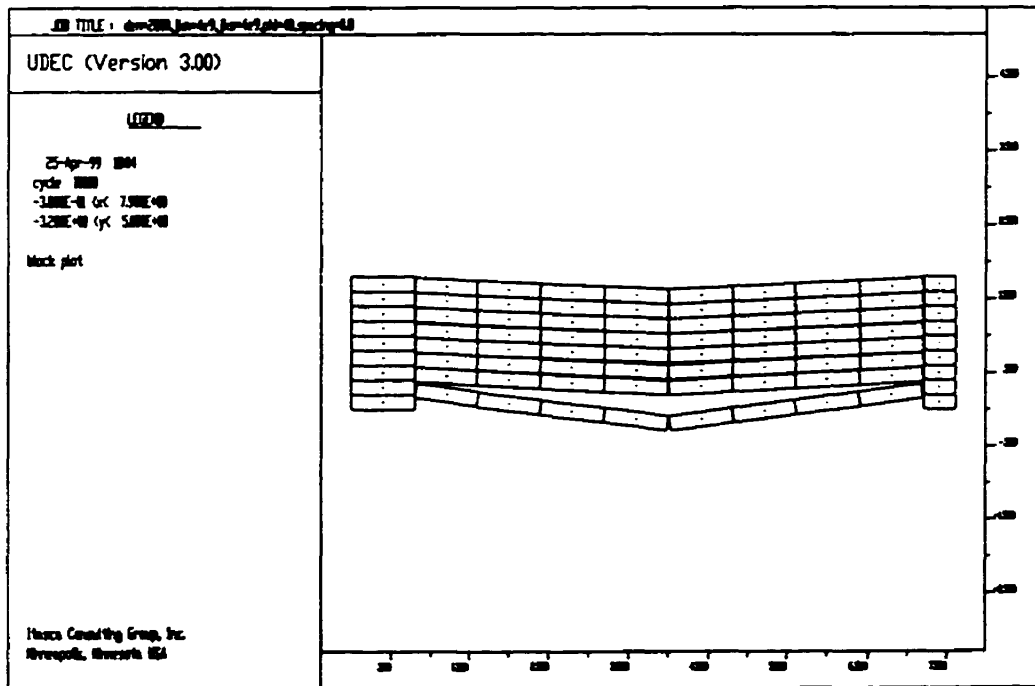
When the friction angle of joints is low, roof failure results from shear failure along the abutments (Figure 4.5a). As the joint friction angle increases, deformation is characterized by opening of joints, individual separation of layers, and buckling failure. For buckling failure, if the number of blocks in the roof is even, failure takes place by a single hinge mechanism (Figure 4.5b) and if the number of blocks in the back is odd, the double-hinged failure mode occurs (Figure 4.5c).

Effect of Dimension of Block

Several block sizes were used to study the dimension effect on failure modes. The width-to-height ratios of block varied from 5 to 0.5. It is shown that when the ratio of width to height is large (i.e. ratio of 5), failure is governed by the double-hinged failure mode (Figures 4.6a and 4.6b). With decrease of the ratio, either partial layer separation or vertical displacement along the abutments takes place, with the roof eventually reaching



a) spacing 1.6m



b) spacing 0.8m

Figure 4.3 Effect of joint spacing on failure modes

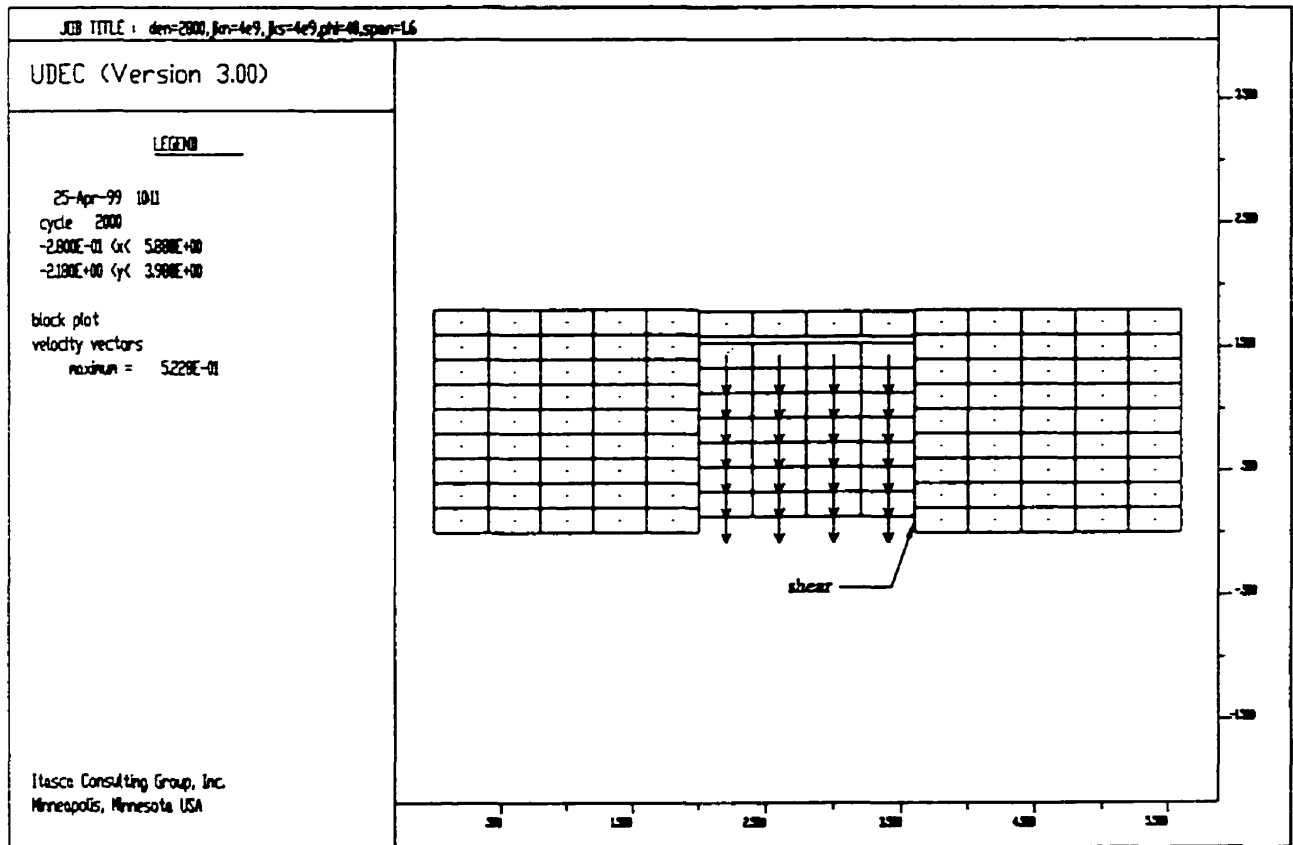


Figure 4.4a Effect of span on the failure modes
 (span 1.6m, arrows are velocity vectors)

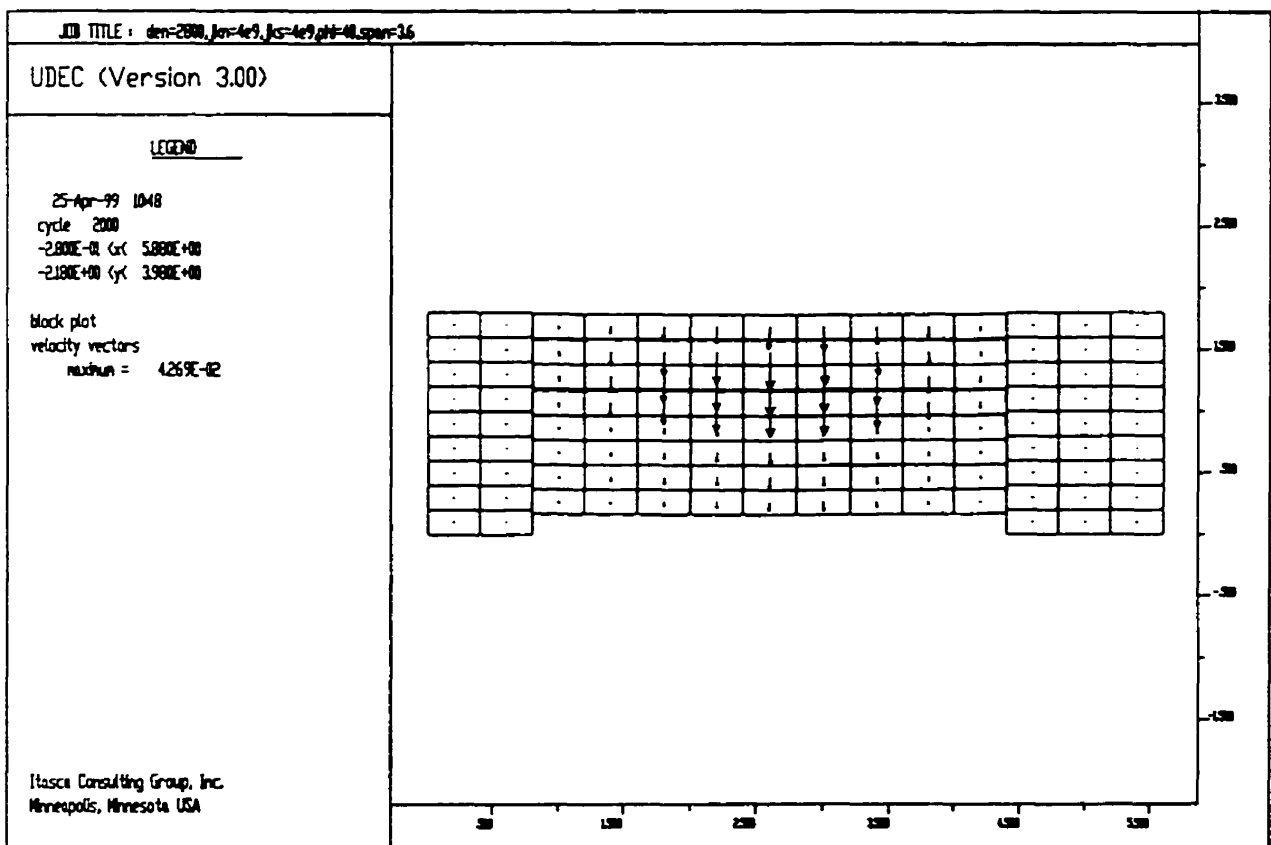


Figure 4.4b Effect of span on the failure modes (span 3.6m)

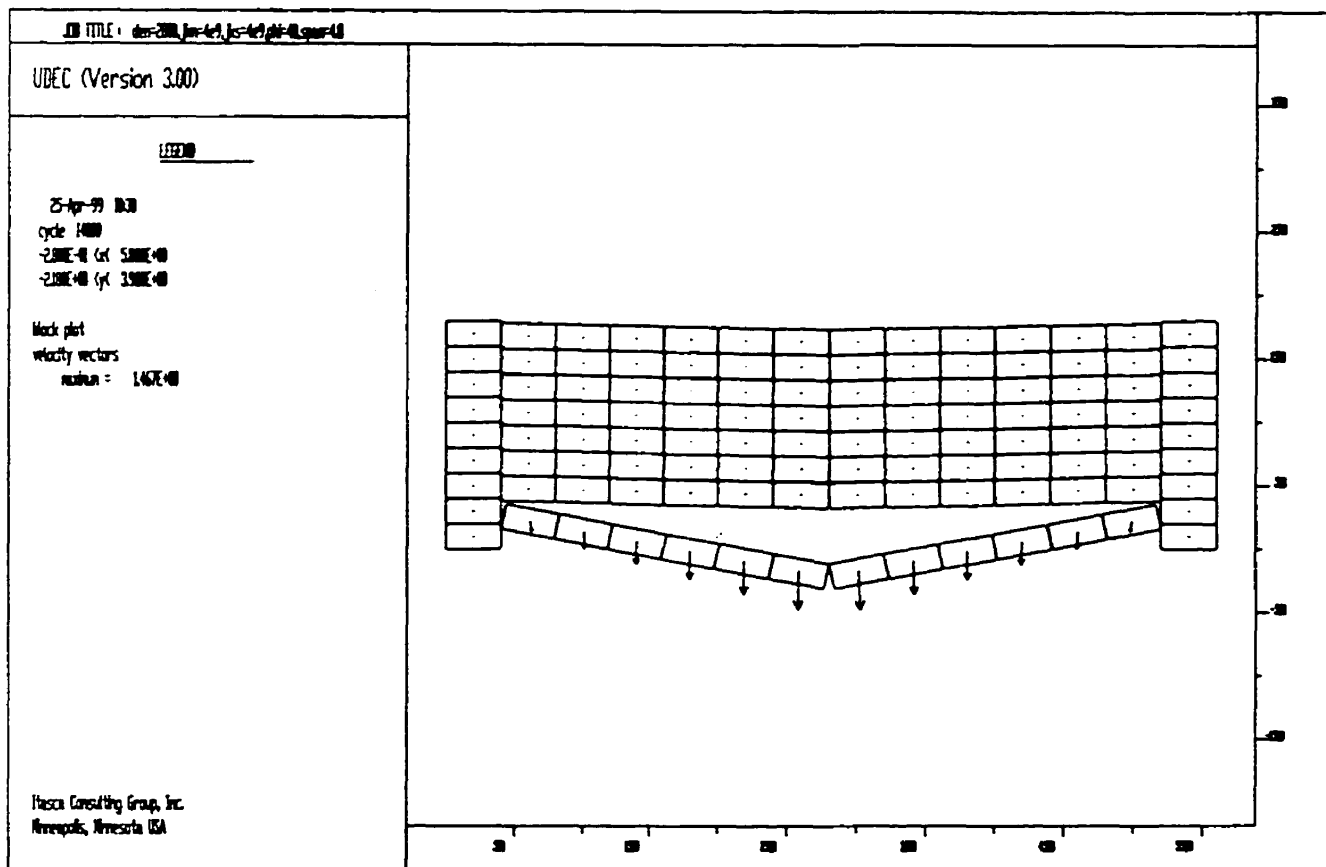


Figure 4.4c Effect of span on the failure modes (span 4.8m)

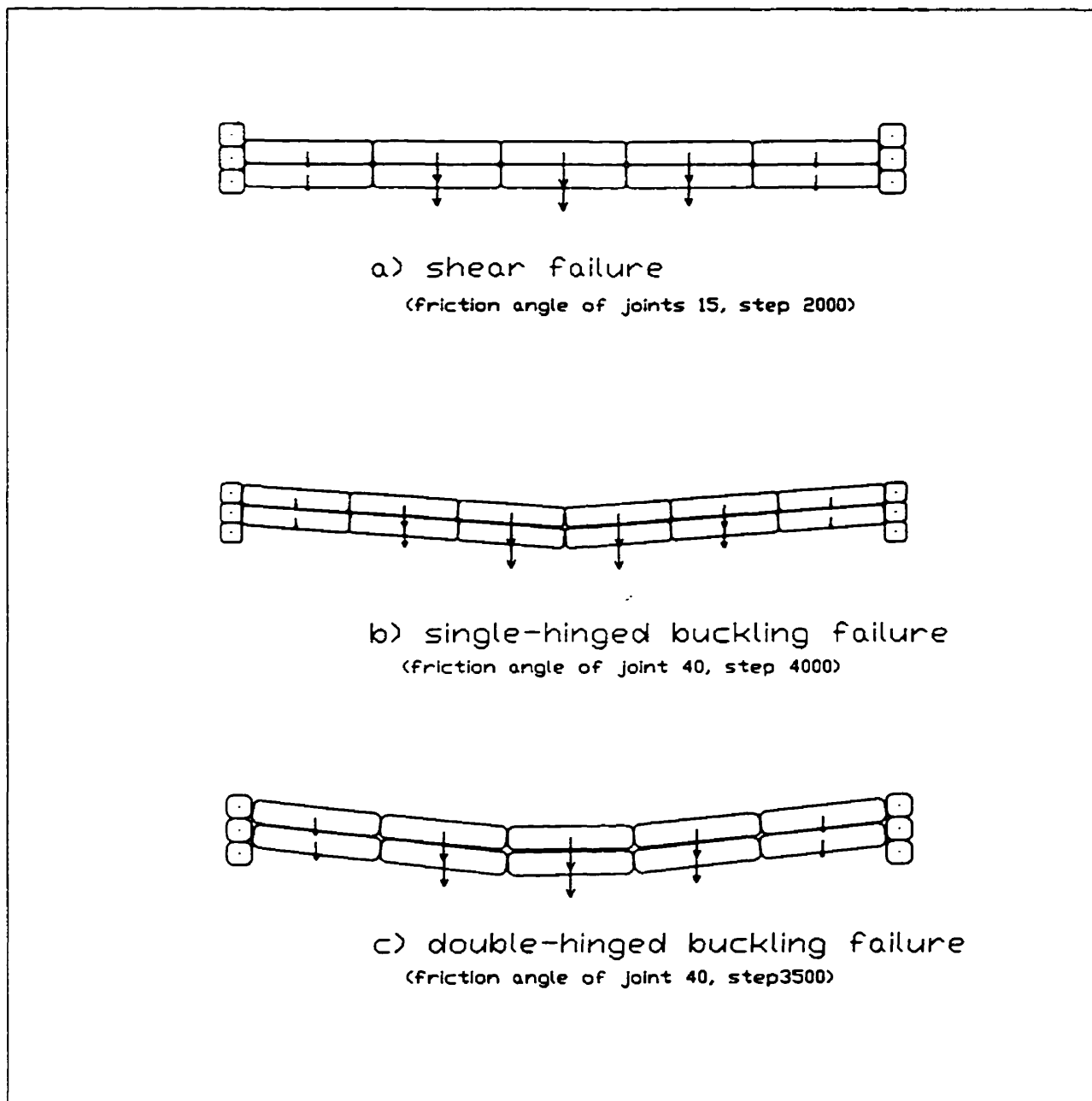
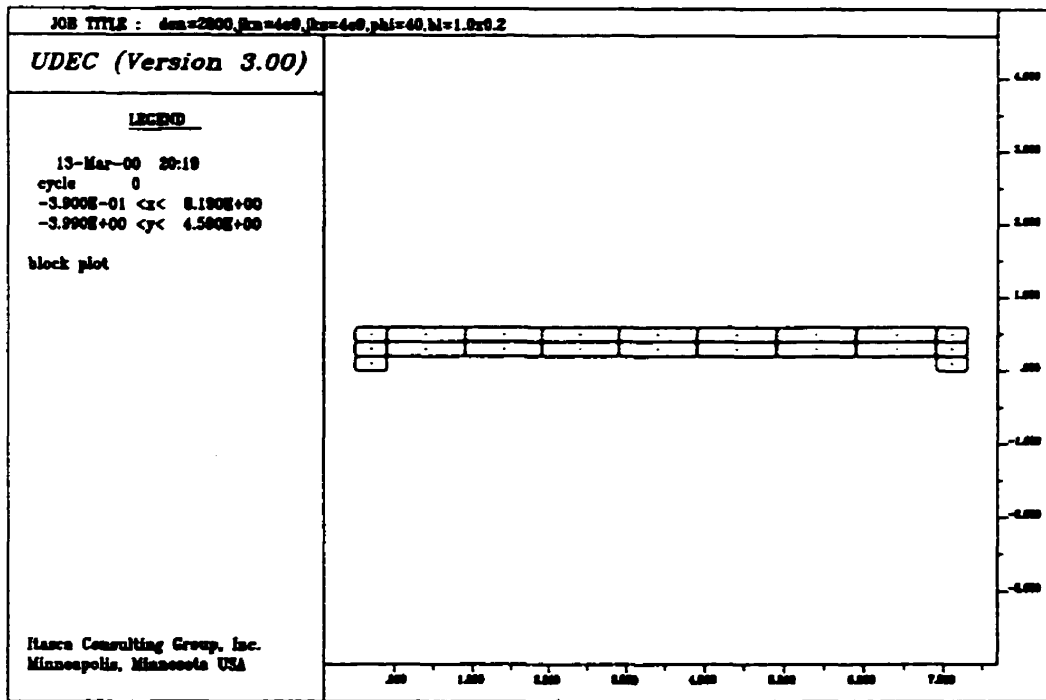
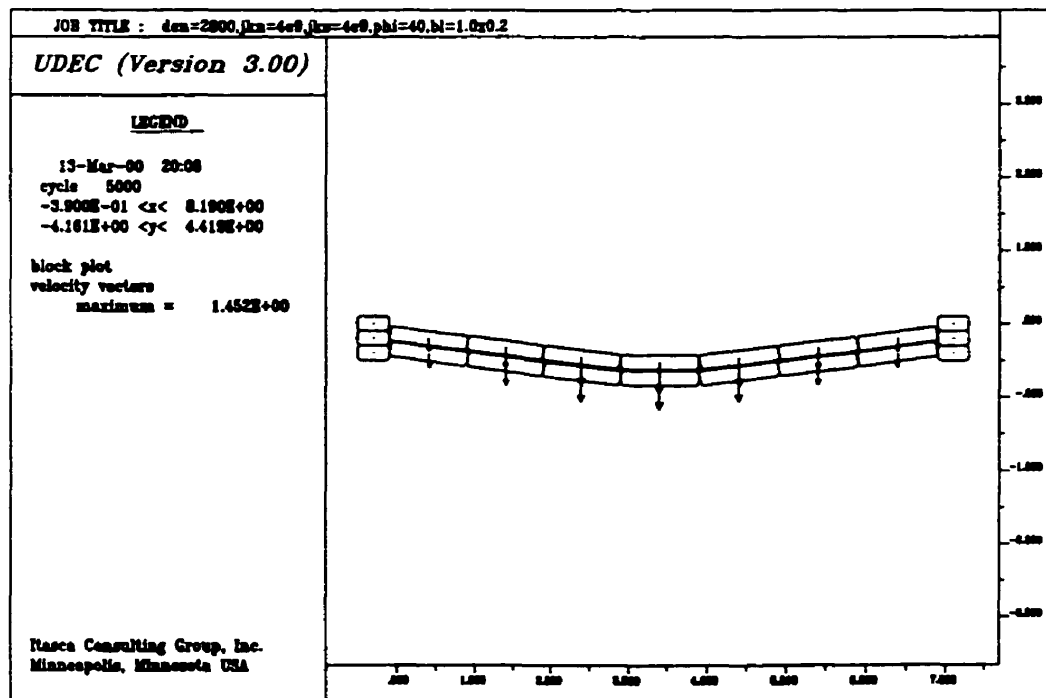


Figure 4.5 Effect of friction angle of joints on the failure modes



a) Initial state t=0



b) Time step: 5000

Figure 4.6 Effect of dimensions on the failure modes (block size: width 1.0m, height 0.2m)

stability by frictional resistance against the downward movement (Figures 4.7a, 4.7b and 4.7c). When the ratio of width to height is small (i.e. 0.5 in Figures 4.8a and 4.8b) failure occurs by shear along the abutments.

4.4 Deformable Block Models

Whereas the main goal of the preceding study of rigid blocks was to “visualize” the dominant failure mechanisms, the following study using UDEC’s deformable block model was carried out to gain further insights into these mechanisms by examining internal block stresses.

The follow parameters were used in the simulation:

a) Size of the individual blocks

Height, 0.2 m

Width, 0.4 m

b) Properties of intact rock:

Density, 2800 kg/m³

Bulk modulus, 8.3 MPa

Shear strength, 6.2 MPa

Cohesion, 3.8 MPa

Friction angle, 45°

c) Properties of joints:

Normal stiffness, 4×10^9 N/m

Shear stiffness, 4×10^9 N/m

Friction angle, 40°

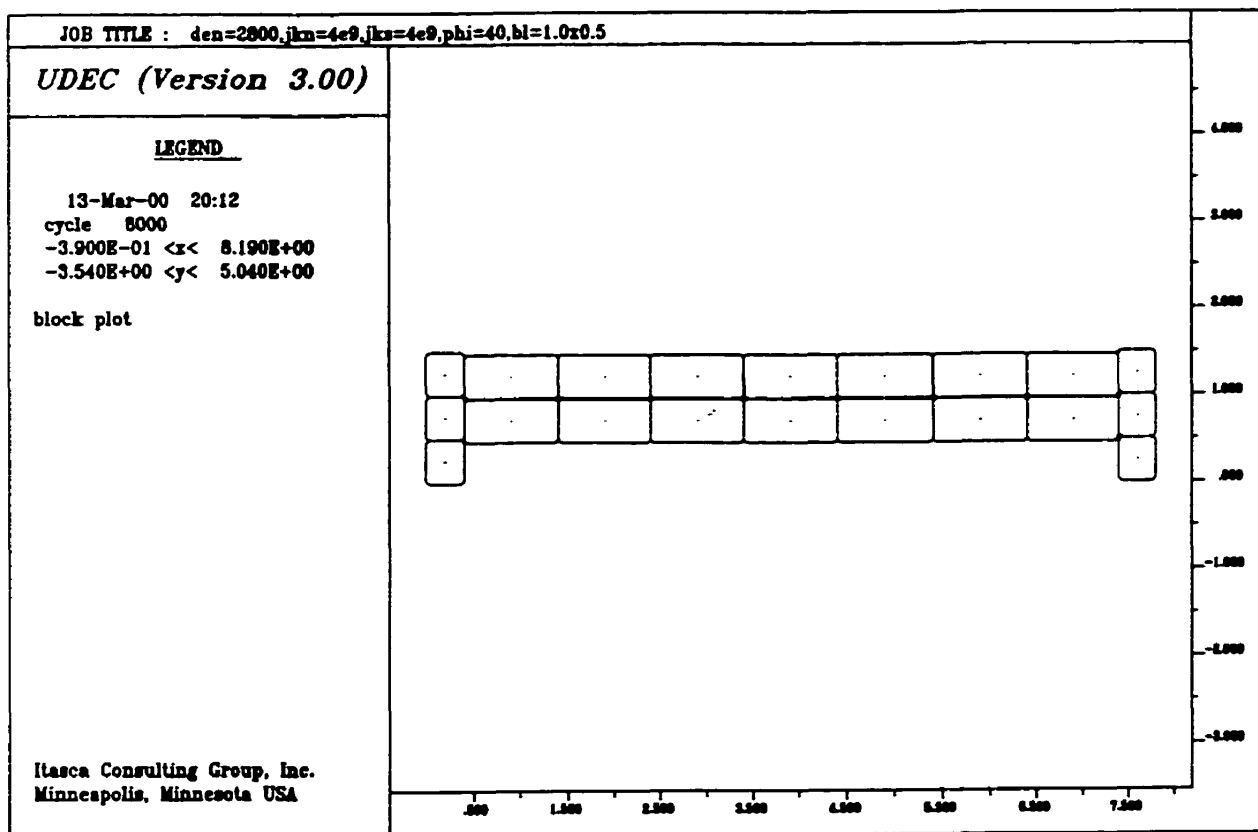


Figure 4.7a Effect of dimensions on the failure modes (Block size: width 1.0m, height 0.5m)

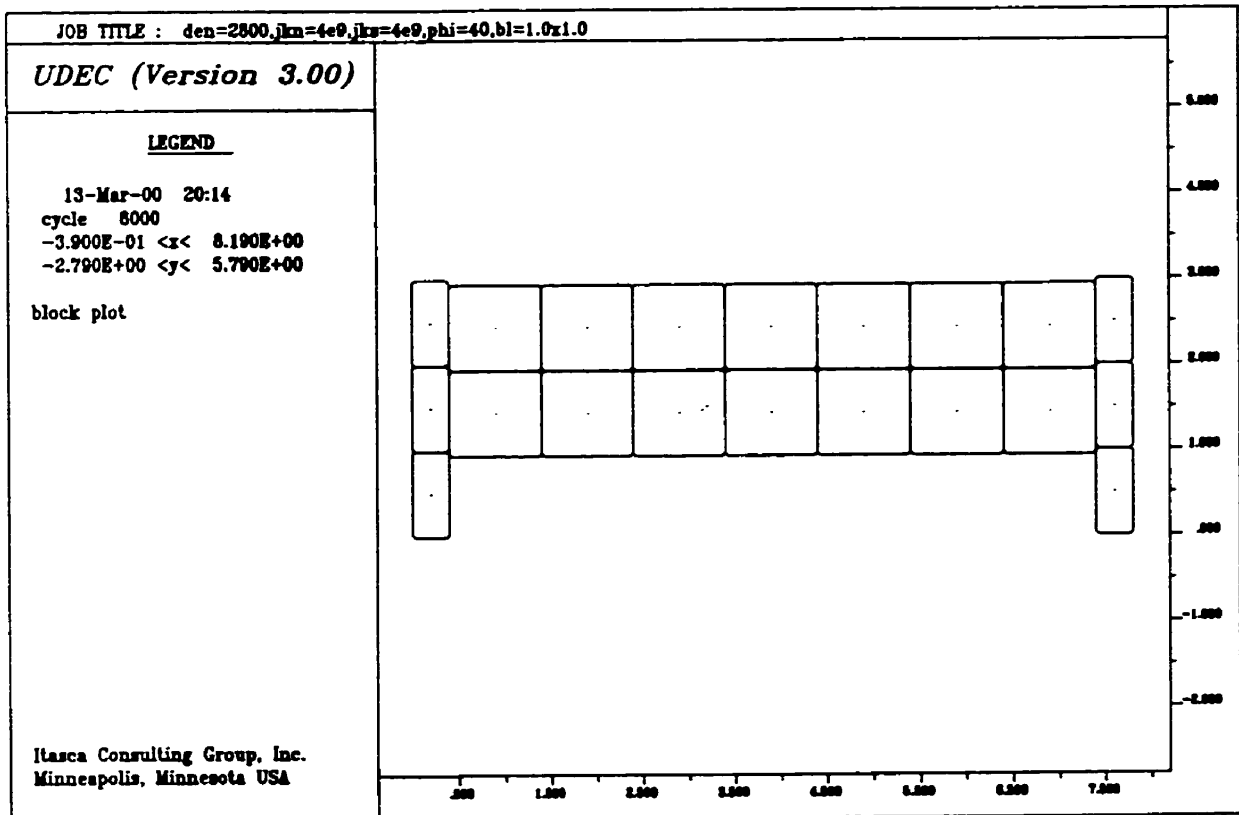


Figure 4.7b Effect of the dimension of blocks on the failure modes (Block size: width 1.0m, height 1.0m)

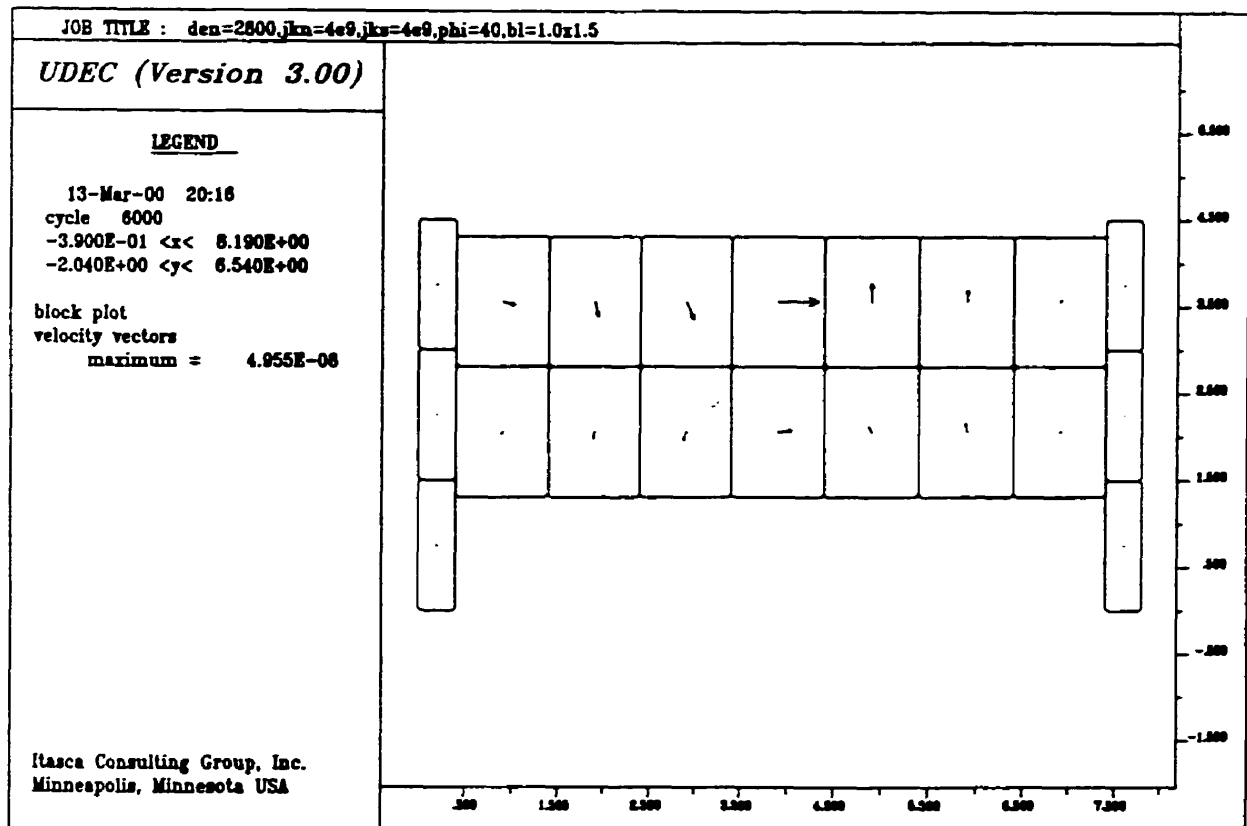
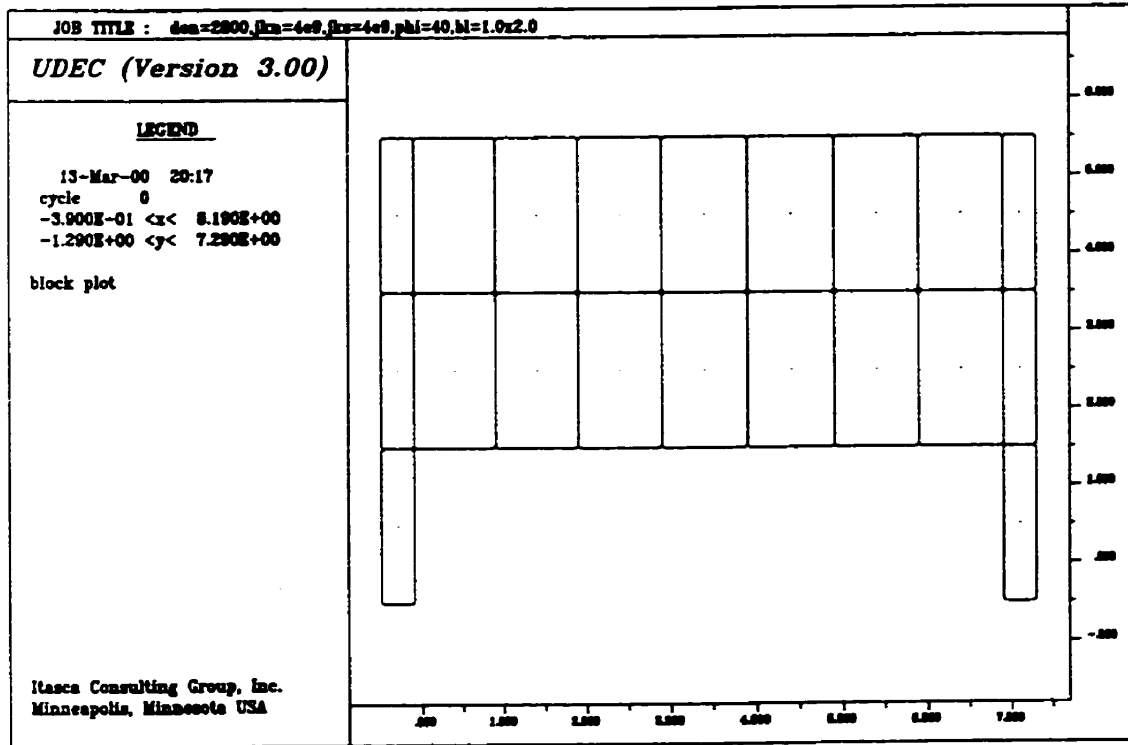
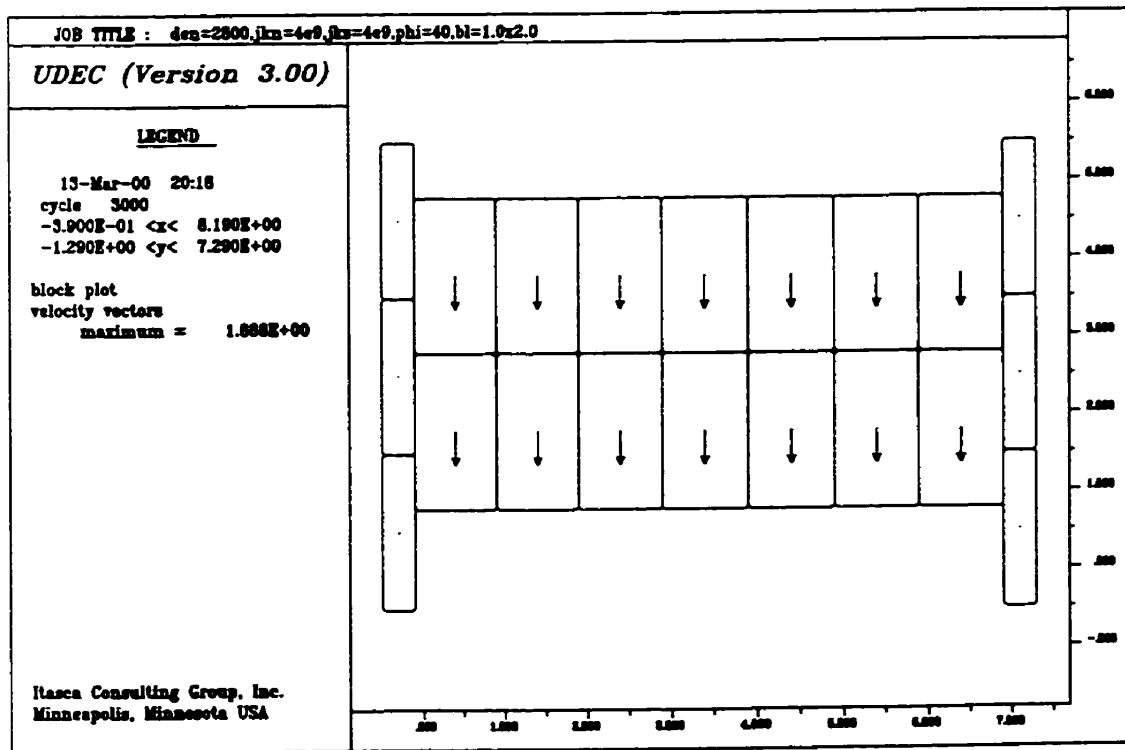


Figure 4.7c Effect of dimensions on the failure modes. The anomalous velocity vectors indicate the whole system is at equilibrium (Block size: width 1.0m, height 1.5m)



a) Time step = 0



b) Time step = 3000

Figure 4.8 Effect of block dimensions on the failure mode (size of blocks: width 1.0m, height 2.0m)

Cohesion, 1.0 MPa

Tensile strength, 0 MPa

The cohesion is eliminated if the joint fails in shear or tension.

d) Boundary conditions:

The external boundaries of the rock mass system are fixed in both horizontal and vertical directions.

Numerical modelling of roof stability first examined a single-layered roof. Stresses at an early stage of deformation are initially concentrated in the upper central region and the lower corners close to the abutments. With the further development of roof deformation, the major principal stress is concentrated in the upper middle region, while the maximum tensile stress is observed in the lower portion of the joints of the middle block (Figures 4.9a and 4.9b). A compressive arch is therefore formed in the roof (Figure 4.10). The roof fails eventually by a double-hinged failure mode when the arching breaks down (Figure 4.11).

If the dimensions of the blocks are changed to a thickness of 0.8 m and a width of 0.4m, the three central blocks displace vertically as a unit (Figure 4.12) but as arching is developed, the movement ceases and the roof is stabilized.

A multiple layered model was also simulated. For this case, the major principal stress is concentrated in the upper central region of each layer (Figure 4.13), while the minor principal stress is observed high in the central joint of the lower layer and the upper joint sections near the abutments (Figure 4.14). The roof sags and rotates around hinges developed at the abutments and at the centre of the span and a compression arch is generated within the roof, rising from the abutments to a high point at midspan (Figure 4.15). This arch produces a resisting moment, formed by the reaction forces at midspan and at the abutments, which acts to resist the destabilizing moment imposed by self-weight.

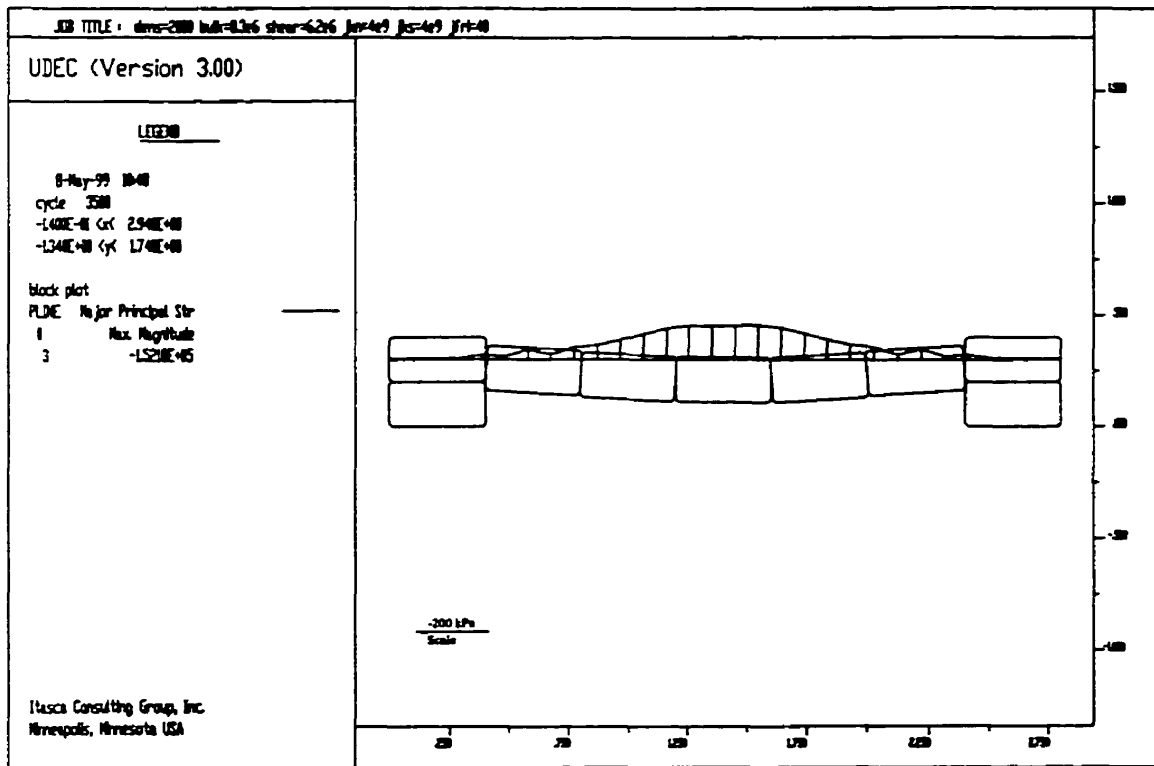


Figure 4.9a Major principal stress distribution

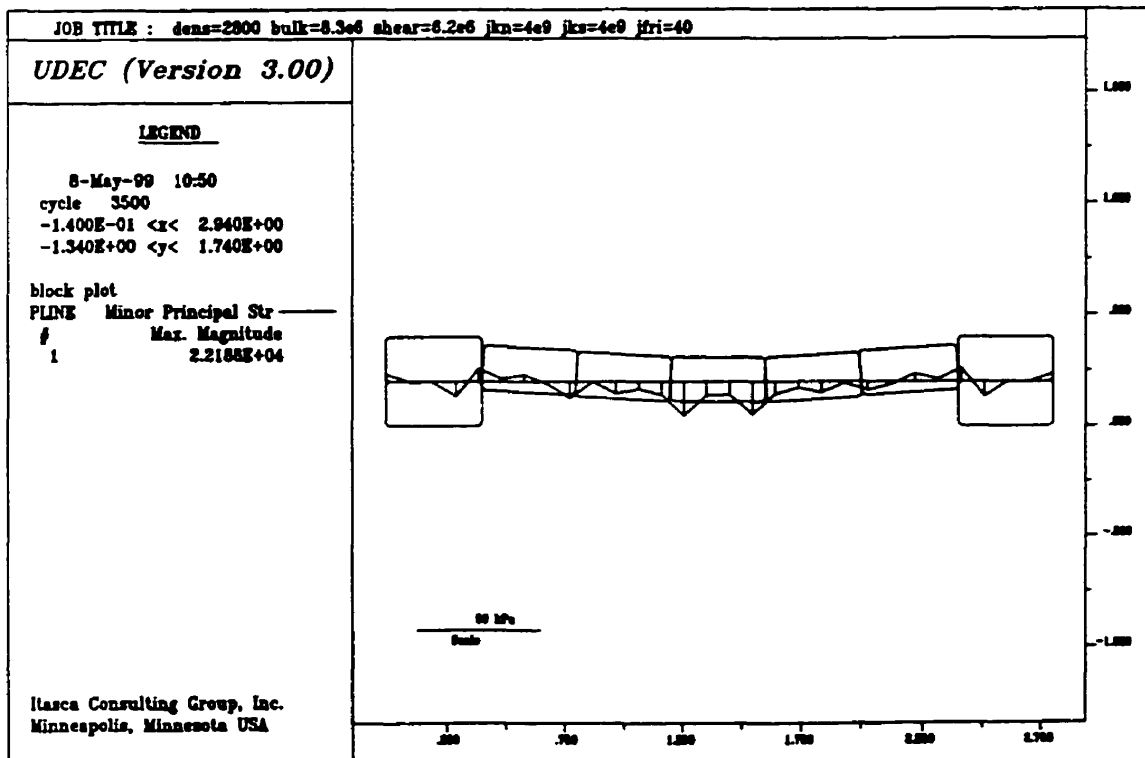


Figure 4.9b Minor principal stress distribution

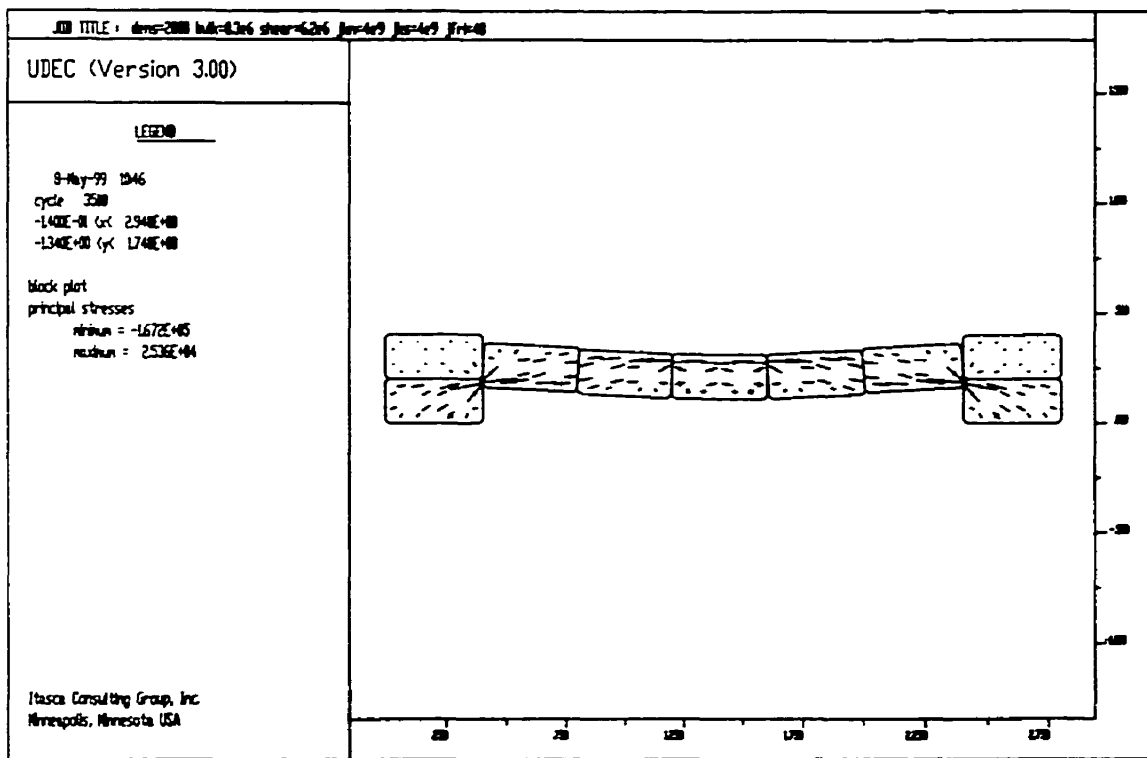


Figure 4.10 Principal stress trajectories show development of a compressive arch

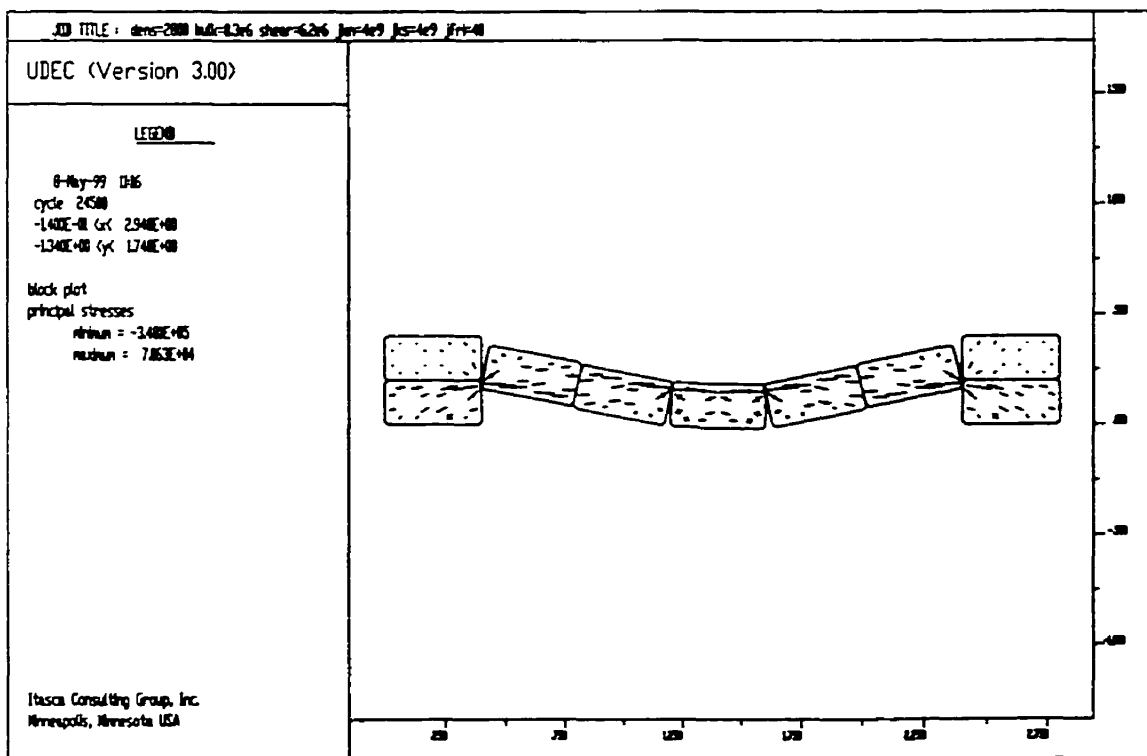


Figure 4.11 Roof failure by the two-hinge failure mode resulting from the collapse of a full arch

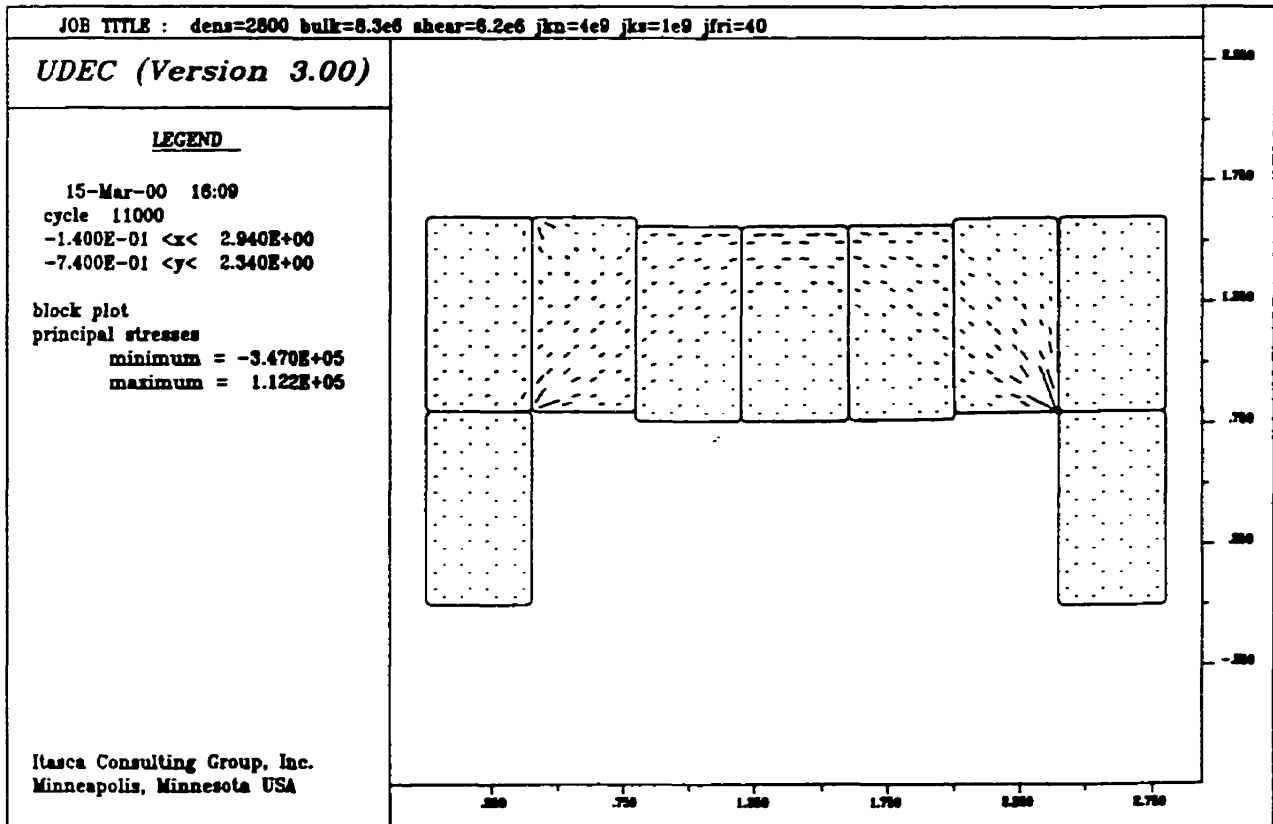


Figure 4.12 Stress trajectories in deformable blocks showing a compressive arch developing in the roof (Size of block: width 0.4m, height 0.8m)

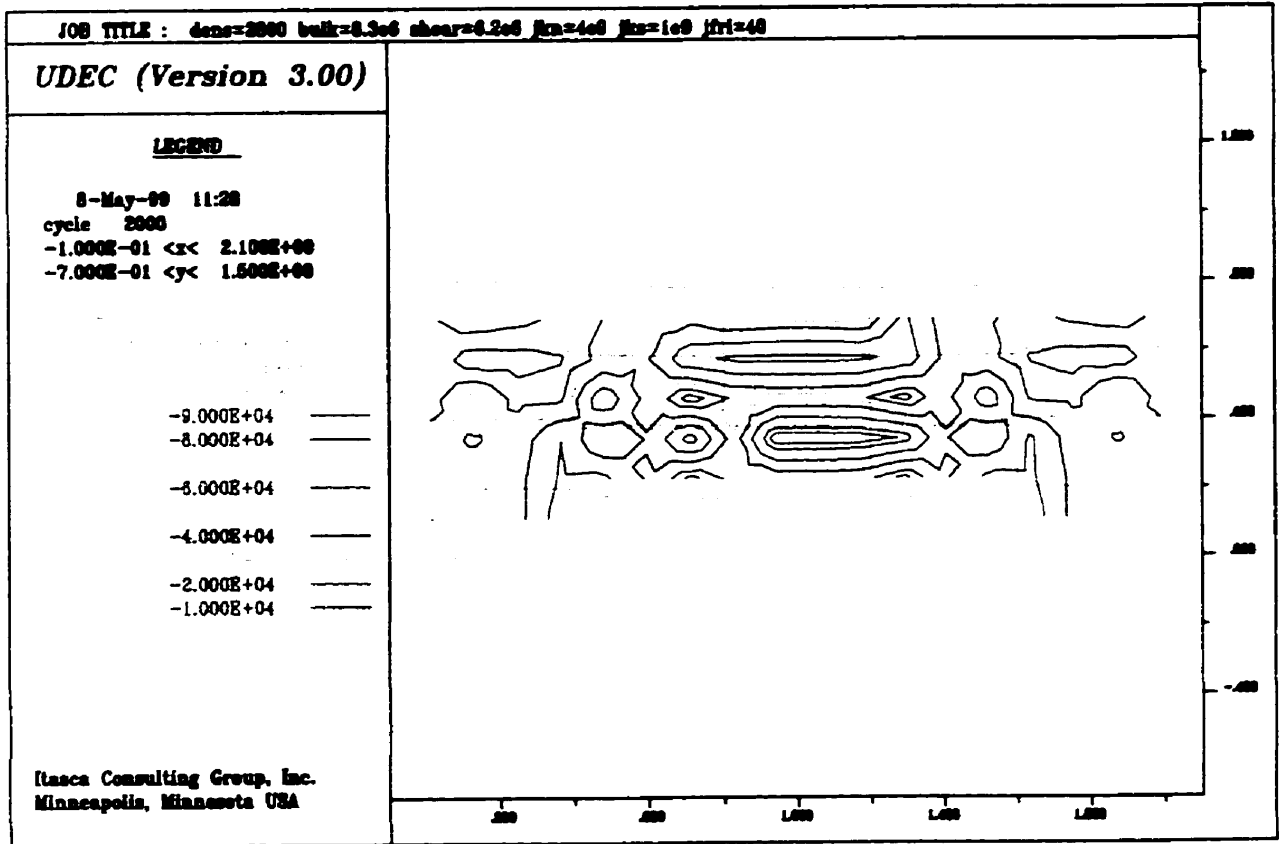


Figure 4.13 Major principal stress contours

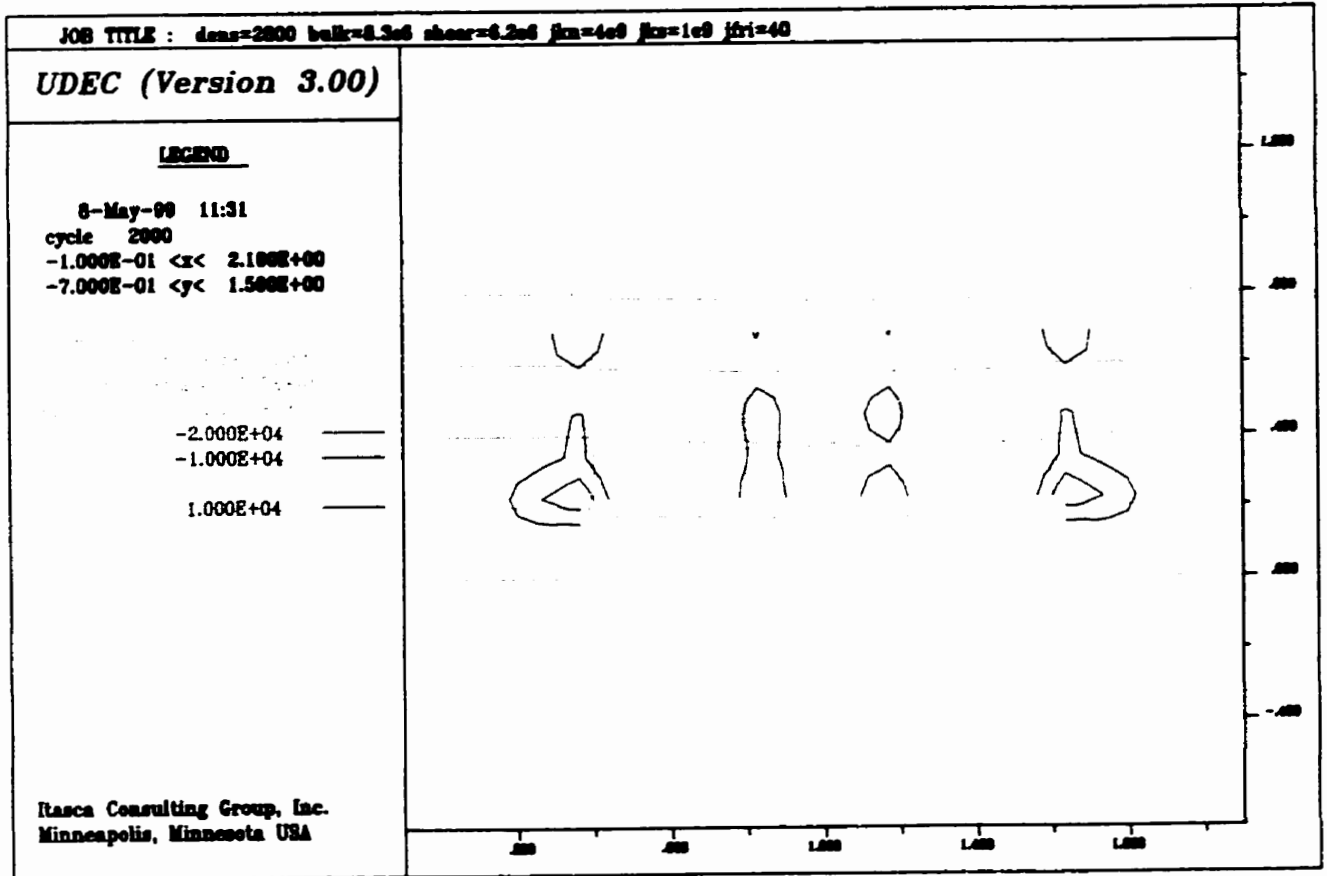


Figure 4.14 Minor principal stress contours

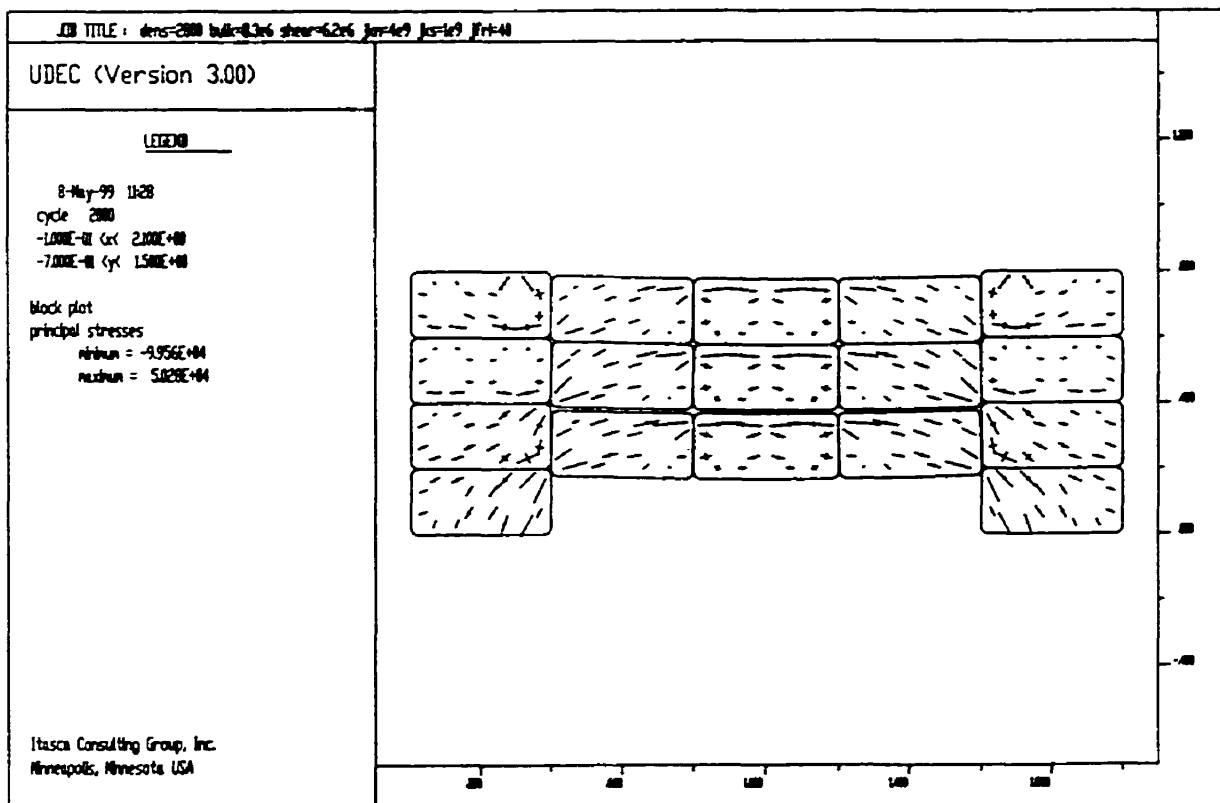


Figure 4.15 Stress trajectories showing the compressive arches developing in each layer

It is also evident that in this layered system, arches develop in each layer (Figure 4.15). It is concluded that for a roof with layers of equal thickness, each layer transfers its weight to the abutments by arching and does not load the layer beneath.

4.5 Physical Modelling

A simple physical model was constructed to simulate the geometry used in the UDEC models (Stimpson, 1989). Rock blocks are represented by layers of gyprock with vertical rough fractures which were produced by a technique for creating tensile fractures (Figure 4.16). The system was unconfined in the horizontal direction. Blocks were removed progressively from the centre of the lowest layer to simulate excavation, i.e. increasing span. The roof failed upwards by sagging progressively (Figure 4.16) in a series of doubled-hinged buckling modes of each layer.

An identical failure process was also observed in the UDEC models when sequential excavation was not modelled (Figures 4.17a and 4.17b). When sequential excavation was modelled in UDEC, another failure mechanism was noted. As the span was opened the initial movement was by vertical shearing (Figure 4.18a). This failure mode may be explained by the span effect noted earlier. The initial “plug failure” results from the small excavation span at early stages of excavation. As the span increases, the downward movement of the central plug initiated a “cantilever” deflection of the bottom layer (Figure 4.18b). The difference between the experiment and the UDEC modelling results from the different friction angles of the joints in the numerical and physical models. The extremely rough “joints” in the gyprock models (estimated at $60^\circ - 70^\circ$) could not be simulated in UDEC.

4.6 Conclusions

Based on the above study of horizontally layered rock with vertical joints above a rectangular opening, it is concluded that:

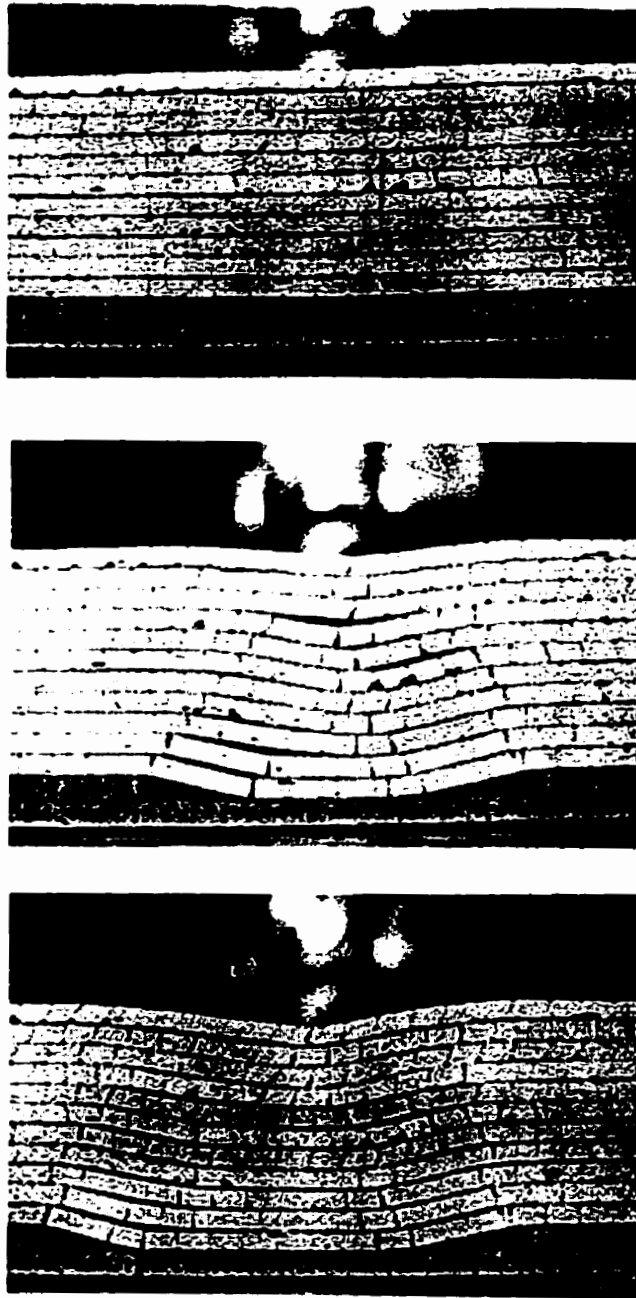


Figure 4.16 Physical modelling of sequential excavation (after Stimpson 1989)

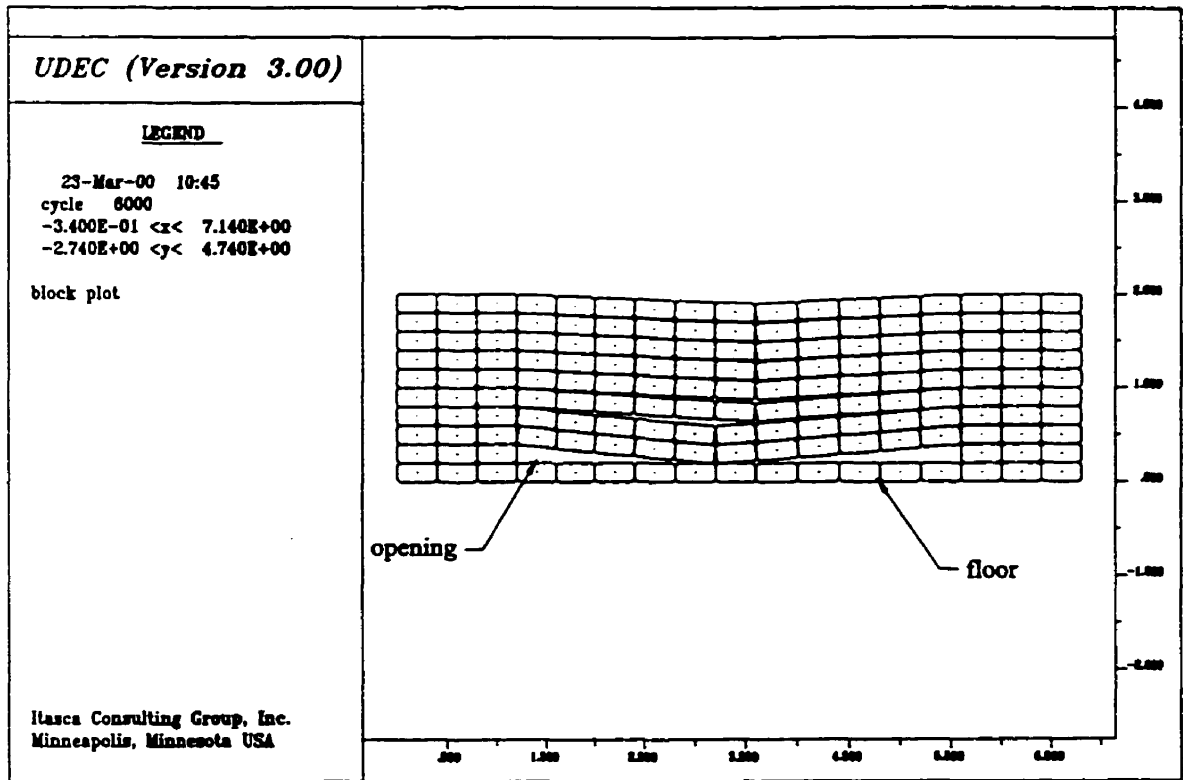


Figure 4.17a Roof failure is characterized by sagging and layer separation (step 6000)

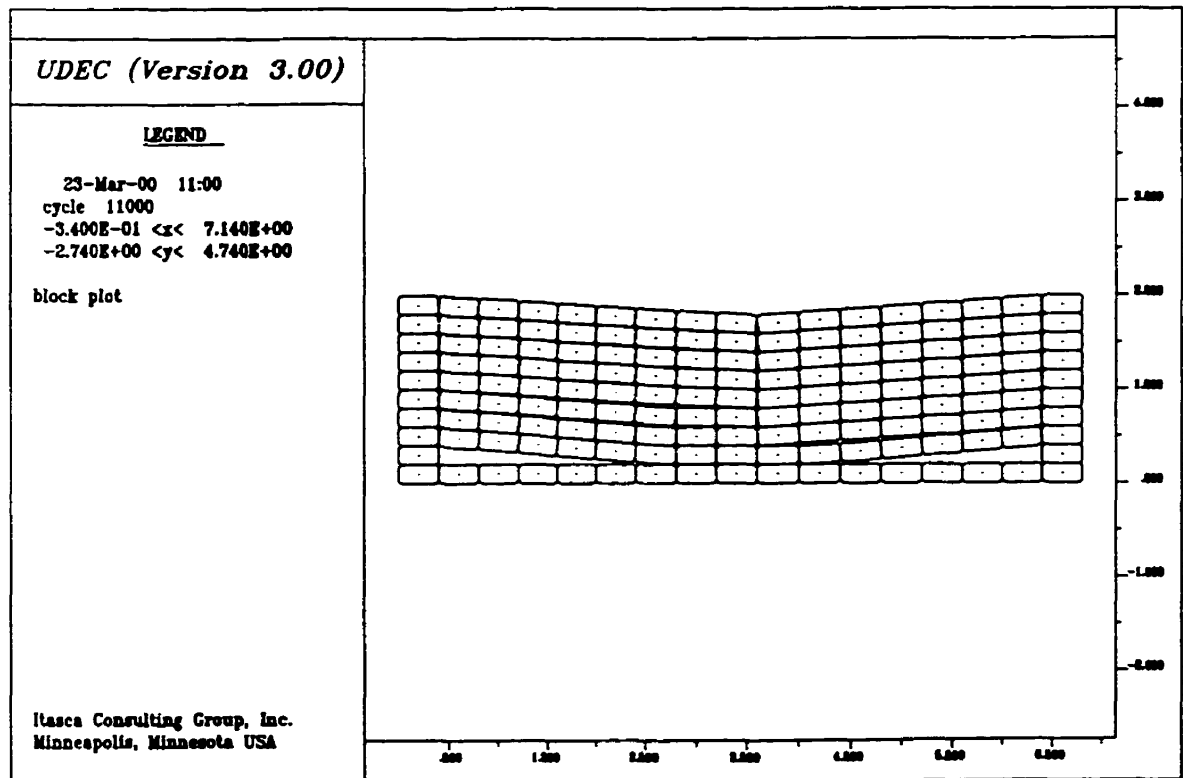
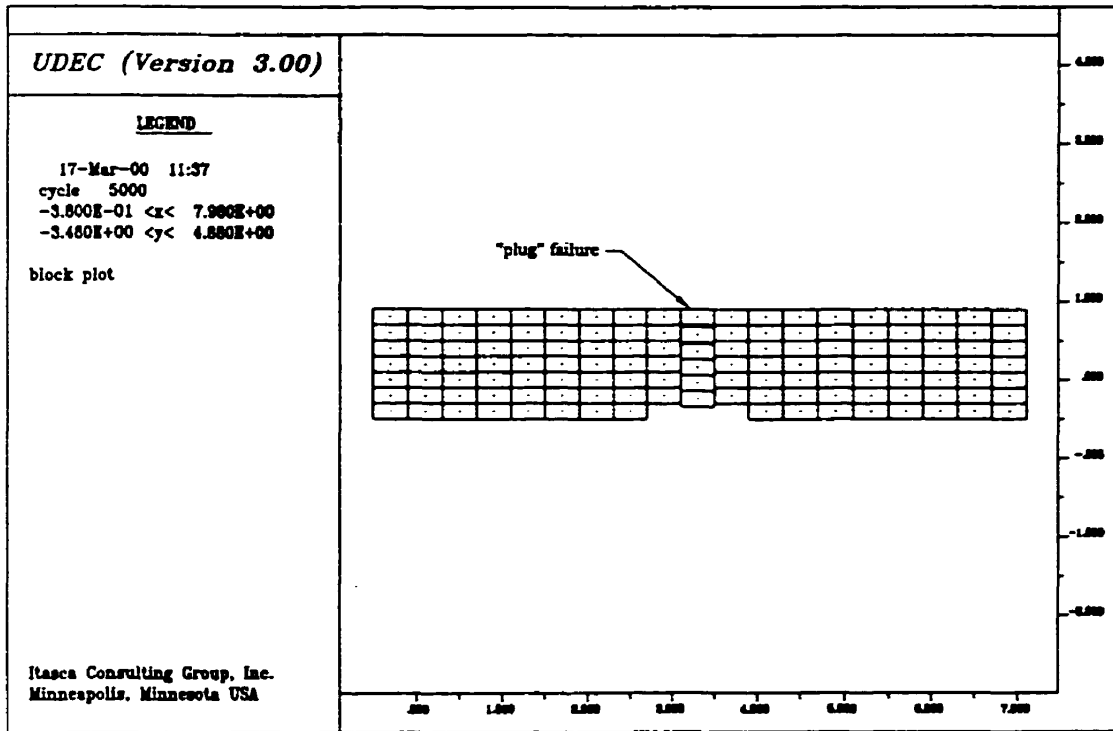
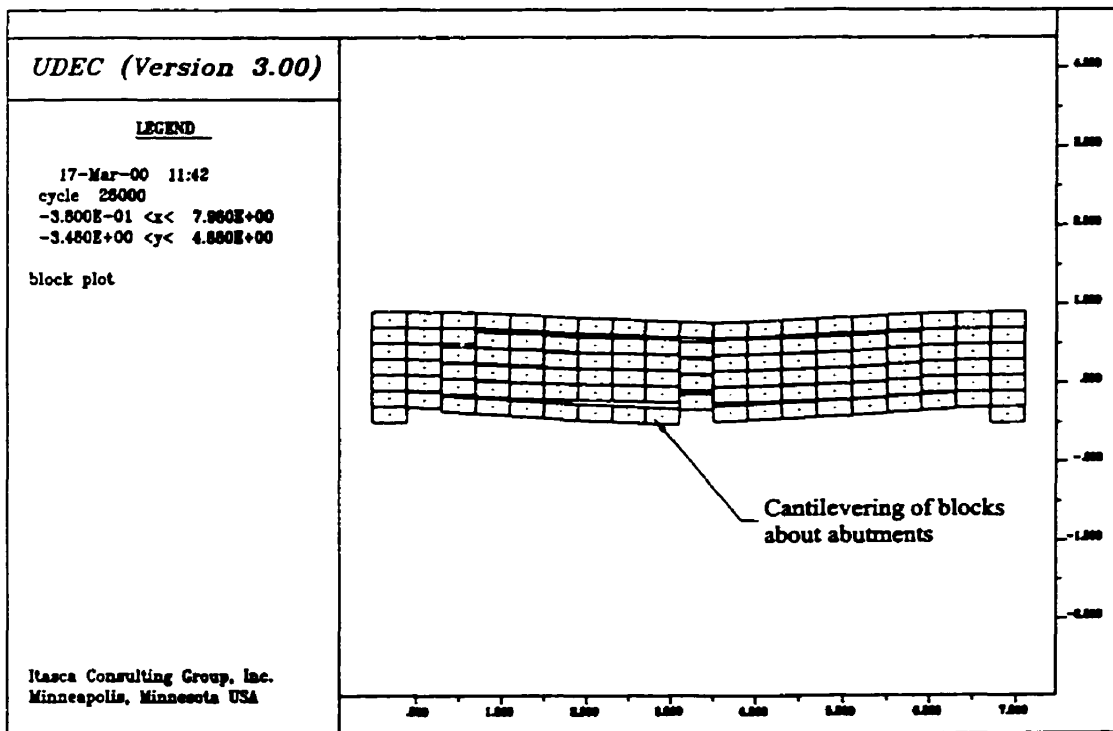


Figure 4.17b Roof failure by the two-hinge mode with increase of span (step 11000)



a) Time step 5000



b) Time step 26000

Figure 4.18 Simulation of sequential excavation

Rigid Block Models

a) The failure modes of the roof of a rectangular opening in horizontally layered, vertically jointed rock are related to the geometry of the opening, joint spacing, bed thickness, and joint friction angle, as well as the mining sequence. Vertical shear failure and buckling failure are identified as the two primary failure modes. Generally, vertical shear failure at the abutments is observed with a low span-to-joint spacing ratio, while buckling failure is observed with high span-to-joint spacing ratios.

b) The joint spacing influences the failure modes such a way that shear failure along vertical joints is associated with widely spaced vertical joints, whereas buckling failure is related to closely-spaced joints.

c) Roof span is also a major factor influencing the failure modes. When the span is small, the roof fails by shear along the abutments. Rotation of blocks, layer separation and sliding begin to play a role with increase of span. However, self-stabilization of the roof can be reached by developing an arching mechanism. When the span is large, the movement of layers is controlled by rotation. The roof fails in buckling by development of hinges at the middle of the roof and at the abutments.

d) The effect of the friction angle of joints was also studied. Shear failure along the abutments was observed for low friction angles. As the joint friction angle increased, roof failure was characterized by buckling failure by either a single or double hinge mechanism.

e) The above conclusions are made based mainly on studies of the blocks with a larger width than height (i.e. ratios of block width to block height > 1). It must be noted that, as the failure modes are influenced simultaneously by multi-factors, failure modes would be much more complex. Based on the results obtained from 9 typical numerical models, a conceptual relationship between the failure modes and the block size/joint spacing/roof span is illustrated in Figure 4.19. Three regions are defined by two lines. The shear/sliding failure at abutments is associated with low ratio of span to joint spacing and increasing ratio of block thickness to block width. The separation/buckling failure is associated with a high ratio of span to joint spacing. Between these two regions there is a region of self-stabilization where the roof reaches stability by frictional resistance against

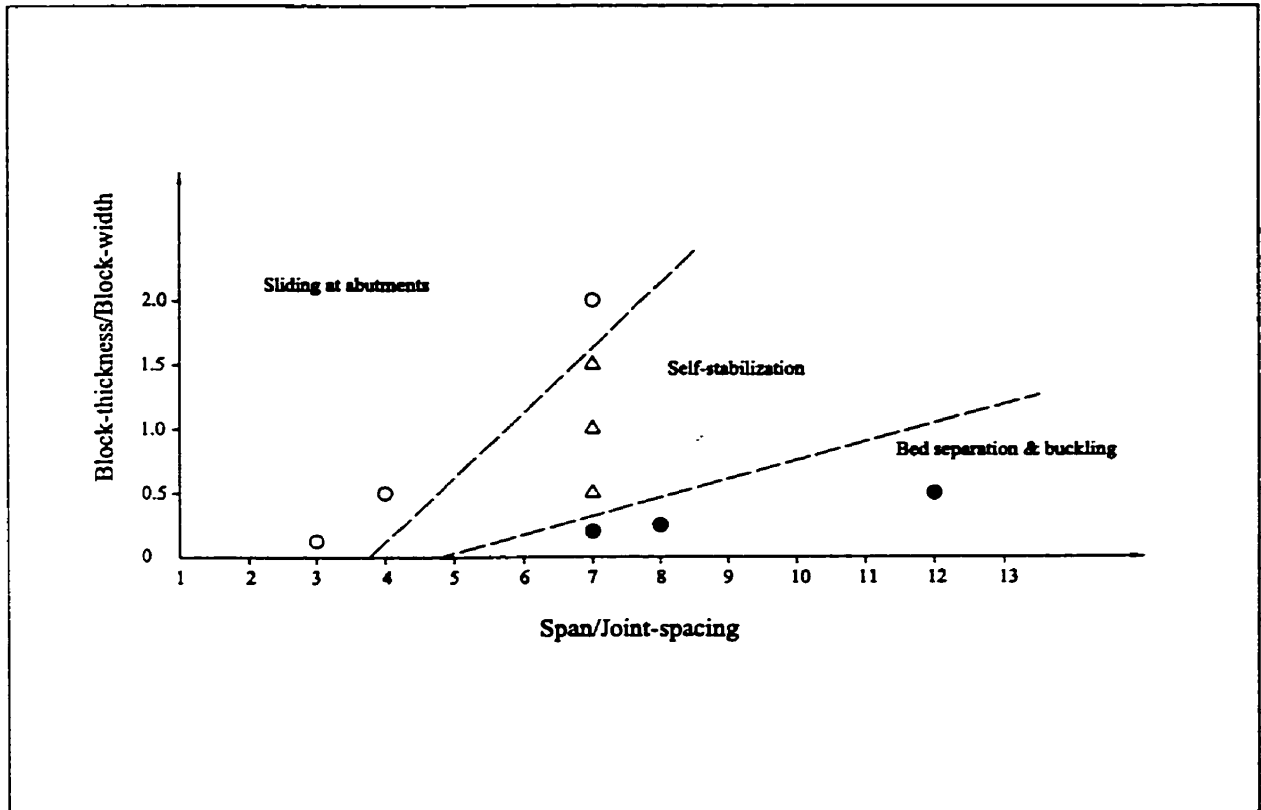


Figure 4.19 Relationship of failure modes to dimensions of block and roof span

downward movement and by development of arching. It is worthy of note that a small span may be unstable and a larger span stable for a given value of ratio of block thickness to block width. It is also worth noting that at very low block thickness/block width ratios, there is a very limited region of self-stabilization. As this ratio increases there is a greater range of spaces where self-stabilization occurs.

f) As to the dimension effect of the blocks, the roof failure modes change from the buckling failure mode to the sliding failure mode when the block width-to-height ratio decreases.

Deformable Block Models

a) Failure modes and mechanisms were also studied for deformable block models. Compressive arches develop in the roof beams with vertical movement of the rock blocks and generate a resisting moment to counteract the destabilizing moment imposed by self-weight. Arching enhances the roof stability.

b) The dimension effect of blocks on the roof stabilization was also observed in the deformable block models. If the width-to-thickness ratio is large, the roof fails by double-hinged buckling failure mode after the compressive arch is broken down. In the case of smaller width-to-thickness ratios, the roof develops a stable arch after a central “plug” of blocks undergoes vertical shear.

c) For the multiple-layer model of uniform thickness where “plug” failure is not operative, each layer transfers its own weight to the abutments by arching and does not load the layer beneath.

These studies demonstrate that UDEC is an invaluable numerical method for gaining insights into failure mechanisms of jointed rock masses.

4.7 Rock Bolting

These UDEC simulations have relevance to the design of rock bolt support patterns. Horizontally layered strata are typically supported by vertical rock bolts. It is evident

from these studies that precautions against the possibility of vertical shear failure at the abutments should be taken by installing inclined bolts at the ends of the span and angling them over the solid abutments.

PART IV SUMMARY

The major objective of this thesis was to investigate how the loosening zone was developed in the roof above an underground opening in both massive and jointed rock. For the massive rock mass, the key issue is the progressive nature of failure. For the jointed rock mass, it is essential to understand how multiple factors (i.e. joint spacing, the frictional angle of joint, and the size of blocks intersected by the joint, the opening span and the sequence of excavation) influence the stability of the roof.

1) Massive Rock

The stress-strength method was adopted in this thesis for studies of the development of the loosening zone above an underground opening in massive salt rock. The essence of this method is to correctly predict stresses around the opening and to use an appropriate strength criterion for the rock mass. As the final state of stress around an underground opening is the resultant of the undisturbed virgin state of stress and the stress induced by the excavation or mining, it is clear that the accuracy of determination of the pre-excavation state of stress is of paramount importance. The initial state of stress is often estimated using Heim's rule. However, the stresses might be modified by tectonism (folding uplift, faulting and etc.), stiffness variations between strata, and by topography. The induced stresses around underground openings can be evaluated by either closed-form solutions such as the Kirsch equation for a circular opening or by numerical solutions. The degree to which analytical and numerical solutions accurately predict the state of stress around an opening depends greatly on selecting the correct boundary conditions and geology.

Damage/failure criteria for massive rock are primarily empirical in nature with a theoretical justification to some degree. The strength of massive rock is typically determined by laboratory testing of intact rock specimens, and is influenced by a scale effect, a loading effect due to different testing conditions and equipment, and sample

disturbance during collection of samples from the field. Other factors can also affect appraisal of strength of the rock mass *in situ*, including “overloading” of the rock ahead of the tunnel face.

Following a review of the literature on salt rock testing, damage criteria were selected for the numerical simulations.

The Proposed Empirical Damage/Failure Criteria

For the Esterhazy salt rock:

Damage initiation: $(\sigma_1 - \sigma_3)$ exceeds 6 MPa (i.e. $0.25\sigma_c$);

Damage growth: $(\sigma_1 - \sigma_3)$ exceeds 18 MPa (i.e. $0.6\sigma_c$);

Failure: $(\sigma_1 - \sigma_3)$ exceeds 24 MPa (i.e. $0.8\sigma_c$).

Field Observations of Cracking Development in the Roofs

Visual inspections of roof fractures above rooms in an Esterhazy potash mine were made by mine staff with a borehole video borescope. It was revealed that visible rock mass damage was characterized by open tensile fractures. These fractures propagated over time forming a dome shaped zone of loosening with the height of the apex being about 3.8 m.

Numerical Modelling Using Phase²

The finite element program, Phase², was used to simulate the development of the zone of damage/failure in the roof of a potash mine and predicted a zone of failure limited to the sidewalls and the roof above the walls for both the Hoek-Brown failure and the Duncan empirical failure criteria. These criteria were not able to predict the zone of failure as to its shape and size compared to the field observations. Using the writer’s failure criterion (Equation 3), the height of the predicted failure zone was 4 m. A dome-shaped zone of damage growth was predicted in the roof with a central height from 3.7 m to 6.8 m using the damage growth criterion (Equation 2). The height of the lower boundary of the

predicted damage zone coincided with the field observation data, but the upper boundary was higher than the observed cracking.

Numerical Modelling Using InSight^{2D}

The propagation of discrete cracks was modelled using InSight^{2D}. The results demonstrated that progressive cracking along the σ_1 direction would lead to a dome shaped zone of loosening with a height of about 3 m above the opening. The predicted zone of cracking matched the field data quite closely.

2) Jointed Rock

Studies of the horizontally layered, vertically jointed rock were carried out to examine the roof failure mechanisms for a rectangular opening in shallower sedimentary rock. Results from numerical modelling using UDEC may be summarized as follows:

- a) Vertical shear failure and buckling failure are identified as the primary failure modes. The development of a particular mode is related to the geometry of the opening, the properties of the intact rock and joints, joint spacing, dimension of blocks, and the mining sequence.
- b) Generally, vertical shear failure at the abutments is observed with a low span-to-joint spacing ratio, while buckling failure is observed with high span-to-joint spacing ratios if the width of the block is larger than the width.
- c) A compressive arch generated in the jointed beam acts to resist the moment imposed by self-weight and thus helps to stabilize the roof.
- d) For layers of uniform thickness and where “plug” failure is not operative, each layer transfers its own weight to the abutments by arching and does not load the layer beneath.
- e) UDEC is an invaluable numerical method for gaining insights into failure mechanisms of jointed rock masses and can also be used for stability analyses.

3) Recommendations for Future Research

Although considerable progress has been made in understanding damage and failure in salt rock, there are several aspects that remain unclear:

- The measurement of far field stresses is required, if possible, for the potash mines at Esterhazy. In this thesis *in situ* stresses were assumed to be hydrostatic.
- Use a 3-D boundary element code such as Phase^{3D} to predict the stress state ahead of an advancing mine panel to determine if the rock strength is degraded before it becomes the periphery of the opening.
- A shear mode stress intensity factor should be incorporated into InSight^{2D} in order to simulate the shear failure.

REFERENCES

Adams, M and G. Sines 1978. Crack extension from flaws in a brittle material subjected to compression. *Tectonophysics*. **49** (1/2):97-118.

Aydan, O., T. Ito and Y. Ichikawa 1993. Failure phenomena and strain localisation in rock mechanics and rock engineering: A phenomenological description. *Assessment and prevention of failure phenomena in rock engineering*, Pasamehmetoglu et al. (ed.), Balkema, Rotterdam, pp. 119-128.

Baar, C.A. 1971. Creep measured in deep potash mines vs. theoretical predictions. *Proc. 7th Canadian Rock Mech. Symp.*, pp. 23-77.

Bieniawski, Z.T. 1967. Mechanism of brittle fracture of rock. *Int. J. of Rock Mech and Min. Sci.*, **4**, pp. 395-430.

Bombolakis, E.G. 1973. Study of the brittle fracture process under uniaxial compression. *Tectonophysics*. **18**: 231-248.

Brace, W.F. 1964. Brittle fracture of rocks. *State of Stress in the Earth's Crust*. Elsevier, New York, NY, pp.111-174.

Brady, B.H.G. 1977. An analysis of rock behaviour in an experimental stoping block at the Mount Isa Mine, Queensland, Australia. *Int. J. Rock Mech. Sci.* **14**, pp. 59-66

Brady, B.H.G 1979. Boundary element methods for mine design. PhD thesis, University of London.

Brady, B.H.G. and E.T. Brown 1985. *Rock Mechanics For Underground Mining*. George Allen & Unwin Ltd.

Budavari, S. 1983. *Rock Mechanics in Mining Practice*. The South African Institute of Mining and Metallurgy.

Carlson, S.R. and R.P. Young 1992. Acoustic emission and ultrasonic velocity study of excavation-induced microcrack damage in the Mine-by tunnel at the Underground Research Laboratory. Atomic Energy of Canada Ltd. RP015AECL, Engineering Seismology Laboratory, Queen's University, Kingston, Canada.

Carter, B.J., E.J.S. Duncan and E.Z. Lajtai 1991. Fitting strength criteria to intact rock. *Geotechnical and Geological Engineering*, **9**, pp.73-81.

Carter, B.J. 1992. Physical and numerical modelling of fracture in rock, with special emphasis on the potash mines of Saskatchewan. Ph.D thesis, University of Manitoba.

Castro, L.A.M. 1996. Analysis of stress-induced damage initiation around deep openings excavated in moderately jointed brittle rock mass. Ph.D. thesis, University of Toronto.

Chen, R. 1993. *In situ* and laboratory studies of potash deformation with reference to Saskatchewan potash. Ph.D thesis, University of Manitoba.

Cundall, P.A. 1971. A computer model for simulating progressive large scale movements in blocky rock systems. In *rock fracture*. Proc. Int. Symp. Rock fracture, Nancy, pp. 2-8.

Desai, C.S. and G. Giod 1990. Numerical methods and constitutive modelling in geomechanics. Springer.

Dey, T.N and C.Y. Wang 1981. Some mechanisms of microcrack growth and interaction in compressive rock failure. *Int. J. Rock Mech. Min. Sci.*, **18** pp.199-209.

Dreyer, W. 1974. Results of recent studies on the stability of crude oil and gas storage in salt caverns. 4th Symp. On Salt, 2 pp.65-92.

Duncan, E.J.S. 1990. Deformation and strength of Saskatchewan potash rock. PhD thesis, University of Manitoba.

Dunn, C.E. 1982. Geology of the Middle Devonian Dawson Bay Formation in the Saskatoon potash mining district, Saskatchewan. report, Sask. Energy and Mines, 194.

Dzik, E.J., E.Z. Lajtai and C.D. Martin 1994. Numerical modelling of discrete fracture in granite. In H.J. Siriwardane (ed.), Proc. 8th Int. Conf. on Computer Methods and Advances in Geomechanics (IACMAG94), Morgantown, West Virginia. A.A. Balkema, Rotterdam.

Eberhardt, E. 1998. Brittle rock fracture and progressive damage in uniaxial compression. University of Saskatchewan, PhD thesis.

Economopoulos, J.N, A. I. Sofianos and N.J. Koronakis 1994. Voussoir beam response of bedded limestone roofs in Greek underground mining excavations. Tunneling and Ground Conditions, Abdel Salam (ed.), Balkema, Rotterdam, pp. 223-229.

Fredrich, J.T., Evans, B. and Wong, T.-F. 1989. Micromechanics of the brittle to plastic transition in Carrara marble. J. Geophysics. Res. 94, pp. 4129-4145.

Fuzesy, A. 1982. Potash in Saskatchewan. *Report*, Saskatchewan Energy and Mines, Report No. 181, pp. 46.

Goodman, R.E. and C.M. St. John 1977. Finite element analysis for discontinuous rocks. Numerical methods in geotechnical engineering (C.S. Desai and J. T. Christian, eds), McGraw-Hill, New York, pp.148-155.

Greenspan, M. 1944. Effect of a small hole on the stresses in a uniformly loaded plate. *Quart. Appl. Math.*, Vol.2, pp.60-71.

Hardy, H.R. and G.L. Mowrey 1976. Study of microseismic activity associated with a longwall coal mining operation using a near-surface array. *Engineering Geology*, **10**, pp.263-81.

Heim, A. 1912. Zur Frage der Gebirgs - und Gesteinsfestigkeit. *Schweiz. Bauztg.* Vol. 50.

Heller, S.R., J.S. Brock and R. Bart 1958. The stresses around a rectangular opening with rounded corners in a uniformly loaded plate. *Trans. 3rd US Cong. Appl. Mech.*, pp.357.

Higdon, A., E.H. Ohlsen, W.B. Stiles, J.A. Weese and W.F. Riley 1985. *Mechanics of Materials*. John Wiley & Sons, Inc.

Hoek, E. and E.T. Brown 1980. *Underground excavations in rock*. London: Instn. Min. Metall.

Hoek, P.K. Kaiser & W.F. Bawden 1995. *Support of Underground Excavations in Hard Rock*. Balkema, Rotterdam.

Indraratna, B. and A. Haque 1977. Experimental study of shear behaviour of rock joints under constant normal stiffness conditions. *Int. J. Rock Mech. & Min. Sci.* **34**, pp.3-4.

Itasca 1996. UDEC version 3.0, User's Manual.

Jaeger, J.C. and N.G.W. Cook 1969. *Fundamentals of Rock Mechanics* (Methuen, London), pp. 513.

Jackson, R. and J.S.O. Lau 1990. The effect of specimen size on the mechanical properties of Lac du Bonnet Grey Granite. In A. Pinto da Cunha, editor, Proc. 1st. Int. Workshop on Scale Effects in Rock Masses, Loen, Norway, pp.165-174. A.A.Balkema, Rotterdam.

Johnston, I.W. 1985. The strength of intact geomechanical materials. Journal of Geotechnical Engineering Division, ASCE, Vol.3, pp.730-749.

Jones, P.R. and F.F. Prugger 1982. Underground mining in Saskatchewan potash. Mining Engineering, pp. 1677-1683.

Kemeny, J.M. and N.G.W. Cook 1987. Crack models for the failure of rock under compression. Proc. 2nd Int. Conf. Constitutive Laws for Eng. Mat. 2, pp.879-887.

Kirsch, G. 1898. Die theorie der elastizitat und die bedurfnisse der festigkeitslehre. Veit. Ver. Deut. Ing., Vol. 42, No. 28, pp. 797-807.

Kranz, R.L. 1979. Crack-crack and crack-pore interactions in stressed granite. International Journal of Rock Mechanics and Mining Sciences & Geomechanical Abstracts. **16** (1), pp.37-47.

Lajtai, E.Z. and E.J.S. Duncan 1988. The mechanism of deformation and fracture in potash rock. Canadian Geotechnical Journal, Vol. 25, No 2, pp.262-278.

Lajtai, E.Z, B.J. Carter and M.L. Ayari 1990. Criteria for brittle fracture in compression. Engineering Fracture Mechanics, **37**(1), pp.25-49.

Lajtai, E.Z, E.J.S. Duncan and B.J. Carter 1991. The effect of strain rate on rock strength, Rock Mechanics and Rock Engineering, **24**, pp.99-109.

Landayi, B. and G. Archambault 1970. Simulation of shear behaviour of a jointed rock mass. Proc. 11th Sym. On Rock Mech., published by AIME, New York, pp.105-125.

Mackintosh, A.D. 1975. Applied rock mechanics: the development of safe travelways at the Comico potash mine. Proceedings of the 10th Canadian Rock Mechanics Symposium. Queen's University, Kingston.

Martin, C.D. 1993. The strength of massive Lac du Bonnet granite around underground openings. PhD thesis, University of Manitoba.

Martin, C.D. and N.A. Chandler 1994. The progressive fracture of Lac du Bonnet granite. International Journal of Rock Mechanics and Mining Sciences & Geomechanical Abstracts, 31(6), pp.643-659.

Mosher, S., R.L. Berger and D.E. Anderson 1975. Fracturing characteristics of two granites. Rock Mechanics. 7 (3), pp.167-176.

Muskhelishvili, N.I. 1953. Some Basic Problems of the Mathematical Theory of Elasticity. Translated from Russian by J.R.M. Radok, Published by Noordhoff, Groningen, 4th edition.

Napier, J.A.L. and M.U. Ozbay 1993. Application of the displacement discontinuity method to the modelling of crack growth around openings in layered media. in "Assessment and Prevention of Failure Phenomena in Rock Engineering", Pasamehmetoglu et al. (eds). Balkema, Rotterdam.

Obert, L and W.I. Duvall 1967. Rock Mechanics and the Design of Structures in Rock. John Wiley & Sons, New York.

Otter J.R.H., A.C. Cassell and R.E. Hobbs 1966. Dynamic relaxation. Proc. Instn Civ. Engrs 35, pp.633-65.

- Pande, G.N, G. Beer and J.R. Williams 1990. Numerical Methods in Rock Mechanincs. John Wiley & Sons Ltd.
- Patton, F.D. 1966. Multiple modes of shear fracture in rock. Proc. 1st Congr. Int. Soc. Rock Mech., Lisbon, 1, pp.509-13.
- Peng, S.S. and A.M. Johnson 1972. Crack growth and faulting in cylindrical specimens of Chelmsford granite. Int. J. of Rock Mech. and Min. Sci. 9, pp.30-41.
- Poulos, H.G. and E.H.Davis 1974. Elastic solutions for soil and rock mechanics. New York, Wiley.
- Rusch, H. 1959. Physical problems in the testing of concrete. Zement-Kalk-Gips (Cement and Concrete Association Library Translation No.86, 1960), pp. 1-9.
- Sangha, C.M. and R.K. Dhir 1972. Influence of time on the strength, deformation and fracture properties of a lower Devonian sandstone. International Journal of Rock Mechanics and Mining Sciences & Geomechanical Abstracts, 9, pp.343-354.
- Sammis, C.G. and M.F. Ashby 1986. The failure of brittle porous solids under compressive stress states. Acta Metall. 34, pp.511-526.
- Savin, G.N. 1961. Stress Concentrations around Holes. Translated from Russian by E. Gros, Published by Pergamon Press, Oxford.
- Scholz, C.H. 1968. Experimental study of the fracturing process in brittle rocks. Journal of Geophysical Research, 73(4), pp.1447-1453.
- Serata, S., 1974. Utilization of stress envelopes in design of solution cavities. 4th Symp. Salt, 2, pp.51-64.

Southwell, R.V. 1940. *Relaxation methods in engineering science*. Oxford University Press.

Sprunt, E.S. and W.F Brace 1974. Direct observation of microcavities in crystalline rock. *International Journal of Rock Mechanics and Mining Sciences & Geomechanical Abstracts*. **11** (4), pp.139-150.

Stacey, T.R. 1981. A simple extension strain criterion for fracture of brittle rock. *International Journal of Rock Mechanics and Mining Sciences & Geomechanical Abstracts*, **18**, pp.469-474.

Steif, P.S. 1984. Crack extension under compressive loading. *Eng. Fract. Mech.* **20**, pp.463-473.

Sterling, R.L. 1980. The ultimate load behaviour of laterally constrained rock beams. In *The State of the Art in Rock Mechanics*, Proc. 21st US Symp Rock Mech., D.A. Summers (ed.), pp.533-42. Rolla: Univ. Missouri.

Stimpson, B. 1989. Ultimate collapse of cross-jointed, thinly bedded, horizontal roof strata. *Int. J. of Mining and Geol. Eng.* Vol. 7, pp.127-146.

Unal, E. 1968. Development of design guidelines and roof control standards for coal mine roofs. Ph.D. Thesis, Pennsylvania State University.

Waversik, W.R. and W.F. Brace 1971. Post-failure behaviour of a granite and disbase. *Rock Mech.* **3**, pp.61-85.

Wiid, B.L. 1966. The time-dependent behaviour of rock: considerations with regard to a research program. CSIR Report MEG 514, Rock Mechanics Division, National Mechanical Engineering Research Institute, Pretoria, South Africa.

Wong, T.-F. 1982 Micromechanics of faulting in Westerly granite. *Int. J. Rock Mech. Min. Sci.* 19, pp. 49-64.

Worsley, N. and A. Fuzesy 1979. The potash-bearing members of the Devonian Prairie Evaporite of southeastern Saskatchewan, south of the mining area. *Economic Geology*, 74, pp.377-388.

Wu, H and D.D. Pollard 1992. Possible secondary fracture patterns due to a change in the direction of loading. *Conf. On Fractured and Jointed Rock Masses, Lake Tahoe*, Vol. 2, pp. 505-512. US Dept of Energy.

Zheng, Z., J. Kemmeny and N.G.W. Cook 1989. Analysis of borehole breakouts. *Journal of Geophysical Research*. 94(B6), pp. 7171-7182.

Zienkiewicz, O.C. 1977. *The finite element method*. 3rd ed. London, McGraw-Hill.

APPENDIX Definition of Stiffness

Stiffness is a mechanical property which defines the ability of a material to resist deformation in the elastic range. It is defined as the slope of the initial straight line portion of the stress-strain diagram. The proportionality of load to deformation was first recorded by Robert Hooke who observed in 1678; this is frequently referred to as Hooke's Law. Thomas Young, in 1807, suggested what amounts to using the ratio of stress to strain to measure the stiffness of a material (Higdon et al. 1985). This ratio is called Young's modulus or modulus of elasticity, and is written as:

$$E = \sigma / \varepsilon$$

or

$$G = \tau / \gamma$$

where σ and τ are normal and shear stresses, and ε and γ are normal and shear strains. The stiffness can also be expressed as:

$$K = \frac{F}{d}$$

where F is the force and d is the deformation produced by the applied force.

Several units, such as GPa, N/m and GPa/m, for stiffness are in use. The selection of the units is mainly problem dependent. For example, in the numerical analyses of jointed rock materials the joints are treated as a special unit and can be modelled by special elements called "joint" elements. For Goodman's joint elements the moduli of elasticity (i.e., the normal stiffness K_n and the shear stiffness K_s) embedded in the stiffness matrix are in N/m, while they are in Pa/m for transversely isotropic parilinear elements (Pande et al. 1990).